2018

SYNTHESIS AND CHARACTERIZATION OF MAGNESIUM - TITANIUM COMPOSITES BY SEVERE PLASTIC DEFORMATION

Baleegh Alobaid
University of Kentucky, baleegh.sood@uky.edu
Author ORCID Identifier:
https://orcid.org/0000-0002-7934-1152
Digital Object Identifier: https://doi.org/10.13023/etd.2018.463

STUDENT AGREEMENT:

I represent that my thesis or dissertation and abstract are my original work. Proper attribution has been given to all outside sources. I understand that I am solely responsible for obtaining any needed copyright permissions. I have obtained needed written permission statement(s) from the owner(s) of each third-party copyrighted matter to be included in my work, allowing electronic distribution (if such use is not permitted by the fair use doctrine) which will be submitted to UKnowledge as Additional File.

I hereby grant to The University of Kentucky and its agents the irrevocable, non-exclusive, and royalty-free license to archive and make accessible my work in whole or in part in all forms of media, now or hereafter known. I agree that the document mentioned above may be made available immediately for worldwide access unless an embargo applies.

I retain all other ownership rights to the copyright of my work. I also retain the right to use in future works (such as articles or books) all or part of my work. I understand that I am free to register the copyright to my work.

REVIEW, APPROVAL AND ACCEPTANCE

The document mentioned above has been reviewed and accepted by the student's advisor, on behalf of the advisory committee, and by the Director of Graduate Studies (DGS), on behalf of the program; we verify that this is the final, approved version of the student's thesis including all changes required by the advisory committee. The undersigned agree to abide by the statements above.

Baleegh Alobaid, Student

Dr. Yang-Tse Cheng, Major Professor

Dr. Matthew J. Beck, Director of Graduate Studies

SYNTHESIS AND CHARACTERIZATION OF MAGNESIUM - TITANIUM COMPOSITES BY SEVERE PLASTIC DEFORMATION

DISSERTATION

A dissertation submitted in partial fulfillment of the
requirements for the degree of Doctor of Philosophy in the
College of Engineering
at the University of Kentucky

By
Baleegh Alobaid
Lexington, Kentucky
Director: Dr. Yang-Tse Cheng, Professor of Materials Engineering,
Lexington, Kentucky
2018

https://orcid.org/0000-0002-7934-1152

ABSTRACT OF DISSERTATION

SYNTHESIS AND CHARACTERIZATION OF MAGNESIUM – TITANIUM COMPOSITES BY SEVERE PLASTIC DEFORMATION

Magnesium alloys are widely used in engineering applications, including aerospace and automobile industries, due to their desirable properties, such as lower density, high damping capacity, relatively high thermal conductivity, good machinability, and recyclability. Researchers have, therefore, been developing new magnesium materials. However, mechanical and corrosion properties are still limiting many commercial applications of magnesium alloys. In this Ph.D. thesis research, I developed Mg-Ti composite materials to offer some solutions to further improve the mechanical behavior of magnesium, such as titanium-magnesium (Ti-Mg) claddings, Mg-Ti multilayers, and Ti particle enforced Mg alloys. Low cost manufacturing processes, such as hot roll-bonding (RB) and accumulative roll-bonding (ARB) techniques, were used to produce Mg-Ti composites and sheets. The microstructural evolution and mechanical properties of composites were investigated using optical microscopy (OM), X-ray diffraction (XRD), scanning electron microscopy (SEM), energy dispersive spectroscopy (EDS), electron backscatter diffraction (EBSD), nanoindentation, and tensile tests.

In the first part of this study, I investigated the bonding strength of the AZ31/Ti to understand the mechanical properties of Mg/Ti composites. Using a single pass RB process, I fabricated AZ31/Ti multilayers with the thickness reduction in a range of 25% to 55%. The hot-rolled AZ31/Ti multilayers were heat-treated at 400 °C for 6, 12, and 24 hours, respectively, in an argon atmosphere. Tensile-shear tests were designed to measure the bonding strength between AZ31/Ti multilayers. Furthermore, the experimental results revealed good bonding of the AZ31/Ti multilayers without forming any intermetallic compounds in the as-rolled and heat-treated AZ31/Ti multilayers. The good bonding between Ti and AZ31 is the result of diffusion bonding whose thickness increases with increasing heat-treatment time and thickness reduction. The shear strength of the Ti/AZ31 multilayer increases with increasing bonding layer thickness.

In the second part of this study, I characterized the microstructure and texture of three-layered Ti/AZ31/Ti clad sheets which were produced by single-pass hot rolling with a reduction of thickness 38% (sheet I) and 50% (sheet II). The AZ31 layer in sheets I and II exhibited shear bands and tensile twins$\{10\bar{1}2\}\langle10\bar{1}1\rangle$. The shear bands acted as local strain concentration areas which led to failure of the clad sheets with limited elongation. Heat treatment caused changes in the microstructure and mechanical properties of clad sheets due to static recrystallization (SRX) on twins and shear bands in the AZ31 layer.

Recrystallized grains usually randomize the texture which causes weaken the strong deformed (0001) basal texture. Twins served as nucleation sites for grain growth during SRX. Tensile tests at room temperature showed significantly improved ductility of the clad sheets after heat treatment at 400°C for 12h**.** The results showed that the mechanical properties of clad sheets II are better than clad sheet I: The clad sheet II shows elongation 13% and 35% along the rolling direction (RD) for as-rolled and annealed clad sheet, respectively whereas the clad sheet I shows elongation 10% and 22% along RD for as-rolled and annealed clad sheet, respectively.

In the final part of this study, I examined the effects of dispersed pure titanium particles (150 mesh) with 0, 2.3, 3.5, 4.9, and 8.6 wt. % on the microstructure and mechanical properties of AZ31-Mg alloy matrix. Mg-Ti composites were processed through three accumulative roll bonding (ARB) steps using thickness reductions of 50% in each pass followed by heat treatment at 400 °C for 12 h in an argon atmosphere. ARB is an efficient process to fabricate Mg-Ti composites. Mechanical properties of Mg- 0Ti and Mg-2.3Ti composite were enhanced by ~ 8% and 13 % in yield strength and ~ 30% and 32 % in ultimate tensile strength, respectively. Meanwhile, the elongation of the composites were decreased by 63% and 70%, respectively. After heat treatment, the results showed a decrease in yield strength and increase in elongation to fracture. The mechanical properties of the Mg-0 and Mg-2.3Ti composite were enhanced: ultimate tensile strength by 9% and 7%, and elongation by 40% and 67%, while the yield strength was decreased by 28% and 36% compared with the initial AZ31. Enhancements of strength and ductility were the results of two mechanisms: a random matrix texture by ARB and ductile titanium particle dispersion.

KEYWORDS: Magnesium alloy AZ31; Titanium; Roll bonding (RB); Accumulative roll bonding (ARB) Heat Treatment; Diffusion Bonding; Mechanical Behavior

Baleegh Alobaid

Author’s signature

November 7, 2018

Date

SYNTHESIS AND CHARACTERIZATION OF MAGNESIUM - TITANIUM COMPOSITES BY SEVERE PLASTIC DEFORMATION

By

Baleegh Alobaid

Dr. Yang-Tse Cheng

Director of Dissertation

Dr. Matthew J. Beck

Director of Graduate Studies:

November 7, 2018

Date

DEDICATION

To My Parents, My Wife, And My Kids

for their endless love and devotion.

ACKNOWLEDGEMENTS

First, I would like to express sincere thanks to my Ph.D. advisor, Prof. Yang-Tse Cheng, for his support, help and career development in my academic research. Dr. Cheng has helped me to become an independent researcher; at the same time, he continues to contribute valuable discussion, feedback, and encouragement.

Second, I would like to express my gratitude to Prof. Fuqian Yang for his valuable contributions, suggestions and in-depth discussion in my research. Prof. Yang has been a substantial influence in developing my research.

I gratefully acknowledge my Ph. D committee members for their efforts and feedback on the preliminary version of my dissertation.

My appreciation also goes to my lab mates and previous group members, Jie Pan, Jiagang Xu, Tao Chen, Alshroofy Mohanad, Yikai Wang, Long Zhang, Jiazhi Hu, for their support and help with my research.

I am particularly thankful to staff and faculty in the department for their understanding and assistance. I am also thankful for the lab manager Nancy Miller of her support and assistance. Thanks to Nicolas Briot, Azin Akbari and Dali Qian from the electron microscopy center.

I greatly acknowledged the Higher Committee for Education Development (HCED) in Iraq for their financial support of my Ph.D. study.

I would like to express my deepest gratitude to my parents and brothers for their unselfish support, encouragement, and prayers.

Finally, I deeply thank my wife and kids. My wife has been greatly supportive, helping and encouraging me most positively.

TABLE OF CONTENTS

List of Tables

List of Figures

CHAPTER 1. Literature Review

1.1. Motivation

There is an interest in engineering applications of lightweight alloys, including solid-state hydrogen storage, aerospace, and automobile industries, because of the increasing demand to reduce fuel consumption and greenhouse gas (e.g., CO_2) emission [1-3]. Also, Mg-Ti alloys have been reported as biodegradable implant materials [4, 5].

AZ31-H24 (Mg-3wt. % Al-1wt. % Zn) is the most common Mg alloy sheet which is produced by hot rolling of the direct chill cast ingot. The hot-rolled AZ31sheets exhibit strong basal texture [6] with limited formability. It has been reported that the forming ability can be improved through modification of texture by weakening the basal or obtaining a random texture. In this work, titanium was added as ductile dispersion. Therefore, it is necessary to understand the effects of Ti on microstructure and texture evolution.

The main objective of this study is to identify the effects of severe plastic deformation and annealing on the microstructure and mechanical behavior of the Mg/Ti composite materials. Composite materials, such as clad sheets, multilayered, and Ti particle additions, consisting of Mg alloy (AZ31) and commercially pure Ti (denoted in this text as AZ31/Ti), were fabricated by single-pass hot rolling (roll bonding; RB) and accumulative roll bonding (ARB), during which there are no interface reactions with as-rolled and heat treated samples at 400°C. A new Mg/Ti composite with a weakened basal texture was developed which exhibits improved room temperature formability.

From the literature review, there has been limited investigations on the mechanical, microstructure and texture of (Mg/Ti) formed by hot rolling and accumulative roll bonding. This study is intended to explore the feasibility of preparing bulk magnesium-titanium composites with acceptable mechanical (improved deformability and toughness). There are a number of unexplored opportunities. Bonding of Mg to Ti has proved difficult because there is no solubility in each other. Therefore, elevated temperature and large deformations are required to obtain good bonding strength. No attempt was made to measure the bonding strength of the Mg/Ti interface made by roll bonding (hot rolling) processes. The first

objective of this study is to fabricate tri-layered Ti/AZ31/Ti alloy and five-layered Ti/AZ31/Ti/AZ31/Ti multi-layered composites by single-pass hot rolling. AZ31/Ti interface bonding strength was investigated. The effects of the reduction and annealing treatments on the bonding strength were also reported. The tensile behavior of three and five layers was investigated. Since no report has been made for the AZ31/Ti interface texture analysis using SEM- electron backscatter diffraction (EBSD), the texture of thick AZ31 sheet cladding with a Ti shim has been studied. Furthermore, since no attempt was made to fabricate AZ31 with Ti particles using the ARB process, AZ31 matrix with different Ti particles (0, 2.3, 3.5, 4.9, and 8.6 wt. %) was studied in details.

A second goal is to design an economically efficient method which can be implemented in industrial production. The microstructure and mechanical properties of the Ti/Mg composites were investigated. Particularly, the AZ31/Ti interface bonding strength and texture were tested. This chapter focuses on two topics:

1. Roll bonding (RB) and accumulative roll bonding (ARB)
2. Challenges and literature review

1.2. Roll bonding (RB) and accumulative roll bonding (ARB)

In this study, two main methods were used, namely, roll bonding (RB) and accumulative roll bonding (ARB). This section gives a brief description of each method. First, the roll bonding is a solid-phase technique that can join similar or dissimilar metals. The metals are bonded by plastic deformation[7, 8]. Figure1.1 illustrates the deformation behavior during the roll bonding process for two different metals (aluminum/steel cladding) [9]. Bonding is a result of diffusion of metals into each other. The bonding process can be accelerated by heat which is generated during plastic deformation and friction. As shown in Figure 1.1b, the bonding mechanism for two different metals can be summarized to four reigns:

1. Before entering the rolling mill: both metals have a surface roughness, and Al sheet has an oxide film on the surface.
2. Entering the rolling mill: The Al layer is deformed and elongated because it has lower flow stress than steel which led to interfacial slide, forming a wavy interface. The new metal surface is generated, and the Al surface oxide film is

broken due to elongation. In addition, the steel has higher entering speed which may contribute to interfacial sliding. High pressure and short rolling time can prevent re-oxidation of the Al surface.

3. Bonding: the metals are heated before entering the rolling mills to temperature 450-500 °C. As shown in figure 1.1c, the diffusion layer is ~1 μm which means that the interface zone temperature is close to the melting point of Al (660 °C) or solid-liquid mixture temperature. Interface temperature is increased as a result of heat generation by plastic deformation and friction. As a result, a local softening zone is generated at the interface which leads to mutual diffusion between metals. During the roll bonding process, surfaces are deformed by shear stress, as shown in figure 1.1d.
4. Exit point: High pressure, heat, plastic deformation, and friction during the rolling process may accelerate the mutual diffusion in the interface zone.

There are several conditions which can affect the bonding strength, such as the number of layers, layer thickness, temperature, time, crystal structure, amount of deformation, surface preparation, and post-heat treatment. Figure 1.2a and figure 1.2b show the effect of the surface preparation and deformation reduction on the bonding strength after rolling [7, 10, 11]. Figure 1.3 is a diagram of a clad sheet production [9]. Roll bonding process can be designed for high quantity production at low cost.

Second, accumulative roll bonding (ARB) is a severe plastic deformation (SPD) process which was invented by Tsuji in 1998 [12-14]. The ARB process is promising for industrial application such as manufacturing ultrafine grained sheet materials[15, 16]. The ARB process can produce bulk materials with ultrafine grains (UFGs). It is well known that the grain size affects the flow stress of a polycrystalline metal which is related to the dislocation density obstacle (grain boundaries and high angle cell boundaries). A higher degree of deformation can be achieved using ARB comparing with other standard rolling procedures.

During ARB, the materials are plastically deformed to the reduction of ~50% (von Mises equivalent 0.80), then cut into two halves, and staked together to maintain the initial thickness followed by rolling. The process of cutting and assembly can be repeated for

several ARB cycles, as shown in Figure 1.4 [17], though the ARB cycles can be repeated without limitation. Therefore extensive plastic deformation can be applied. As discussed above, surface treatment, degreasing, and wire-brushing are used to prepare the surface of the materials to increase the bonding strength. The ARB process is carried below the recrystallization temperatures of materials. UFGs of about 1μm can be obtained by several ARB cycles [17]. During the ARB process, the layers are joined together by rolling, which is the same as in a conventional roll-bonding process.

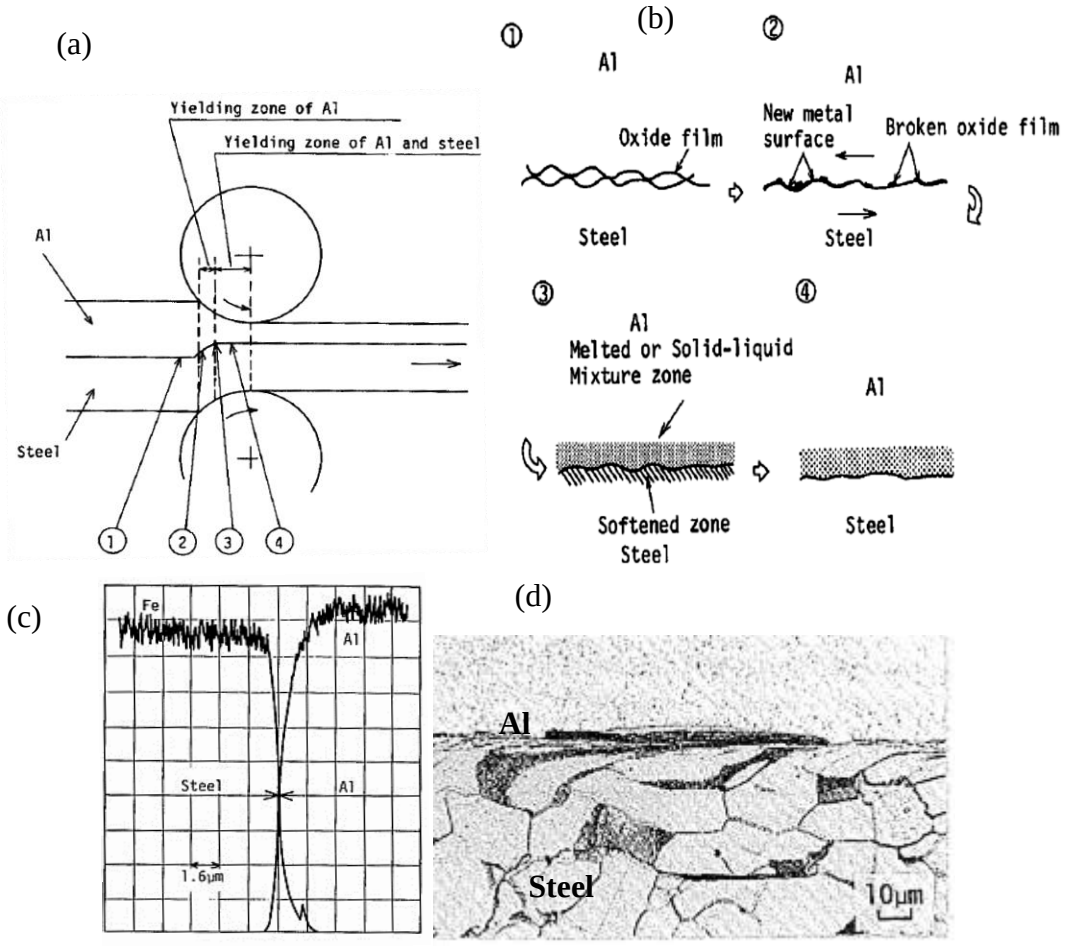

Figure 1.1 Schematic of the roll bonding mechanism for two different metals (aluminum clad steel plate) [9].

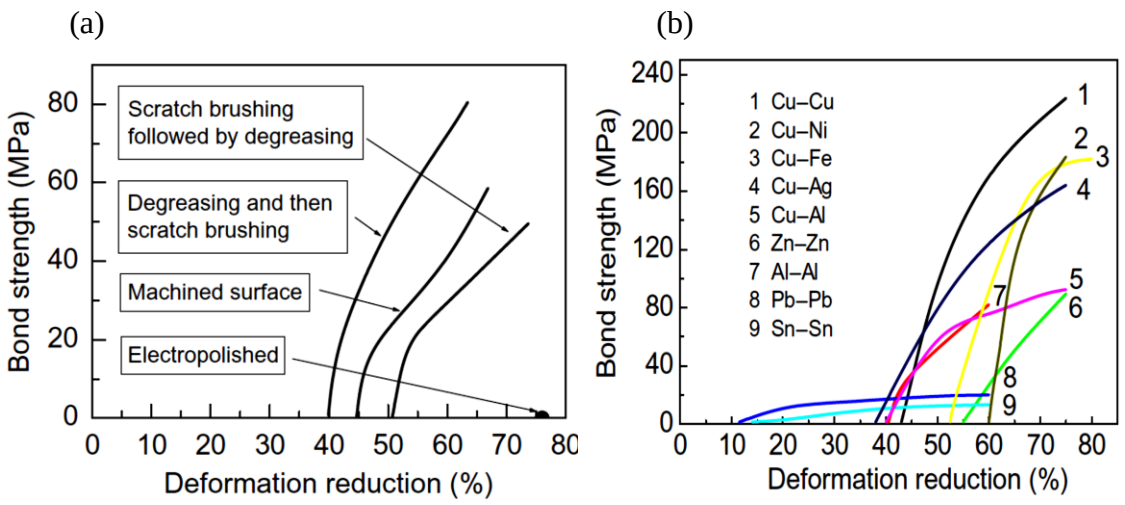

Figure 1.2 (a) Effect of surface preparation on bonding strength, and (b) roll bonding strength as a function of deformation reduction [11].

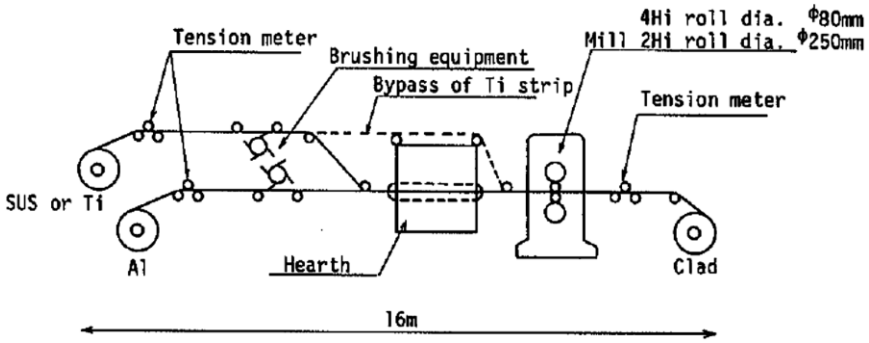

Figure 1.3 A diagram of clad sheet production [9].

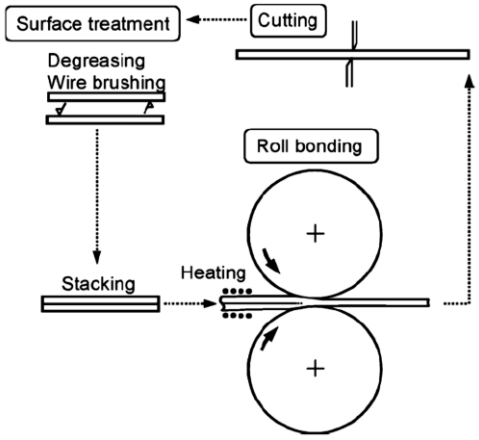

Figure 1.4 Principle of accumulative roll bonding (ARB) [17].

1.3. Literature review on Mg-Ti

The melting point of Ti (1668°C) is higher than the boiling point of pure Mg (1091°C). Mg-Ti binary phase diagram is shown in figure 1.5. It has very low solubility. Thus, Ti/Mg alloy cannot be produced by conventional rapid solidification and/or melting methods. The non-equilibrium processes can produce Mg-Ti alloys such as physical vapor deposition, vapor quenching, magnetron sputtering, and high-energy ball milling [5, 18-23]. Brazing and friction stir welding has been reported as processes to join Mg to Ti and Al [24-29]. Mg/Al multilayers and clad composites have been fabricated by single-pass hot rolling and ARB [16, 30, 31].

Magnesium has a hexagonal closed packed (hcp) crystal structure with lattice parameters (a = 0.32 nm, c = 0.52 nm). It has low symmetry and the limited of slip systems which cause insufficient strength and ductility. Magnesium has a 1.624 axial ratio (c/a), smaller than the ideal value of ?, which results in low critical resolved shear stresses [32]. In general, hcp materials have slip plane systems: basal $\{0001\}<11\bar{2}0>$, prismatic $\{10\bar{1}0\}<11\bar{2}0>$ and pyramidal $\{10\bar{1}1\}<11\bar{2}0>$ systems [33-35].

Figure 1.6 shows the slip and twinning pane and directions in Mg alloys. It is difficult to form Mg and its alloys at ambient temperature. Only basal slip systems are active at room temperature, while the other slip systems (prismatic and pyramidal) are inactive. Therefore, insufficient plastic deformation occurs at room temperature [36-39]. Magnesium deforms by the basal slip at room temperature because the critical resolved shear stress (CRSS) for the basal slip is ~ 1/100 less than that of the non- basal slip systems. The Mg formability improves greatly at 230-400 °C due to a decrease of the CRSS of prismatic and pyramidal systems with increasing temperature. During severe plastic deformation processing (e.g., hot rolling), other non-basal slip systems or twinning systems are activated. The twinning systems are provided with extra independent deformation modes in addition to other dislocation slip systems. There are various twinning systems in Mg alloys: double twins (DTWs; $\{10\bar{1}1\}-\{10\bar{1}2\}\langle 10\bar{2}0\rangle$); compression twins (CTWs; $\{10\bar{1}1\}\langle 10\bar{2}0\rangle$); tensile twins (TTWs; $\{10\bar{1}2\}\langle 10\bar{1}1\rangle$) [40, 41]. The double twins and compression twins are associated with the formation of shear bands, as shown in figure 1.7.

The shear bands are observed at angles < ±35° to the RD, which are caused by high local stress concentration[42, 43].

There has been a considerable amount of research to improve the electrochemical and mechanical behavior of magnesium and its alloys due to its lightweight, high specific strength, and recyclability [44] [13, 45-48]. Mg and its alloys cannot meet the electrochemical and mechanical demands because of the poor forming ability and corrosion resistance at room temperature which is why composite materials, such as clad, multilayers, and powder metallurgy are of interest. The composite materials have been processed by various manufacturing methods such as diffusion bonding, roll bonding, and accumulative roll bonding. The mechanical properties of Mg were improved by the addition of Ti particles which was attributed to load transfer trough Mg/Ti interface. This is caused by good interfacial bonding without intermetallic phase formation at the Mg/Ti interface.

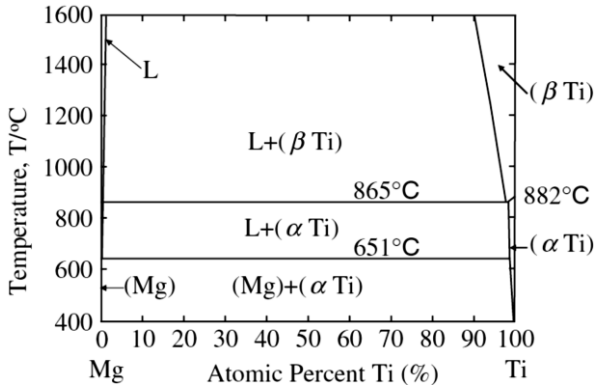

Figure 1.5 The Mg-Ti phase diagram [49].

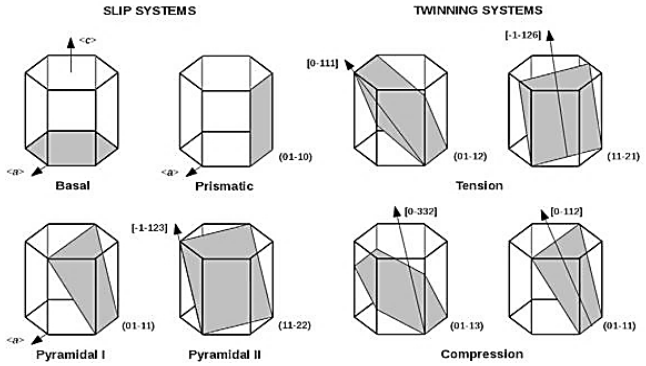

Figure 1.6 Shows deformation modes in hcp Mg alloys [35].

Perez et al. [22, 50], Hassan et al. [51] and Umeda et al. [52] reported improvement of the mechanical properties by adding Ti as reinforcement in Mg by powder metallurgy method.

Asano et al. [34] have synthesized Mg-Ti alloys by using a ball milling process. BCC Mg-Ti alloy was formed in the form of spherical particles with a mean diameter of 1mm. Danaie et al. [1] synthesized Mg-Ti multilayer composites by accumulative roll-bonding (ARB) for hydrogen storage applications. Samples with a thickness of 0.7mm were prepared by the repetitive folding and cold rolling of Ti and Mg foils. The Mg-Ti composite showed a good hydrogen absorption rate.

Kawamoto et al. [32] studied strain transfer through the Mg/Ti interface using a crystallographic method. They suggested that the dispersion of Ti particles in the Mg-based composite can improve the deformability of Mg by the strain transfer through the Mg/Ti interface. They concluded that a larger Schmid factor and lower residual strain energy are essential for the movement of a prismatic slip system in Ti grains.

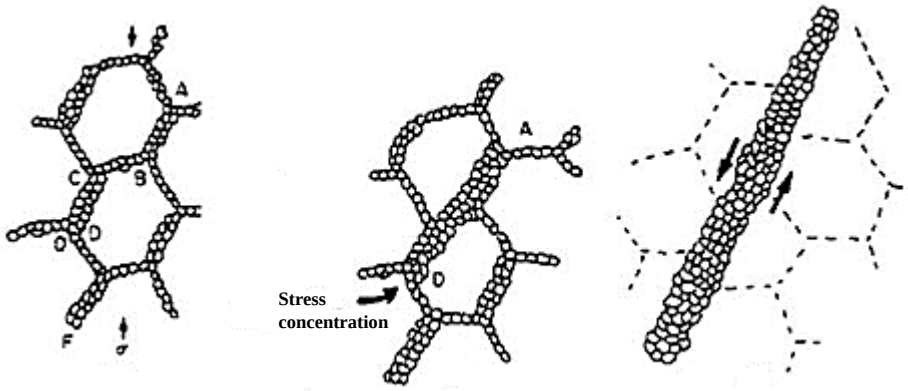

Figure 1.7 Shows Ion et al. [42]model for the formation of localized deformation shear bands.

Kitazono et al. [53] synthesized Mg/Ti composites by accumulative diffusion-bonding (ADB). The mechanical properties of the AZ91Mg alloy were improved by the dispersion of Ti particles in the AZ91matrix. They suggested that an improvement in ductility was caused by the development of a random texture due to severe plastic deformation and stress relaxation in Ti particles.

Alam et al. [54] claimed that there is an improvement in the microstructure and mechanical properties of AZ41 and AZ50 Mg alloys by adding nano-sized Al_2O_3 particles and Ca. Disintegrated melt deposition technique was used to prepare the nanocomposites, which results in an improvement in the 0.2% yield strength and ultimate tensile strength in comparison to AZ41 and AZ51 alloys.

Kumar et al. [55] synthesized Mg/Ti nanocomposites through the disintegrated melt deposition technique followed by hot extrusion. They claimed that the prepared Mg/Ti nanocomposites had superior mechanical properties over pure magnesium.

Esen et al. [19] prepared Ti–Mg composite rods by hot rotary swaging from elemental powders of titanium and magnesium. The composite was in-vivo tested in Ringer's solution. They suggested that Ti–Mg composite can be used in the human body.

Teng et al. [56] investigated the micro-machinability of Mg-based composites reinforced with Ti and TiB_2 nanoparticles by using an ultraprecision desktop micro machine tools (micro-end milling process using AlTiN-coated carbide end mills).

Kumar et al. [57] studied the effects of adding Y_2O_3 nano- reinforcement on compression, damping, and thermal expansion of Mg–3Al–2.5La alloy. The composite was prepared by a disintegrated melt deposition technique followed by hot extrusion. There was a significant improvement in the compression yield strength and ultimate compressive strength.

Dai et al. [58] analyzed the effects of the Mg/Ti interface on the stability and adsorption of hydrogen for hydrogen storage applications. They assumed two interface configuration (symmetrical and anti-symmetrical). Their result showed that anti-symmetrical configuration was the more stable interface configuration.

Duygulu et al. and Motevalli et al. [59, 60] suggested that zirconium and aluminum can be used to increase the bonding between magnesium and titanium due to good solubility of Zr and Al in both Ti and Mg, leading to mutual solubility or intermetallic compound formation at the interface.

CHAPTER 2. Microstructure and mechanical behavior of hot-rolled AZ31/Ti multilayers

2.1. Summary

Using a single pass hot-rolling process, we fabricate AZ31/Ti multilayers with the thickness reduction in the range of 25% to 55%. The hot-rolled AZ31/Ti multilayers are heat-treated at 400 °C for 6, 12, and 24 hours, respectively, in an argon atmosphere. Optical microscopy, scanning electron microscopy, energy dispersive spectroscopy, and x-ray diffraction are used to characterize the microstructure of the AZ31/Ti multilayers; nanoindentation, tensile, and shear tests are used to measure the mechanical properties of the AZ31/Ti multilayers. The experimental results reveal good bonding of the AZ31/Ti multilayers without forming any intermetallic compounds in the as-rolled and heat-treated AZ31/Ti multilayers. The good bonding between Ti and AZ31 is the result of diffusion bonding whose thickness increases with increasing heat-treatment time and thickness reduction. The shear strength of the Ti/AZ31 multilayer increases with increasing bonding layer thickness.

2.2. Introduction

Titanium and magnesium have been widely used in a variety of engineering areas. In particular, magnesium has attracted great interest in automobile industry. It is desirable to have a material with a combination of properties of Ti and Mg, such as lightweight, high strength, and low cost [32]. This interest has stimulated the research of developing Ti/Mg composites.

Mg-based composites can exhibit improved formability and toughness with the dispersion of ductile particles, which are deformed plastically at a stress level lower than the strength of Mg matrix. These ductile particles can limit stress concentration and cracking at the grain boundaries of Mg. Ti may be used as the strengthening phase in Mg matrix since Ti has a very low solid solubility in Mg, and intermetallic compounds are not present in the equilibrium Mg-Ti phase diagram [27, 32, 59, 61]. It is impossible to form Ti/Mg solid solutions by conventional means to improve the strength of Mg-based materials.

Multilayer structrures are a type of composites, which have been widely studied for engineering applications. There are several methods to join Mg with Ti, including friction

stir welding, transient liquid phase welding, cold metal transfer welding, tungsten inert gas welding, and laser welding [24, 27, 29]. All of them require significant energy consumption, and are not suitable for the fabrication of Ti/Mg multilayer structures. Other techniques, such as sputtering and evaporation, for the fabrication of Ti/Mg multilayer structures require expensive devices and systems, and cannot produce Ti/Mg multilayer structures in large quantities [30, 62-66].

Roll bonding is a simple technique to produce multilayers, which consist of two or more alloys [67-69]. Using hot-roll bonding, Naga et al. [70] formed a tri-layer structure, consisting of stainless steel, Ta, and X (X: Ti-5Ta, Zr or Ti). Ma et al. [71] fabricated Ti-6Al-4V/Al 3003/Ti-6Al-4V laminated composites by hot-roll bonding, and found that the laminated composites exhibited a good Ti/Al interfacial bonding with straight interfaces. Lou and Acoff [72] used a cyclic cold-roll bonding/annealing process to produce multi-layered Ti/Al composites. Ma et al. [73] fabricated Al 6061/Ti-6Al-4V/Al6061 laminated composites by hot-roll bonding, and studied the effect of rolling temperature and thickness reduction on the microstructure and mechanical properties of the laminated composites. Using single-pass hot rolling followed by thermal annealing at 200 °C, Nie et al. [74] produced tri-layer Al5052/AZ31/Al5052 clad sheets with the thickness reduction of 33% and 48%, and found that the annealed clad sheets with 33% thickness reduction and limited recrystallization exhibited the largest elongation of 22.5% and higher ultimate tensile strength than the annealed clad sheets with 48% thickness reduction. Currently, roll-bonding has not been reported as a process for fabricating AZ31/Ti multilayer structures.

Considering the potential application of Ti/Mg composites in biomedical, automotive, and aerospace industries, we have fabricated AZ31/Ti multilayers via a single hot-roll bonding process. The microstructure and mechanical behavior of the prepared AZ31/Ti multilayers were systematically studied as functions of heat treatment and the thickness reduction.

2.3. Experimental details

The materials used in this work were commercially pure titanium grade-2 (annealed, TIMETAL 50A) plates and magnesium tempered-alloy (AZ31B-H24, Magnesium Elektron) plates, whose chemical compositions and mechanical properties are listed in Tables 2.1 and 2.2, respectively. Prior to rolling, the surfaces of all the plates were

roughened manually by a steel wire brush, and degreased ultrasonically in an acetone bath for 15 min. The dimensions of un-deformed Ti layers were 0.58±0.05 mm in thickness, 25 mm in width, and 50 mm in length, and the dimensions of un-deformed AZ31 sheets were 0.80±0.1 mm in thickness, 25 mm in width, and 50 mm in length. Stacked-layered structures (three layers and five layers) of Ti/AZ31/…/AZ31/Ti, which were assembled from the cleaned plates, were heat-treated in a furnace at 450 °C for 10 min in an argon atmosphere. Steel wires were used to secure the stacked-layered structures to prevent slipping between layers during hot rolling.

After being removed from the furnace, the stacked-layered structures were immediately rolled in a rolling mill to form sandwiched structures, as shown schematically in figure 2.1 for a three-layer structure. The roll bonding was conducted without lubricant in the rolling mill, which has a 101.6 mm diameter roller operating at 24 revolutions per minute. The thickness reductions was set at 25%, 38%, 50%, and 55% in a single pass. Portions of the sandwiched structures were then annealed at 400 °C for various durations. The sandwiched structures of three layers were designated as AS325, AS338, AS350, and AS355 for as-rolled structures with the thickness reductions of 25%, 38%, 50%, and 55%, respectively, and AN338, AN350, and AN355 for the corresponding structures annealed at 400 °C in Ar gas. The sandwiched structures of five layers with the thickness reduction of 50% were denoted as AS550 for as-rolled structures and AN550 for annealed structures, respectively.

Table 2.1. Chemical composition of commercially pure titanium grade-2 and AZ31 (wt. %)

Chemical composition (wt. %)													
	C	Al	Zn	Mn	Ca	Cu	Fe	Ni	Si	O2	N	Mg	Ti
AZ31	-	2.5-3.5	0.7-1.3	0.2-1.0	0-0.04	0-0.05	0-0.005	0-0.005	0-0.05	-	-	Bal	-
Ti	0.02	-	-	-	-	-	0.13	-	-	0.13	< 0.01	-	Bal

Table 2.2. Mechanical properties of the commercial pure titanium grade-2 and Mg alloys (AZ31)

	Yield Strength (MPa)	Ultimate tensile stress (MPa)	Elongation (%)
AZ31	224-227	290-291	17
Ti	332-365	431-488	31

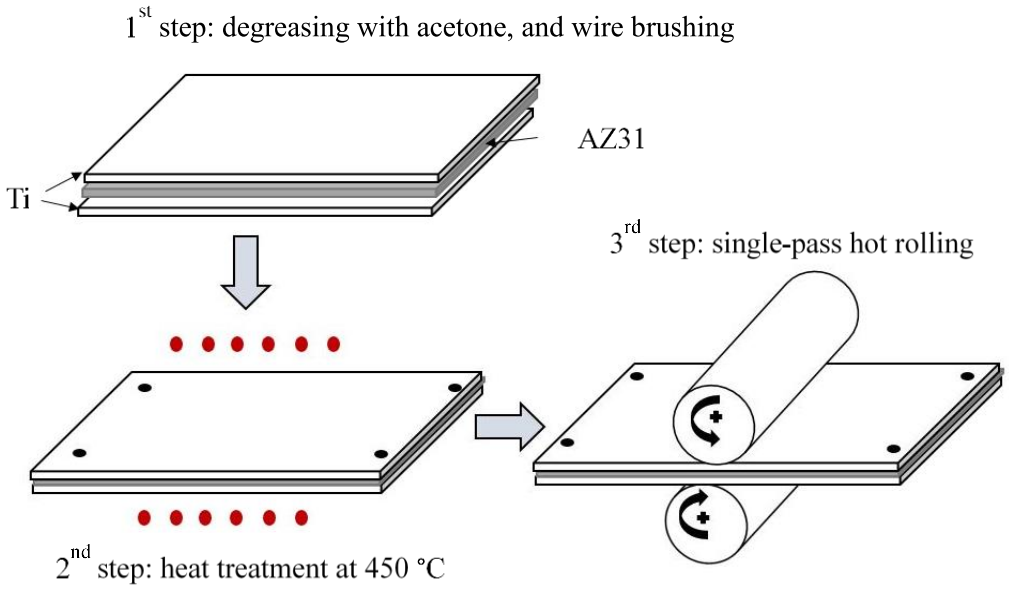

Figure 2.1 Illustration of the fabrication of Ti/AZ31/Ti sandwiched structures.

The microstructure and chemical compositions of the materials near the Ti/AZ31 bonding interface were characterized on the transverse-direction (TD) plane by optical microscopy (OM), energy *dispersive* X-ray spectroscopy (EDX), and scanning electron microscopy (SEM). X-ray diffraction (XRD) analysis of the sandwiched structures with patterns recorded in a range of 30-80^{o} was performed on a Siemens D500 at 40 kV and 30 mA with a Cu Kα radiation source.

The mechanical behavior of the sandwiched structures was studied by nanoindentation (Agilent G200), tension test, and shear test (Instron 3345 machine). The indentation load was 30 mN. The cross-head speed for the tension and shear tests was 0.5 mm/min. Figure 2.2 shows the geometry of the specimens for the tension and shear tests [75, 76].

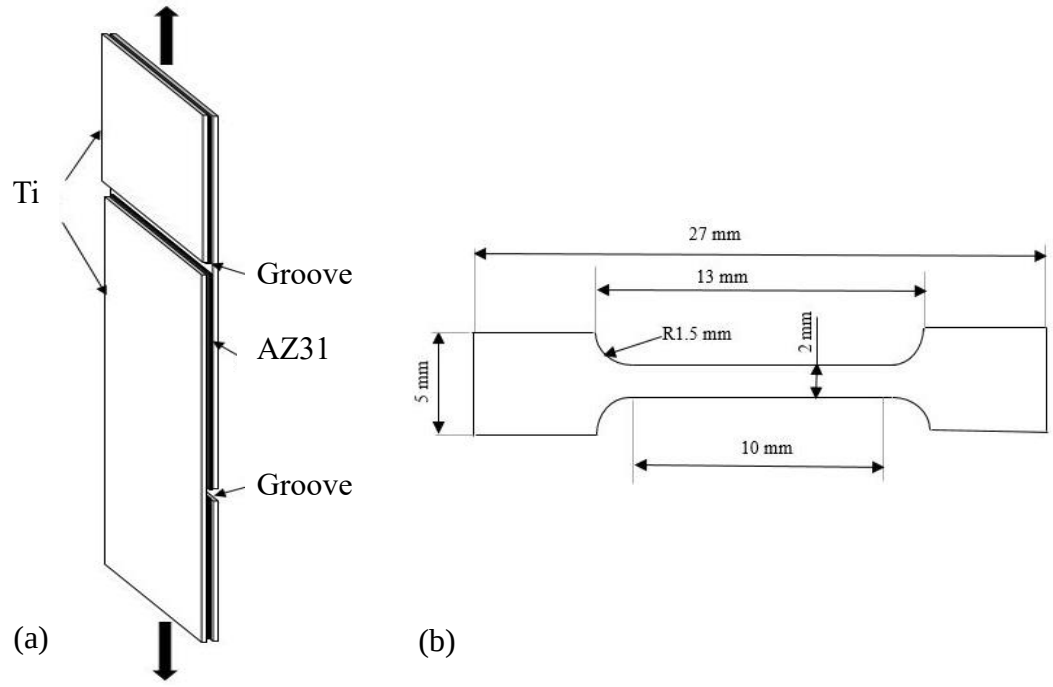

Figure 2.2 (a) Schematic of the shear test of a trilayer Ti/AZ31/Ti sandwiched structure, and (b) geometrical dimensions of the tension specimens.

2.4. Results and discussion

2.4.1. Microstructures of Ti/AZ31 interface

For the Ti/AZ31/Ti sandwiched structures with the thickness reduction of 25%, the bonding strength is insufficient to hold layers together, which suggests that a critical thickness reduction is needed to increase the bonding strength for the fabrication of the Ti/AZ31/Ti sandwiched structures. Figure 2.3 shows the optical micrographs of the sandwiched structures of Ti/AZ31/Ti and Ti/AZ31/Ti/AZ31/Ti with the thickness reductions of 38% and 50%, respectively. There are no pores, voids, and local de-bonding observed along the interface the AZ31 and Ti layers. The Ti/AZ31 interfaces are wavy in contrast to the flat surfaces of the un-deformed Ti and AZ31 plates, as shown in figure 2.3b. The change in the morphologies of the interface/surface is controlled by the rolling-induced plastic deformation, the surface interaction, and the mismatch in the mechanical behavior between Ti and AZ31 [9, 11]. The local plastic deformation can increase local temperature, which causes the softening of both Ti and AZ31 and the increase of the plastic strain as well as the migration of atoms across the AZ31/Ti interfaces.

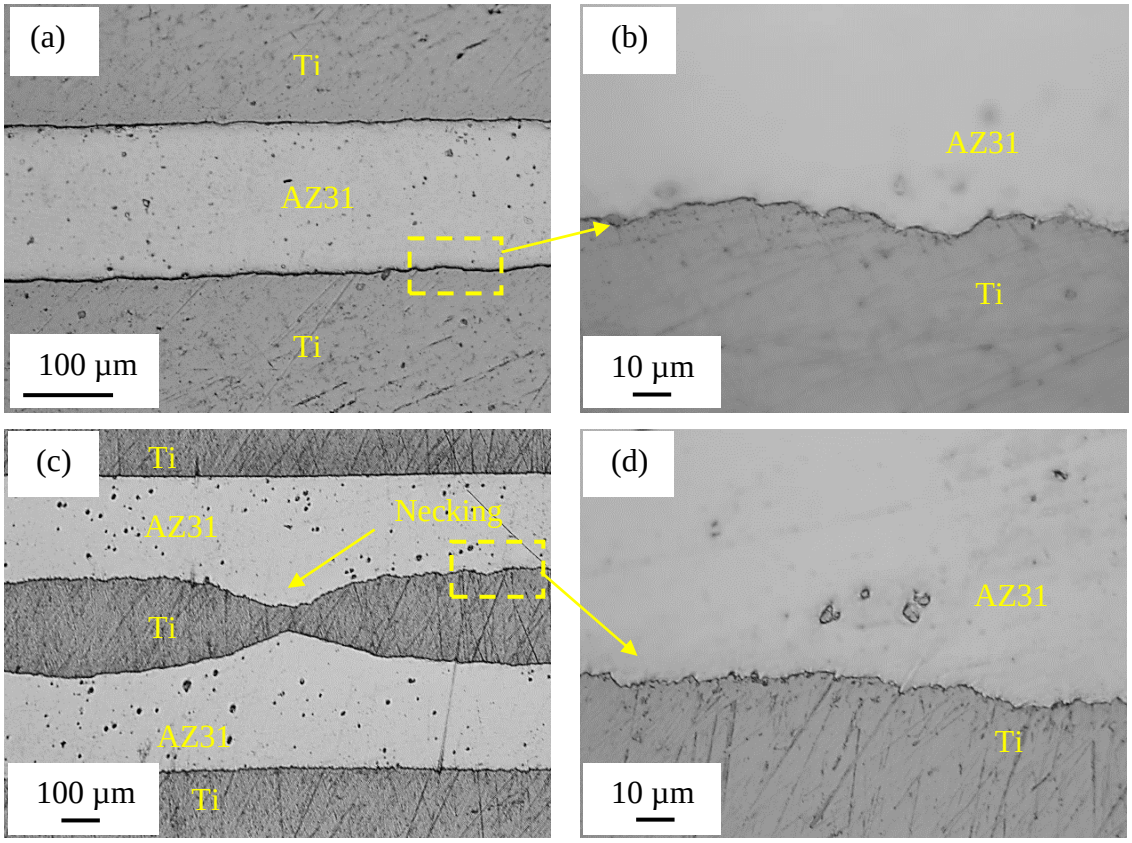

Figure 2.3 Optical images of sandwiched structures: (a) AS338, (b) high magnification of AS338 interface, (c) AS550, and (d) high magnification of AS550 interface.

The AZ31 plate experiences more severe plastic deformation than Ti plates because the flow stress of AZ31 is lower than Ti [9, 65, 77]. Figures 2.3c and 2.3d are optical micrographs of a Ti/AZ31/Ti/AZ31/Ti sandwiched structure and the corresponding Ti/AZ31 interfaces. The Ti layer experiences local necking, as shown in figure 2.3c, which is in accord with the results that rolling causes the necking and fracture of hard layers due to the difference in the mechanical properties between soft layer and hard layer [64, 65, 78]. This result is likely due to the plastic flow of AZ31 towards local weak spots in the Ti layers, which causes a local reduction in thickness.

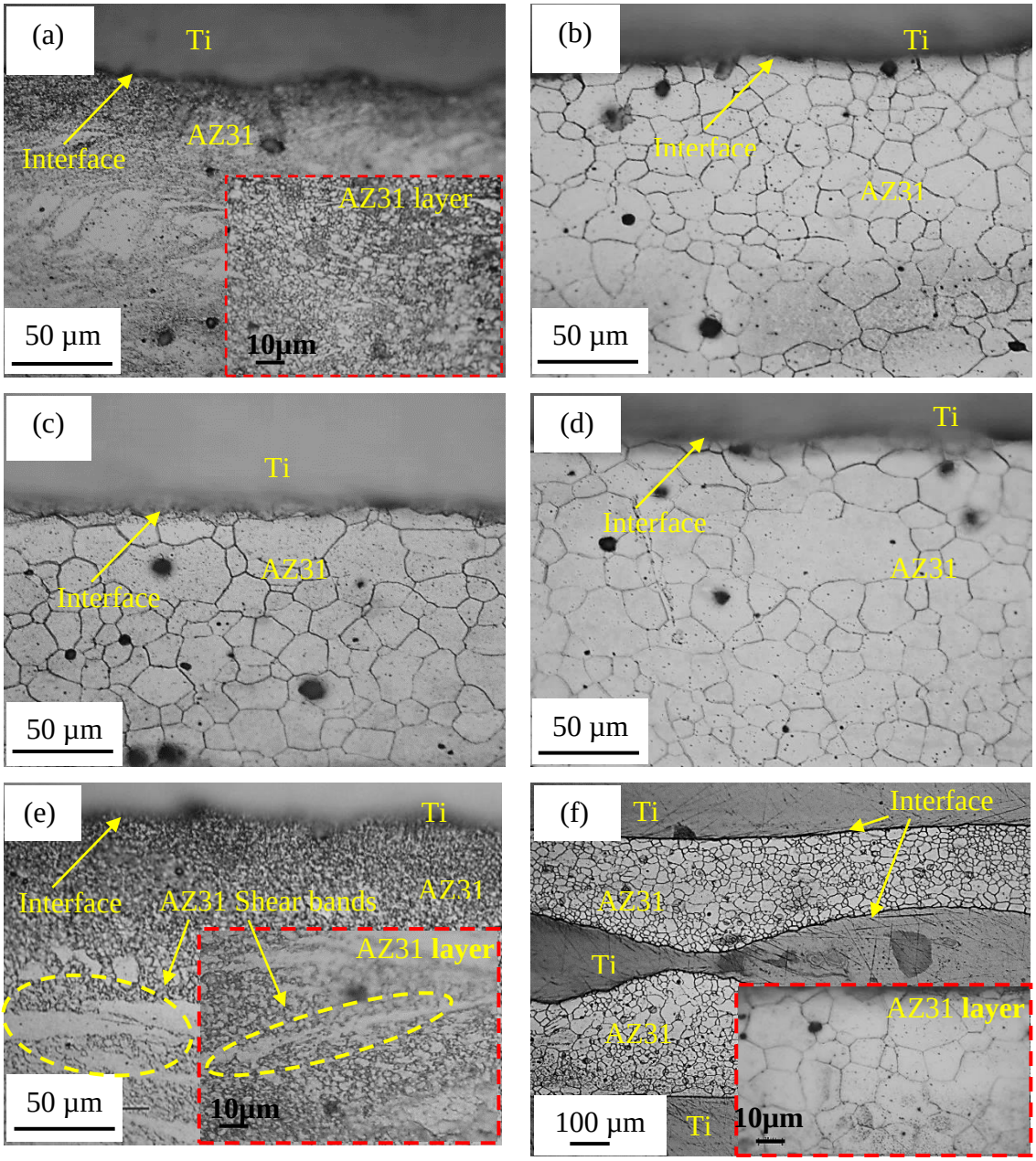

Figure 2.4 Optical images of the Ti/AZ31 interfaces before and after heat treatment: (a) AS350, (b) AN350 with annealing time of 6 hours, (c) AN350 with annealing time of 12 hours, (d) AN350 with annealing time of 24 hours, (e) AS550, and (f) AN550 with annealing time of 24 hours.

Figure 2.4 shows optical images of the sandwiched structures before and after the heat treatment. Relatively uniform, fine grains are present in the AZ31 layer for the as-rolled Ti/AZ31/Ti sandwiched structures with the thickness reduction of 50% (AS350),

suggesting that the rolling caused dynamic recrystallization (DRX) of Mg due to the release of heat associated with the rolling-induced plastic deformation [79, 80]. DRX occurred during the rolling process and involved the formation of fine grains.

The annealing of the as-rolled AS350 at 400 °C (AN350) led to grain growth, as shown in figure 2.4b-4d for the heating times of 6, 12 and 24 hours, respectively. Static recrystallization process (SRX) took place during the heat treatment [81, 82]. The average grain size of the AN350 increases with annealing time, as expected, to reduce the resultant grain-boundary energy. For comparison, the optical images of AS550 and AN550 with the annealing time of 24 hours are depicted in figure 2.4e and figure 2.4f. It can be seen that the microstructure of AS550 consists of fine grains and shear bands. The AZ31 layers in the five-layer structure experienced severe plastic deformation, leading to the formation of shear bands (many fine DRX grains). The shear bands acted as local strain concentration, and led to the reduction of elogation [83]. Similar to the AN350, the annealing of the as-rolled AS550 for 24 hours led to grain growth, and the average grain size is slightly larger than AN350 with the same annealing time. Plastic deformation plays an important role in the grain growth during the annealing.

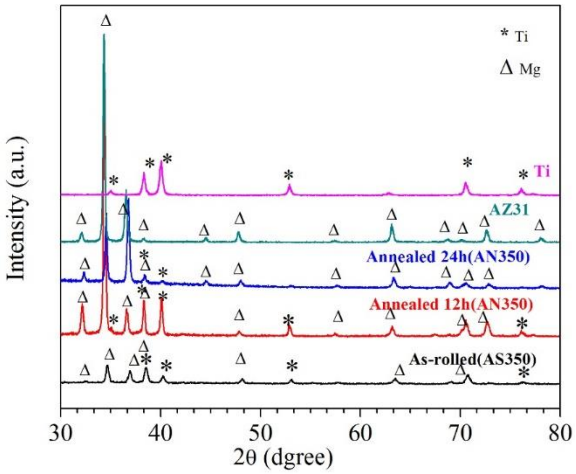

Figure 2.5 XRD patterns of AZ31 plate, Ti plate, as-rolled Ti/AZ31/Ti, and the annealed Ti/AZ31/Ti at 400 °C for 12 and 24 hours.

XRD analyses of the sandwiched structures were performed to investigate if any new phases/intermetallic compounds were formed. Figure 2.5 shows the XRD patterns of

the AZ31 plate, Ti plate, and the materials on the fractured surfaces of the as-rolled Ti/AZ31/Ti and the Ti/AZ31/Ti annealed at 400 °C for 12 and 24 hours. There are only Ti and Mg phases presented in the sandwiched structures, suggesting that both the hot rolling and annealing did not lead to the formation of intermetallic compounds. This result is consistent with that the mutual solubility between Ti and Mg is very low [19, 32, 53, 58]. The bonding between the AZ31 plate and the Ti plate is therefore controlled by the inter-diffusion of Ti and Mg across the Ti/AZ31 interface [65].

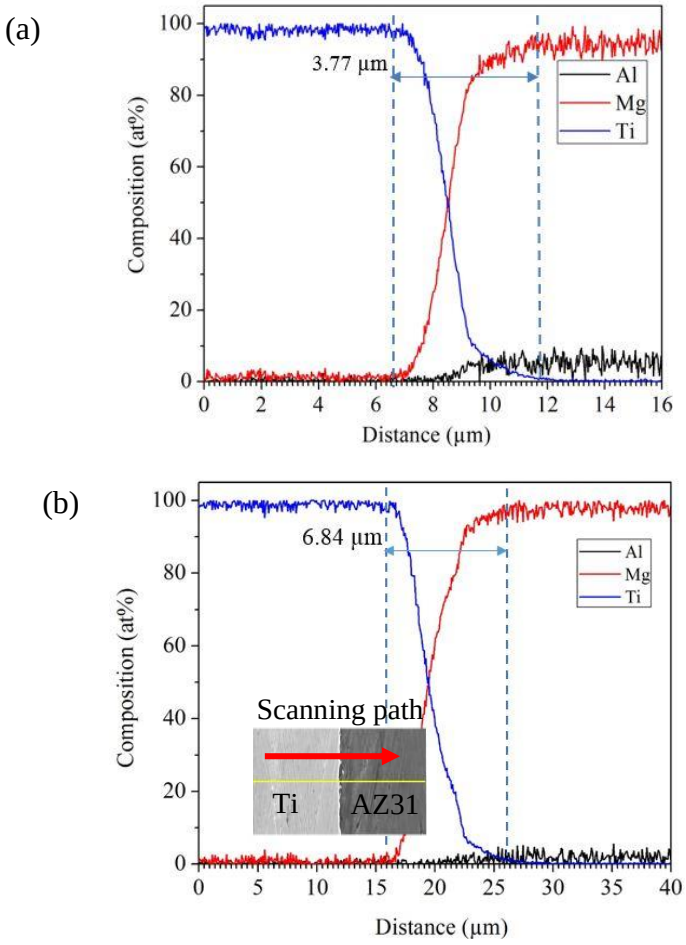

Figure 2.6 EDS line scan and EDS mapping around the Ti/AZ31 interface; (a) AS355 and (b) AN355.

Figures 2.6 shows the EDS line scan of the Ti/AZ31 interface of the AS355 and AN355 annealed at 400 °C for 12 hours, respectively. There is a small fraction of Al in the AZ31 matrix for both the AS355 and AN355, as expected, and Al diffuses across the

Ti/AZ31 interface. Also, there exists inter-diffusion of Ti and Mg across the Ti/AZ31 interface of AS355 and AN355, respectively. As discussed above, there is no intermetallic compound at the Ti/AZ31 interface. Figure 2.7 shows SEM image and EDS mapping of cross section of AN355 annealed at 400 °C for 12 hours. The inter-diffusion is driven by the concentration gradient across the interface. From figure 2.6, it is evident that the thickness of the inter-diffusion layer of the AS355 is less than that of AN355 annealed at 400 °C for 12 hours, which reveals the temperature-dependent diffusion process in accordance with diffusion being a thermally activated process. The higher the temperature, the faster is the diffusion. The EDS patterns for both the AS355 and AN355 reveal that there are no Mg in the Ti matrix and Ti in the AZ31 matrix except within the inter-diffusion layer across the Ti/AZ31 interface, which supports the occurrence of the inter-diffusion.

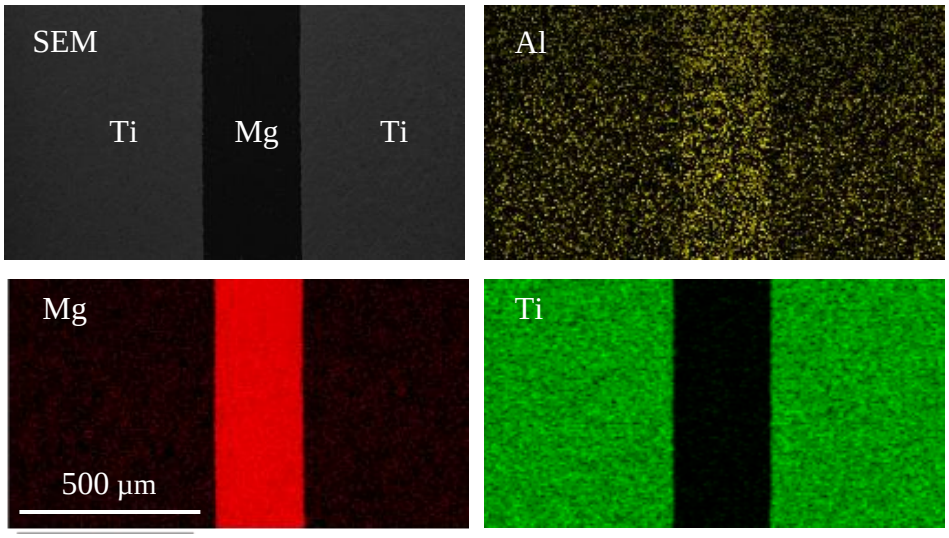

Figure 2.7 SEM image and EDS mapping of cross section of AN355 annealed at 400 °C for 12 hours.

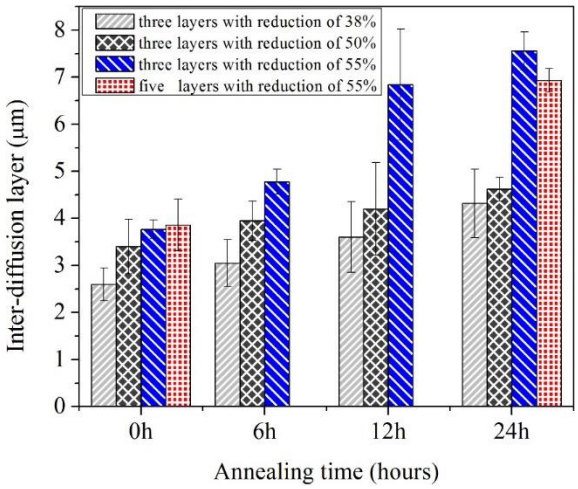

Figure 2.8 Thickness of inter-diffusion layer across the Ti/AZ31 interface.

Figure 2.8 shows the thickness variation of the inter-diffusion layer across the Ti/AZ31 interface with the annealing time for AN338, AN350, AN355, and AN550, respectively. The thickness of the inter-diffusion layer increases with increasing annealing time and the thickness reduction of the sandwiched structures due to the time-dependent diffusion and the stress-limited diffusion. The larger the plastic deformation, the higher is the dislocation density. There exists the contribution of dislocation pipe diffusion, which accelerates the diffusion of Ti and Mg across the Ti/AZ31 interface [65, 84].

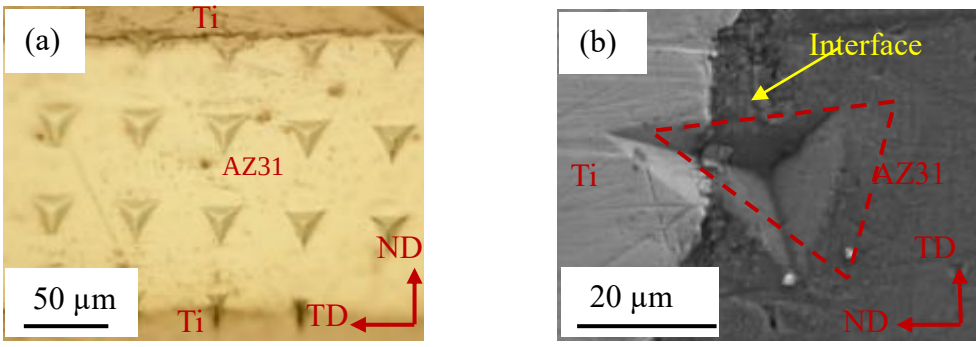

Figure 2.9 Indentation marks across AZ31 layer and Ti/AZ31 interface of AS350; (a) optical image, and (b) SEM image.

2.4.2. Mechanical behavior

Nanoindentation was performed across the Ti/AZ31 interface, using a Berkovich indenter with the maximum indentation load of 30 mN. Figure 2.9 shows the indentation

marks across the Ti layers, AZ31 layer and Ti/AZ31 interface over the surface of an AS350 sandwiched structure. For the same indentation load, the sizes of the indentation marks over the AZ31 region are larger than those near the Ti/AZ31 interface, suggesting that there is a larger resistance to the penetration of the indenter near the Ti/AZ31 interface than that on the surface of AZ31. Figure 2.10 depicts spatial distribution of the indentation hardness of the as-rolled Ti/AZ31/Ti three-layer structures and Ti/AZ31/Ti/AZ31/Ti five-layer structures. The indentation hardness of AZ31 is smaller than that of Ti, as expected. A hard interface was not observed for both sandwiched structures in accordance with the above discussion that there is no intermetallic compound formed near the Ti/AZ31 interface.

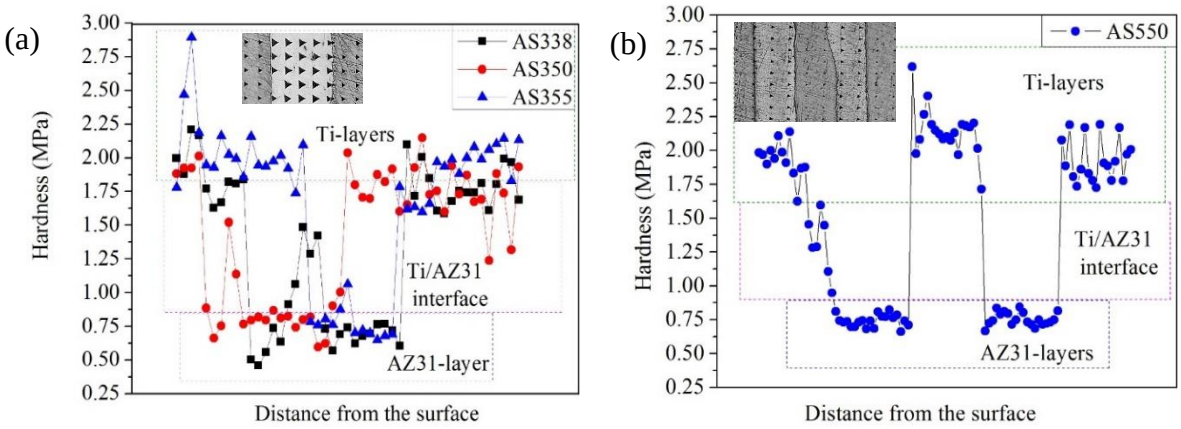

Figure 2.10 Spatial distribution of indentation hardness of the as-rolled sandwiched structures; (a) Ti/AZ31/Ti, and (b) Ti/AZ31/Ti/ AZ31/Ti.

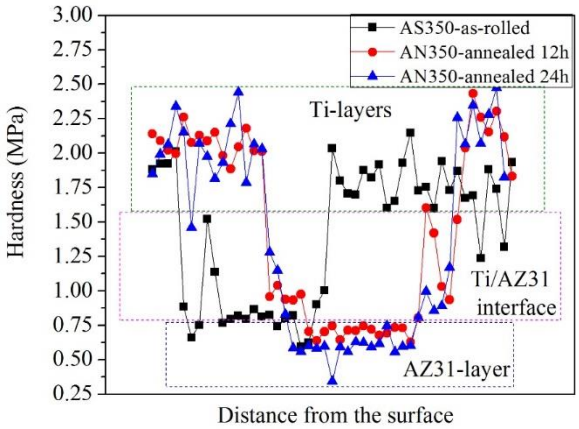

Figure 2.11 Spatial distribution of indentation hardness of the as-rolled and annealed Ti/AZ31/Ti sandwiched structures.

The indentation hardness of the AZ31 is in a range of 0.5 to 0.75 GPa for the as-rolled Ti/AZ31/Ti three-layer structures, and in a range of 0.67 to 0.8 GPa for the as-rolled Ti/AZ31/Ti/AZ31/Ti five-layer structures; the indentation hardness of the Ti is in a range of 1.5 to 2.5 GPa for the as-rolled Ti/AZ31/Ti three-layer structures, and in a range of 1.75 to 2.5 GPa for the as-rolled Ti/AZ31/Ti/AZ31/Ti five-layer structures. There exists a slight difference between the corresponding indentation hardness values, which is likely due to the difference in the thickness reduction. In general, the indentation hardness of crystalline metals increases with increasing dislocation density [33, 85, 86]. The larger the thickness reduction, the larger is the dislocation density [31, 87, 88].

Figure 2.11 shows the spatial distribution of the indentation hardness of the as-rolled and annealed Ti/AZ31/Ti three-layer structures. The AZ31 after the annealing has smaller indentation hardness than that without the annealing. The annealing of the sandwiched structures at 400 °C leads to grain growth and the decrease in dislocation density, which results in the decrease of the resistance to the penetration of the indenter into AZ31.

It is known that the bonding strength between the AZ31 plate and the Ti plate plays an important role in determining the structural application of the sandwiched structures. The double notch shear test of the sandwiched structures was performed, and the shear strength was calculated as

$$\tau = F / A \tag{1}$$

where F is the force causing the separation of the AZ31 plate from the Ti plate, and A is the contact area between the AZ31 plate and the Ti plate.

Figure 12a shows the variation of shear strength with the thickness reduction for as-rolled and annealed Ti/AZ31/Ti sandwiched structures. For the same heat-treated sandwiched structures, the bonding strength increases with the increase of the thickness reduction, and for the same sandwiched structures, the bonding strength increases with the increase in the annealing time. These trends reveal the strong effect of the inter-diffusion layer on the bonding strength of the sandwiched structures.

Pripanapong et al. [89] studied the bonding between pure Ti and Mg alloys (AZ31B, AZ61, AZ80, and AZ91) fabricated by spark plasma sintering (SPS) at high temperature

and pressure. They obtained a tensile strength of 129.8 MPa for the Ti/AZ31 interface bonded at 400 ºC for 1 hour, and suggested that the Ti_3Al intermetallic layer led to the improvement of the bonding strength between Ti/Mg. Xu et al. [29] reported the joining of the AZ31B magnesium alloy to TC4 titanium alloy by tungsten inert gas welding–brazing, and obtained the joining strengths of 32 MPa and 190 MPa with the welding currents of 40 A and 70 A, respectively. They attributed the increase of the bonding strength with the welding current to the formation of $Mg_{17}Al_{12}$ reaction layer at the interface.

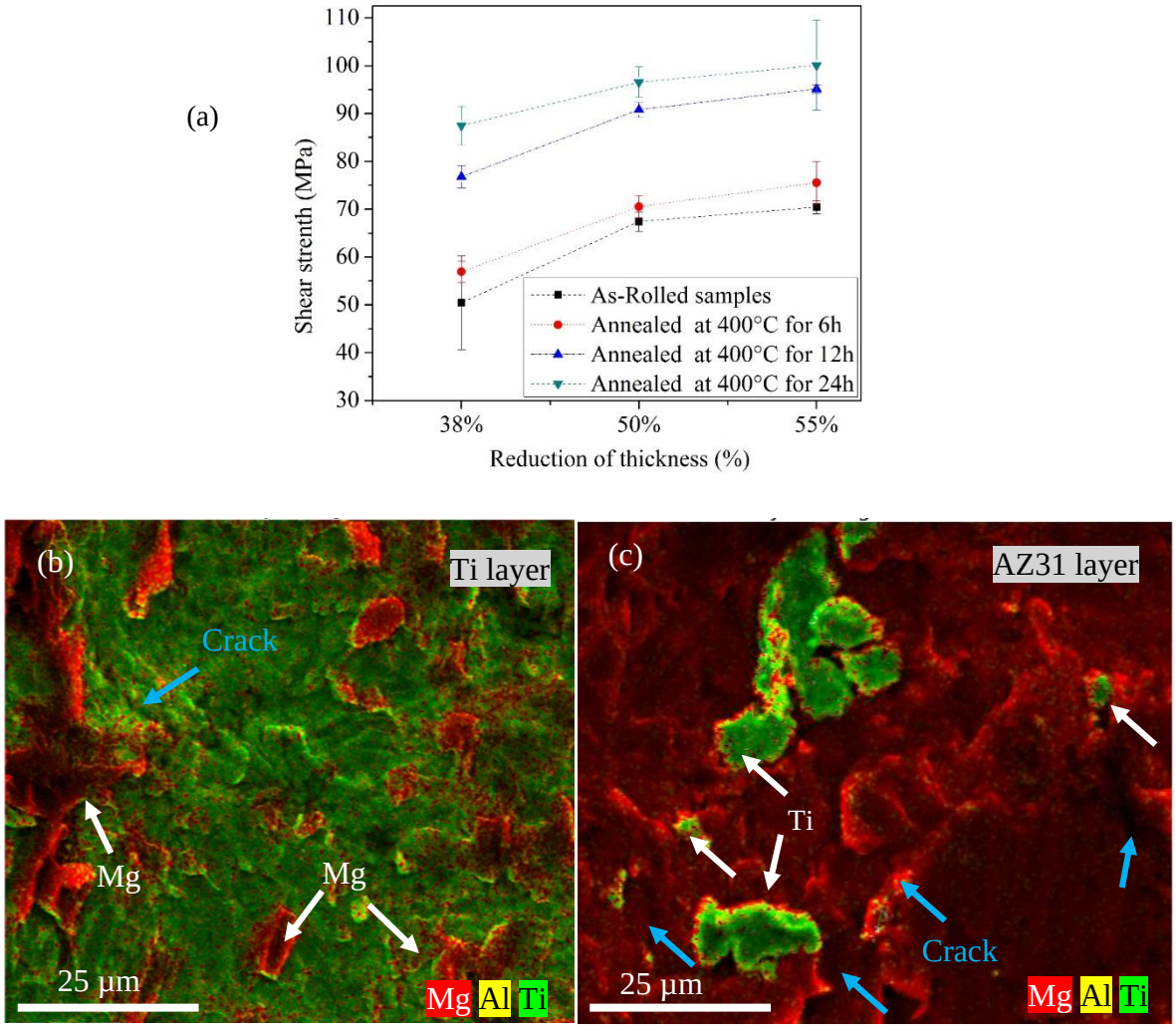

Figure 2.12 (a)Variation of shear strength with the thickness reduction for as-rolled and annealed Ti/AZ31/Ti sandwiched structures; (b) and (c) SEM-EDS mapping of fractured surface of sheared AN350 with annealing time of 12 hours for both Ti side and AZ31 layers; respectively.

Tan et al. [27, 90] used laser welded-brazed method to join Ti64 /AZ31 with AZ31 and AZ91 as filler metal. There was a Ti_3Al reaction layer at the interface for the AZ91 filler, and no intermetallic compound formed for the AZ31 filler. They reported the increase of the joint tensile-shear strength with the increase of Al in the filler and the laser power at low welding speed. The joint strengths were approximately 1000 N and 2000 N with the use of the AZ31 and AZ91 filler metal, respectively. The joint efficiencies are 25.5±5% and 47.37±1.5%, compared with AZ31.

According to figure 2.12a, the maximum bonding strength achieved is 100±9 MPa with the AN355, which is 75% of the shear strength of AZ31B. The shear results agree qualitatively with the results reported in the literature for dissimilar joining of AZ31/Ti alloys [24, 27, 29, 89-91]. It needs to point out that the failure of some of the sandwiched structures initiated either at the Ti/AZ31 interface or at the notch, but all the failures occurred at the Ti/AZ31 interface. This observation implies that the Ti/AZ31 interface is the weakest part in the sandwiched structures. Since Ti and AZ31 differ in mechanical properties at room temperature, strain concentration at the interface can occur [61]. Figure 2.12b and 2.12c show SEM-EDS analysis of the fractured surface of the sheared specimen AN350 with annealing time of 12 hours. There are residues of Ti and Mg adhered to the fracture surface of the Ti and AZ31 layers, respectively.

The fracture surface of the Ti layer exhibits mixed failure features of tear ridge and cracks (figure 2.12b), and the fracture surface of the AZ31 layer displays tear ridge and fractured Ti islands (figure 2.12 c). Accordingly, we can conclude that the good interface bonding between the Ti and AZ31 formed during single- pass hot rolling. Tensile tests of the as-rolled sandwiched structures were performed to examine the effect of the AZ31 on the tensile fracture of the sandwiched structures. Figure 2.13a shows the tensile stress- strain curves of the as-rolled samples with three and five layers, which were deformed along the RD direction at room temperature. The three-layer samples exhibit high tensile strength and low elongation, which is attributed to the strain hardening in both the Ti and AZ31 plates. The ultimate tensile strength of the five-layer structure is about 418 MPa with elongation of 15%. There are small load drops for the five-layer structures which are likely due to the cracks and voids formed in the AZ31 layers. Figure 2.13b and 2.13c show optical images of the tensile-fractured surface of the as-rolled sandwiched structures. There are

many cracks and voids formed in the AZ31 plate, since AZ31 is much weaker and less ductile than Ti. Under the action of tensile loading, the AZ31 plate likely fails first, and the Ti plates may continuously carry the load until the initiation of local failure/fracture in the Ti plates. Further increases in the tensile load can lead to the failure/fracture of the sandwiched structures. The Ti/AZ31 interface has little effect on the failure of the sandwiched structures under the action of tensile loading. There is no opening/separation observed at interfaces due to fracture.

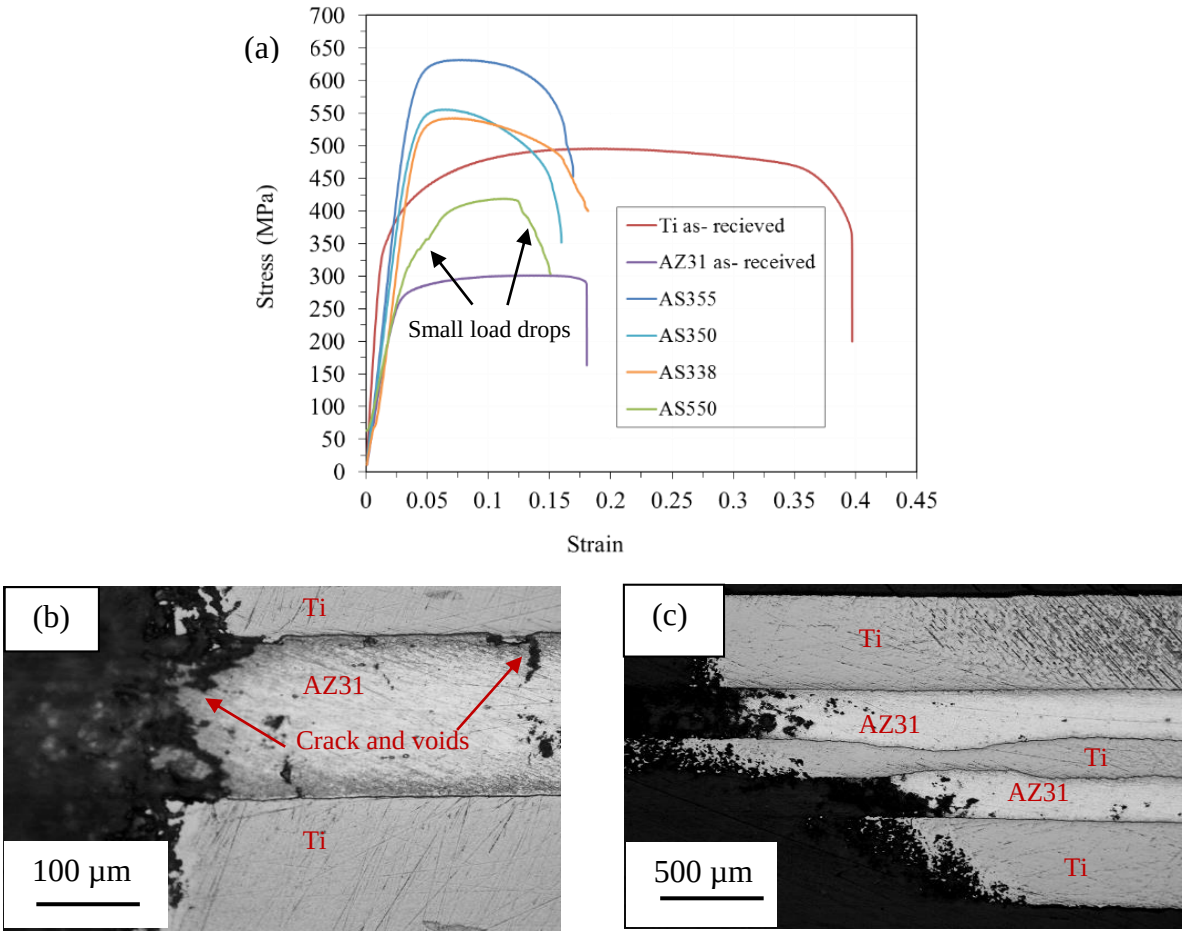

Figure 2.13 (a) Tensile stress-strain curves; (b) optical images of tensile-fractured surface of as-rolled sandwiched structures Ti/AZ31/Ti, and (c) Ti/AZ31/Ti/AZ31/Ti.

2.5. Conclusions

Ti/AZ31 multilayer structures have been successfully fabricated, using single pass hot-rolling process. The effects of the thickness reduction and annealing at 400 °C on the evolution of the microstructures and bonding strength of the multilayer structures have been investigated. Several conclusions can be drawn as follows.

1. Plastic deformation (rolling deformation) and heat treatment cannot cause formation of intermetallic compounds near the AZ31/Ti interface.
2. There exists inter-diffusion of Ti, Mg, and Al across the AZ31/Ti interface, which is driven by the concentration gradient. The plastic deformation associated with the thickness reduction enhances the inter-diffusion.
3. The thickness of the inter-diffusion layer increases with the increase of the annealing time and the thickness reduction.
4. The indentation hardness of the AZ31 plates in the sandwiched structures decreases with increasing annealing time due to the grain growth and the decrease in the dislocation density.
5. For the same heat-treated sandwiched structures, the bonding strength increases with the increase of the thickness reduction; for the same sandwiched structures, the bonding strength increases with the increase in the annealing time and temperature.
6. Under the action of tensile loading, the AZ31 plate fails first in the sandwiched structures.

CHAPTER 3. Three layered Titanium Clad-AZ31 Magnesium alloy Sheet by Single-Pass Hot-Rolling

3.1. Summary

In the present study, three-layered Ti/AZ31/Ti clad sheet was produced by single-pass hot rolling. Metallurgical bonding between Ti and AZ31 was successfully achieved with a 38% (sheet I) and 50% (sheet II) reduction of thickness. The microstructure and mechanical behavior were analyzed using optical microscopy (OM), X-ray diffraction (XRD), scanning electron microscopy (SEM), energy dispersive spectroscopy (EDS), electron backscatter diffraction (EBSD), nanoindentation, and tensile tests. The AZ31 layer in sheets I and II exhibited microstructures of shear bands and tensile twins$\{10\bar{1}2\}\langle 10\bar{1}1\rangle$. The shear bands acted as local strain concentration areas which led to the failure of the clad sheets with limited elongation. Heat treatment caused changes in the microstructure and mechanical properties of clad sheets due to static recrystallization (SRX) on twins and shear bands in the AZ31 layer. Recrystallized grains usually randomize the texture which weaken the strong deformed (0001) basal texture. Twins served as nucleation sites for grain growth during SRX. Tensile tests at room temperature showed significantly improved ductility of the clad sheets after heat treatment at 400°C for 12h. The results showed that the mechanical properties of clad sheet II is better than clad sheet I: The clad sheet II shows elongation of 13% and 35% along the rolling direction (RD) for as-rolled and annealed clad sheet, respectively whereas the clad sheet I shows elongation of 10% and 22% along RD for as-rolled and annealed clad sheet, respectively.

3.2. Introduction

Magnesium composite materials have been produced with various materials such as Al[87], Zn[62, 64], Ni[65] and Cu[92] to improve its mechanical and heat conductivity properties. Also, Mg alloys have been clad by various type of materials such as aluminum[67, 93], steel[94], and titanium [95, 96]. Metal-metal composite materials were fabricated by bonding multilayers, which has advantages of their mechanical properties. Kawamoto et al. [32] studied strain transfer through the Mg/Ti interface using a crystallographic method. They suggested that dispersion of Ti particles in the Mg-based composite can improve the deformability of Mg by strain transfer through the Mg/Ti interface. Clad sheets component are minimized Mg alloys weakness and provide a new application area. The ductile metal component can attribute to failure prevention by

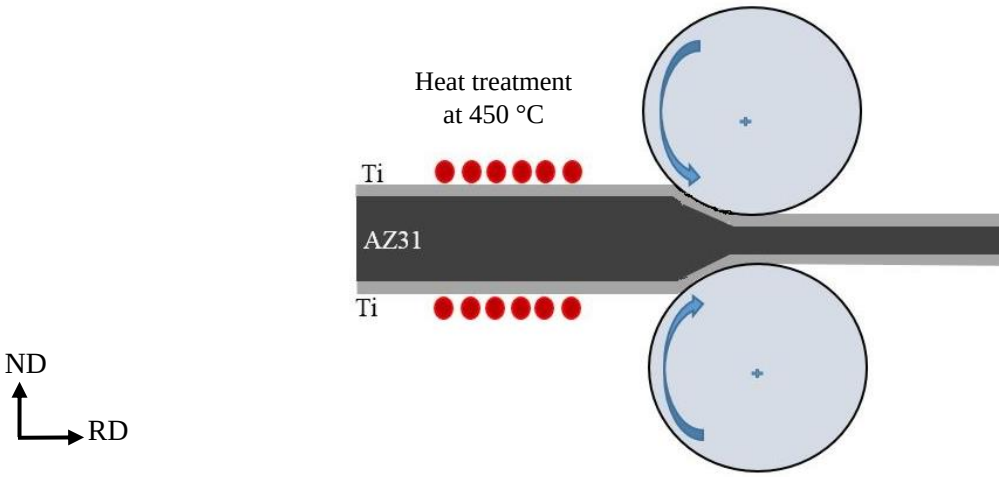

Figure 3.1 Illustration of the fabrication of Ti/AZ31 clad sheet.

necking less ductile phase, which will be necking at the higher strain that depends on the their bonding properties [94]. Therefore, it is important to obtain a suitable method to fabricate Ti/AZ31/Ti Clad sheets. There are many processes to manufacture Mg multilayer composite materials such as accumulative roll bonding (ARB) [87, 97], diffusion bonding (DB)[59, 98], brazing and friction stir welding[24-29, 99], and roll bonding(RB)[31, 67]. The roll bonding process has been reported as a conventional method to fabricate and bond clad sheet by cold or warm rolling[9].

In this work, the Ti/AZ31/Ti clad sheets were fabricated by single-pass hot rolling. AZ31 Mg alloy has relatively poor tensile ductility; therefore, utilizing advantages of both

Mg and Ti may improve its performance in structural applications. Moreover, the clad sheet gains the corrosion resistance equivalent to that of Ti alloys. The microstructure and mechanical of the clad sheets were investigated, and the Ti/ AZ31 interface texture orientation was studied as well. The relation between texture and mechanical properties at the interface were discussed.

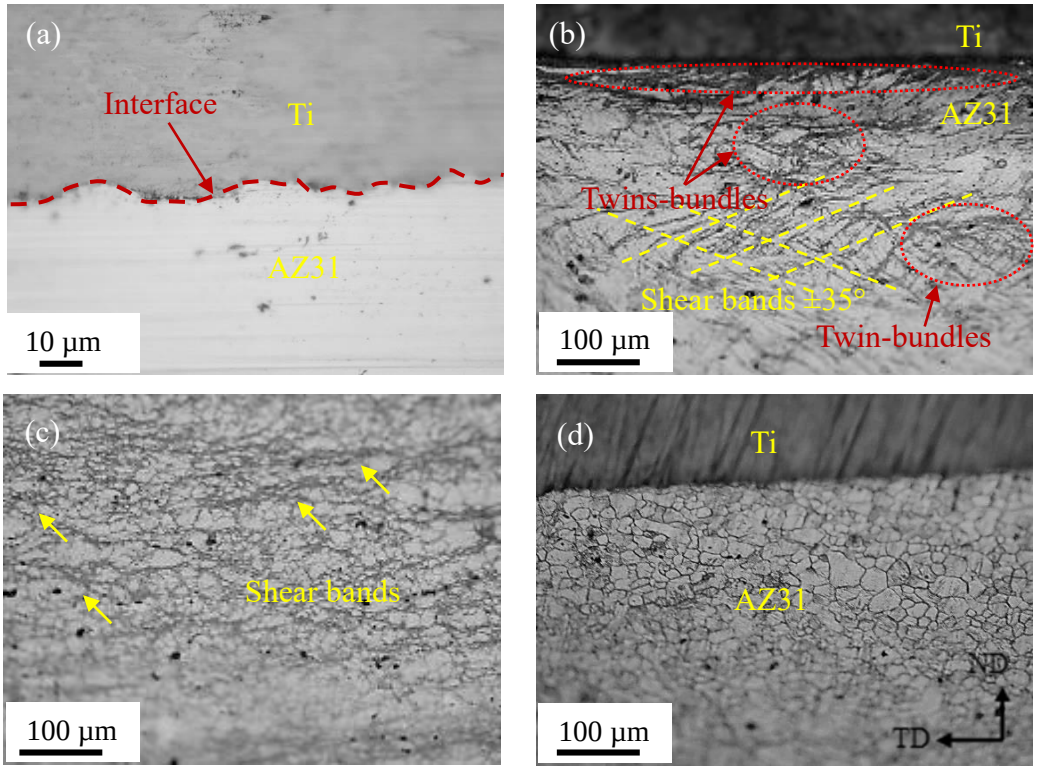

Figure 3.2 OM images of the Ti/AZ31 interfaces. (a-b)as-rolled clad sheet II; (c) AZ31 hot rolled with 50% reduction;(d) annealed clad sheet II.

3.3. Experimental procedures

The materials were used commercially pure Ti grade 2 (Ulbricht) (C 0.012, N 0.005, Fe 0.09, and balance Ti wt. %), and AZ31B magnesium alloy (Magnesium Electron) (Al 3.06, Zn 1.04, Mn 0.4, Cu 0.001, Si 0.004, Fe 0.0035, and balance Mg wt. %). Three layered Ti/AZ31/Ti clad sheets were produced by single-pass hot rolling. Then, the AZ31 and Ti sheets were cut into rectangular pieces of 75mm×50mm×3.06±0.10mm and 75mm×50mm×0.2±0.02mm, respectively. Sandwiched samples were heated in a furnace at 450°C for 15 min and then fed through a rolling mill with 38% and 50% reduction of thickness in a single pass, as shown in figure 3.1. The samples were designated as the clad sheet I and II for reduction of thickness 38% and 50% reduction of thickness, respectively. The AZ31 and Ti plates were decreased by an ultrasound bath using acetone for 15 min and roughed by using a rotating stainless steel wire brush before assembly. Sample surface preparations were carried out to achieve a good bonding strength between layers. The degreasing and surface roughing steps were required to avoid sheets sliding to obtain an excellent bonding strength between layers[11]. The roller diameter was 101.6 mm, and the rotational speed of the roller was 24 revolutions per minute. Heat treatment was carried out in an argon atmosphere furnace at 400°C for 12 h.

The Ti-clad Mg alloy sheets were observed along the (TD) plane using optical microscopy (OM), scanning electron microscopy (SEM), X-ray diffraction (XRD), energy dispersive X-ray (EDX), and electron backscatter diffraction (EBSD) patterns. Samples were prepeared using silicon carbide abrasive papers of grit size 320, 1200, and 2000. Preparations of EBSD samples were difficult because the Ti and AZ31 required different solutions and methods for surface polishing. Therefore, the polishing was performed layer by layer. Suter's electrochemical polisher was employed to polish AZ31 layer; an electrolyte (methanol: ethanol: nitric acid = 10:10:3) at room temperature and voltage of 27-30V. Ti layers were chemically polished using (nitric acid: hydrofluoric acid =1:1) to obtain high-quality EBSD patterns[49, 100]. EBSD was performed on the as-rolled and annealed samples using FEI (Helios NanoLab 660) equipped with electron backscatter diffraction (EBSD) system. The EBSD data were analyzed using HKL channel 5 software. The mechanical behavior was evaluated by nanoindentation (Agilent G200), and tensile-

test. The tensile test samples were cut parallel to both (RD) and (TD) directions. The tensile strength test was performed at room temperature using an Instron (model 3345) machine with an initial strain rate of 0.5 mm/min. The tensile test spacemen were machined by an electric discharge machine (EDM) and have a gauge length of 10 mm and 2mm width, as shown in figure 2.2b [76].

3.4. Results and discussion

3.4.1. Microstructural characterization

Ti/AZ31/Ti clad sheets were fabricated with a thickness reduction of 38% and 50% (sheet I and II). Optical microscopy (OM) observations appear without any visible defects such as pores, voids, cracks, interface debonding, or delamination (figure 3.2a). High plastic deformation was occurred at the interface which causes a zig-zag mode at the interface due to different flow stress

of the Ti and AZ31. The interfacial zig-zag mode is a favor geometric shape that enhances the bonding strength between layers [9, 11, 101].

It is suggested that plastic deformation and friction could increase the temperature at the interface. This led to softening of both the Ti and the AZ31, and increasing the plastic strain as well as the migration of atoms across the AZ31/Ti interfaces[31, 65]. Figure 3.2b shows microstructure of the as-rolled clad sheet which is observed as a mixed microstructure of parallel shear bands inclined by ±35° and tensile twins $\{10\bar{1}2\}\langle 10\bar{1}1\rangle$ in areas far from the interface of the Ti/AZ31 layer. While ultrafine dynamic recrystallization (DRX) grains were found close to the Ti/AZ31 interface, a high friction interaction between both layers occurs during the rolling; that means the main deformation mechanisms during hot rolling were controlled by basal $\langle a\rangle$ slip system ($\{0001\}\langle 11\bar{2}0\rangle$) and twining $\{11\bar{2}0\}$[102, 103]. Figure 3.2c illustrates microstructure of the as-rolled AZ31 sheet with reduction of thickness 50%. DRX occurred during the hot rolling, which produced homogenous equiaxed fine grains with small fractions of shear bands, as previously reported [79, 104-107].

Compared with the as-rolled clad sheet microstructure, the clad sheet samples were deformed under the high strain rate along the normal direction (ND) which generated the shear bands (many fine DRX grains) and twin microstructures[108]. The shear bands act as local strain concentration areas which cause to failure the clad sheet with lower elogation

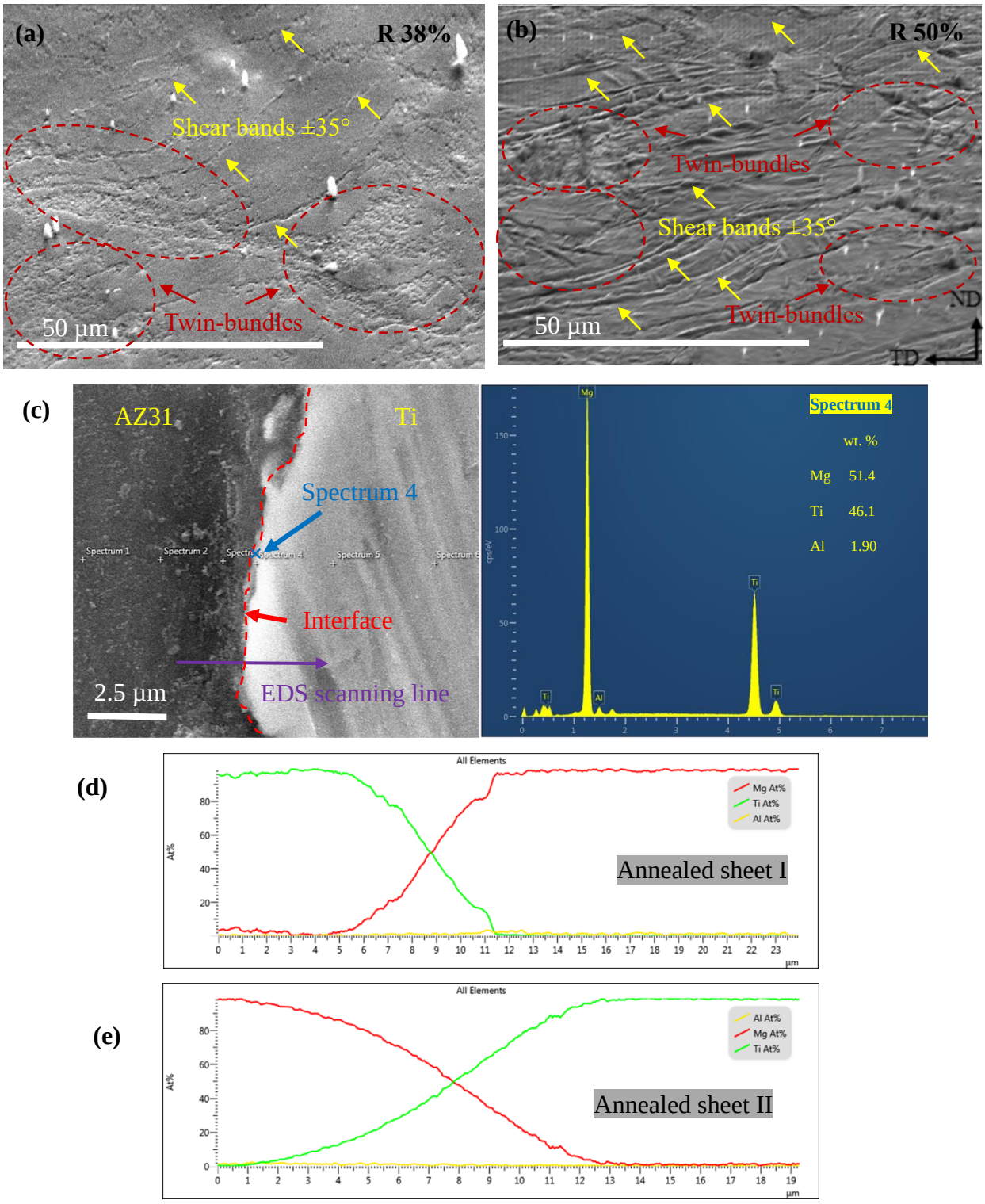

Figure 3.3 Shows SEM images: (a) sheet I as-rolled AZ31 layer;(b) sheet II as-rolled AZ31 ;(c) point scanning of annealed sheet II interface;(d-e) line scanning of annealed sheet I and II interface.

[109-111]. Annealing of the clad sheets can improve the ductility of Athe Z31 layer and the bonding strength between theTi and AZ31[95]. Further annealing, the microstructures

of the AZ31 layer showed uniformm equiaxed recrystallized grains, as shown in figure 3.2d. Optical microscopy cannot provide high magnication views of shear bands. SEM of shear bands are shown in figure 3.3a-b. The shear bands′ density were increased with the increase of the reduction strain from 38% to 50% during the hot rolling process. The shear band form during high strain process is associated with DRX. During hot rolling, the normal strain and high temperature cause softening and local strain. Under this condition, dislocation density become more concentrated which leads to the formation of the shear bands [42, 83, 112]. The SEM image of annealed sheet II shows no visible intermetallic compound; EDS point analysis provides further support as shown in figure 3.3c. In addition, EDS line scan of the annealed sheet I and II are given in figure 3.3d, which show the effect of reduction strain and heat treatment. A thin diffusion reaction layer observed at the Ti/AZ31 interfacial zone. This resulted in the diffusion of atoms which occurred despite the short rolling time. Since a Ti-Mg binary phase diagram shows tiny mutual solid solubility, they do not react with each other; no exist of intermetallic phase[32].

Therefore, the bonding between Ti and Mg may occur by interdiffusion or intermixing at an atomic level [58, 96, 113]. The bonding strength is a function of surface roughness and post heat treatment. It has been reported that severe plastic deformation can produce significant mixing, such as ball milled powders and roll bonding [34, 114].

The results showed that no enrichment of “Al element” found across the interface of the Ti/AZ31 after annealing heat treatment (figure 3.3c). Thus, there is no possibility of forming of brittle intermetallic compounds between Ti-Al and Mg-Al at the interfaces. Figure 3.4 showed XRD patterns of Ti, AZ31, as-rolled and annealed clad sheet II. The AZ31 presents strong XRD diffraction peak (0002) basal plane texture.

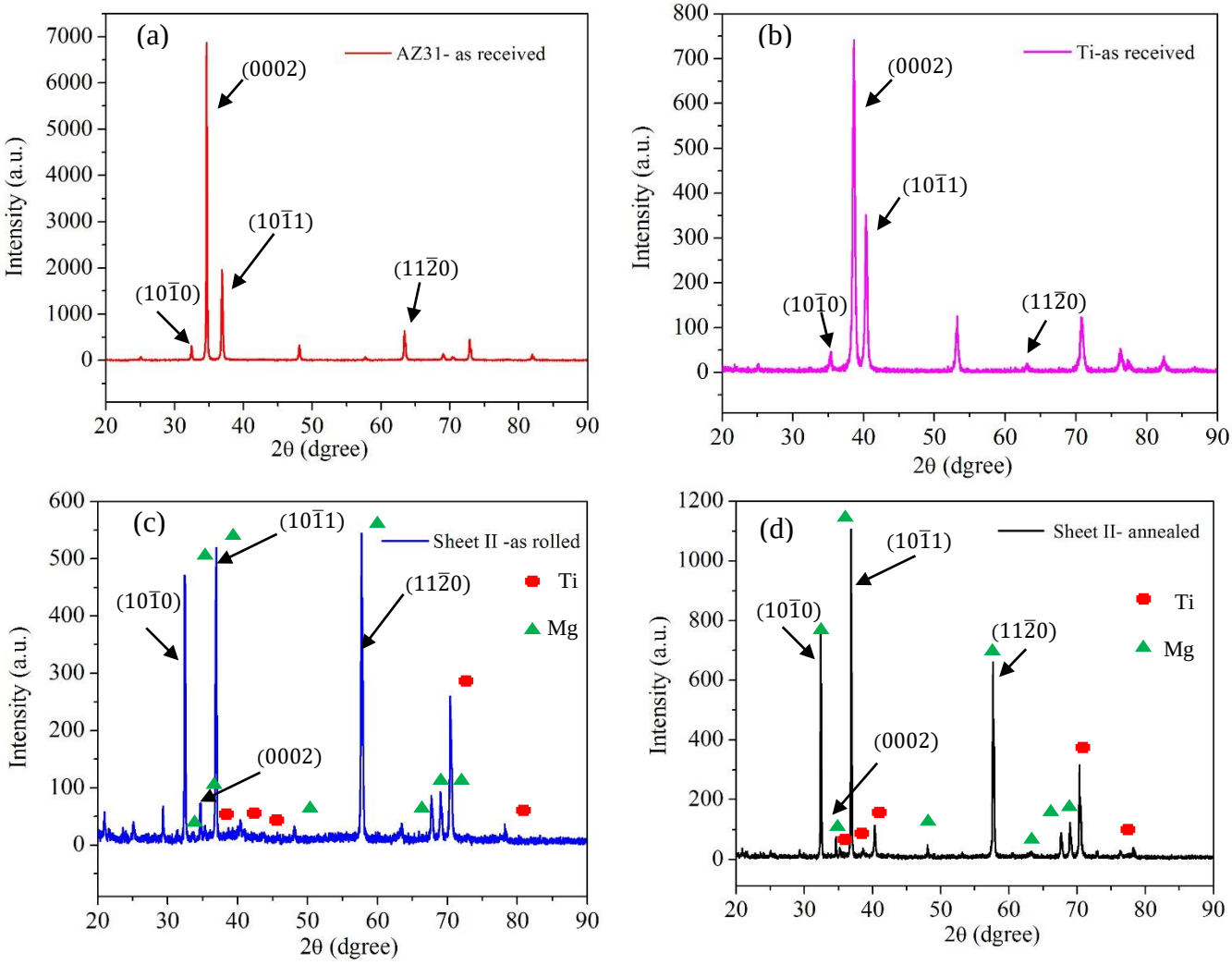

Figure 3.4 Shows X-ray diffraction patterns of (a) AZ31-as received;(b) Ti-as received;(c) sheet II-as rolled; (d) sheet II-annealed.

Furthermore, there is no evidence for intermetallic compounds obtained from Ti, AZ31, as-rolled and annealed sheet II diffraction patterns, as shown in figure 3.4c and figure 3.4d.

After hot rolling, (10$\bar{1}$1), (10$\bar{1}$0), and (11$\bar{2}$0) show strong XRD diffraction peak while (0002) shows weak diffraction peak which means the material is exhibiting texture evaluation. The peak intensity should be attributed to the relative number crystal planes parallel to the surface [81, 115]. In addition, the reorientation of lattice had occurred by twinning that lead to weak the strong basal texture. Therefore, the strong peak

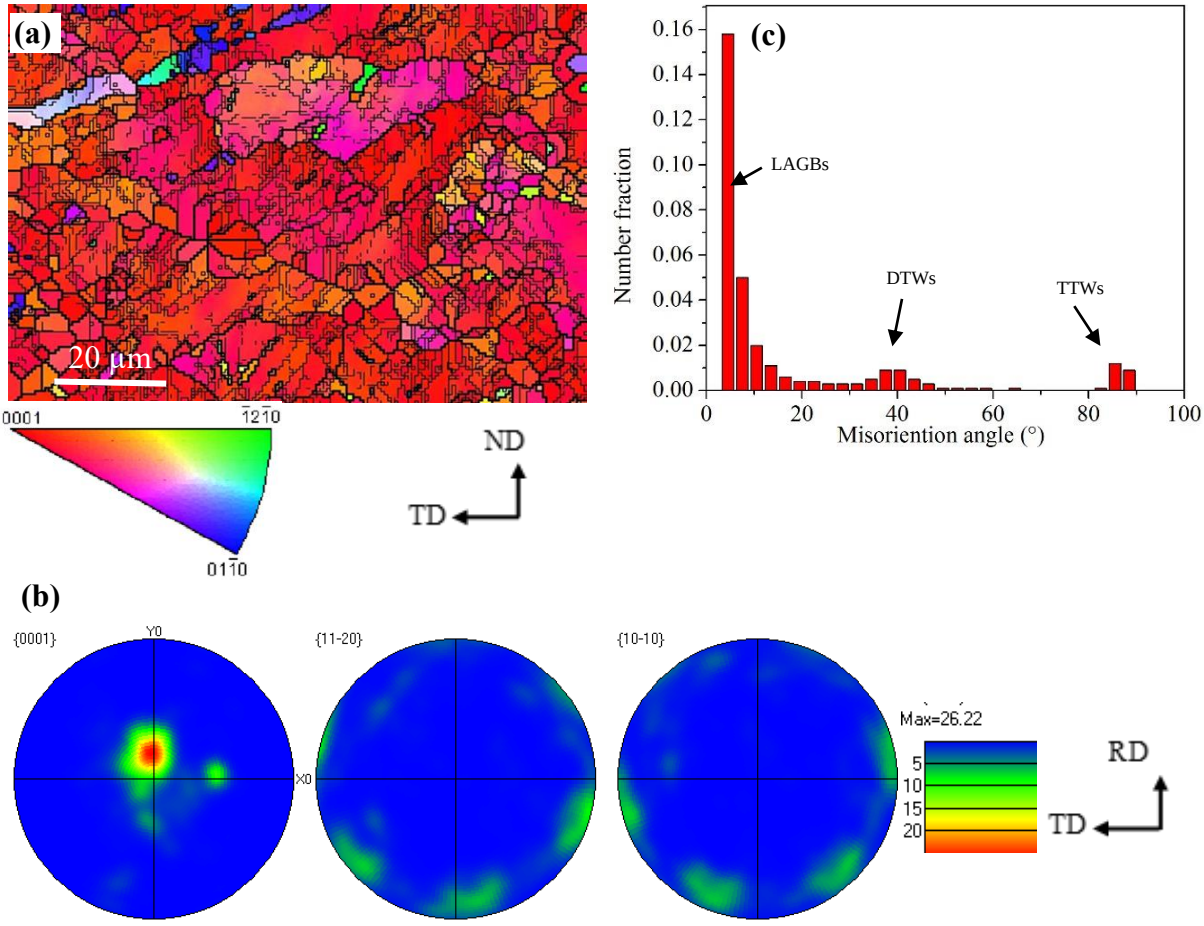

Figure 3.5 Shows AZ31 layer of the as-rolled sheet I. (a) EBSD IPF image of the AZ31 layer; (b) pole figures; (c) distributions of misorientation angle.

corresponding to the higher crystal plane. After annealing, the strong peaks remained same, with the intensity increasing obviously.

3.4.2. Texture Evolution of clad sheets

3.4.2.1. The AZ31 Layer

The AZ31 layer is the largest substantial component of the clad sheet, and its texture significantly affects the mechanical properties. EBSD analysis was used to investigate the texture of the AZ31 layer before and after annealing heat treatment. Figure 3.5 shows the EBSD inverse pole figure (IPF) map, pole figures (PF), and distributions of misorientation angle; these were obtained from areas far from the AZ31/Ti interface of the as-rolled sheet I (central part of the AZ31 layer). Figure 3.5a shows IPF map and grain boundaries (GBs) which are a columnar grains structure containing deformed and fine substructure grains

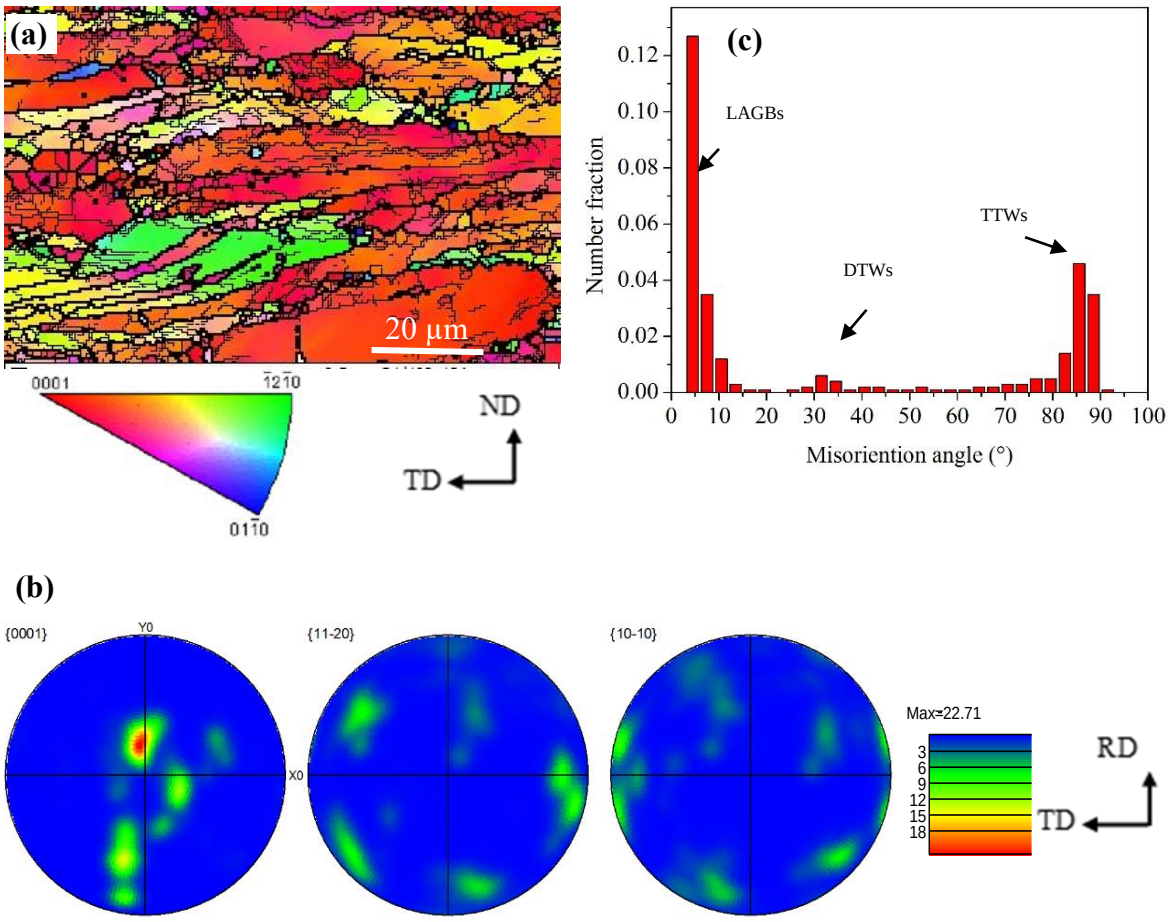

Figure 3.6 Shows AZ31 layer of as-rolled sheet II. (a) EBSD IPF image of the AZ31 layer; (b) pole figures; (c) distributions of misorientation angle.

with average grain size 6.36 µm. The average grain size calculated from IPF maps. The different color in the EBSD map means different crystal orientation. The fine grains are found as resulting of the DRX during hot rolling, as discussed in the previous section. The as-rolled AZ31 layer developed strong basal crystallographic textures. The maximum pole intensity of the (0001) PF was 26.22 which tilted at 14° away from normal direction ND toward RD, as shown in figure 3.5b. It has been reported that deformation by the basal $\langle a \rangle$ slip system ($\{0001\}\langle 11\bar{2}0\rangle$) and twining $\{11\bar{2}0\}$ can effect texture orientation by rotation of many grains from c-axes to the RD [31, 103, 116].

Various terms used to describe the distribution of misorientation angle such as low angle grain boundaries (LAGBs; misorientation angle <15°); high angle grain boundaries (HAGBs; misorientation angle >15°); double twins (DTWs; $\{10\bar{1}1\}-$

$\{10\bar{1}2\}\langle 10\bar{2}0\rangle$) around 35°; compression twins (CTWs; $\{10\bar{1}1\}\langle 10\bar{2}0\rangle$) around 56°;

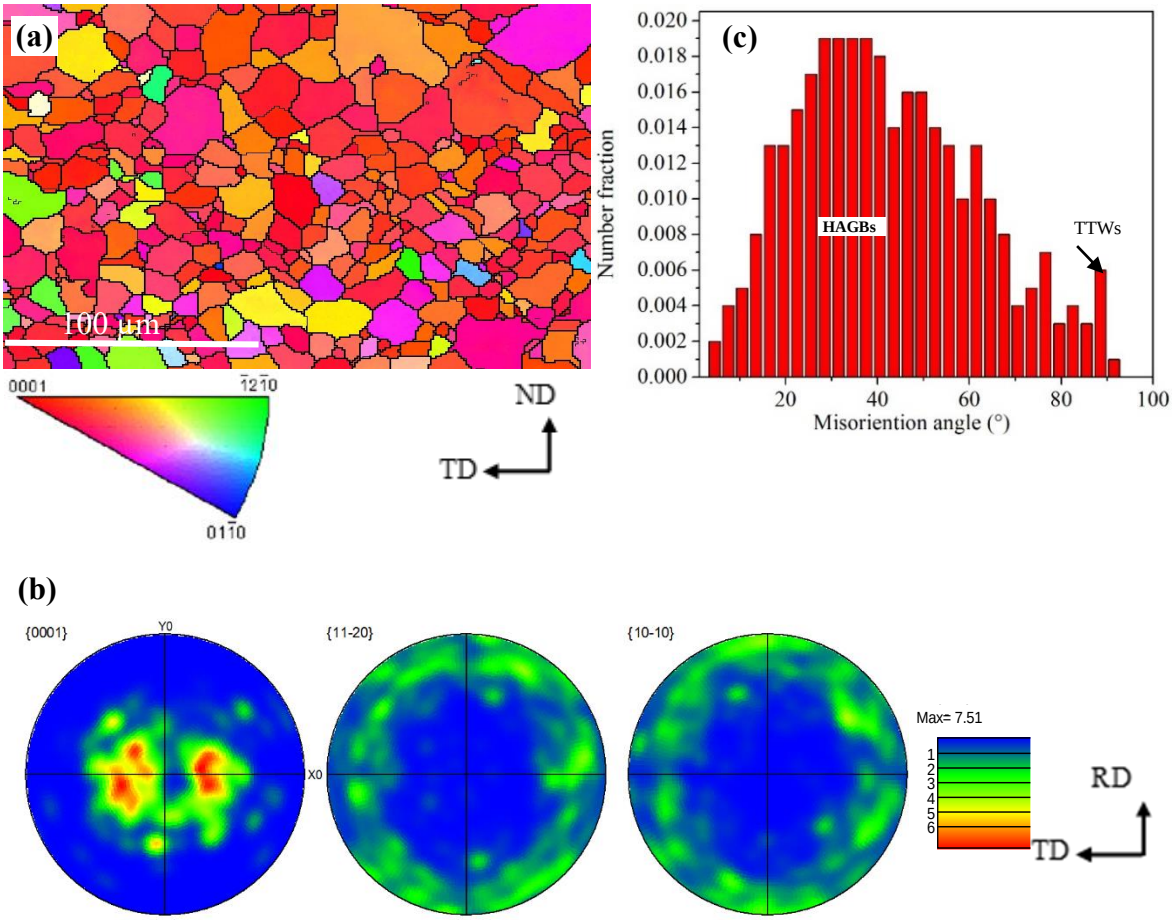

Figure 3.7 Shows middle of the AZ31 layer for the annealed sheet I. (a) IPF figure of the AZ31 layer; (b) pole figures; (c) distributions of misorientation angle.

tensile twins (TTWs; $\{10\bar{1}2\}\langle 10\bar{1}1\rangle$) around 86° [40, 41]. The distributions of misorientation angle are dominated by a large peak around 8° (LAGBs), and there are two small peaks around 40° (DTWs) and 86° (TTWs), as shown in figure 3.5c. Therefore, it is evidence that twins (TWs) and LAGBs cause the formation of shear bands during hot-rolling[83, 112].

Tan.et al. [117] have demonstrated that rolled AZ31 at a temperature ranging between 200°C to 400°C with high strain level (60-80%) led to grains refinement. The IPF map contains non-indexed areas (TTWs) which subjected high local strain (sheared during high deformation) [118]. Guan et al.[82] reported that deformed grains boundaries, deformed twins, shear bands, and second phase particles are the main contribution to nucleation sites during recrystallization of Mg alloys.

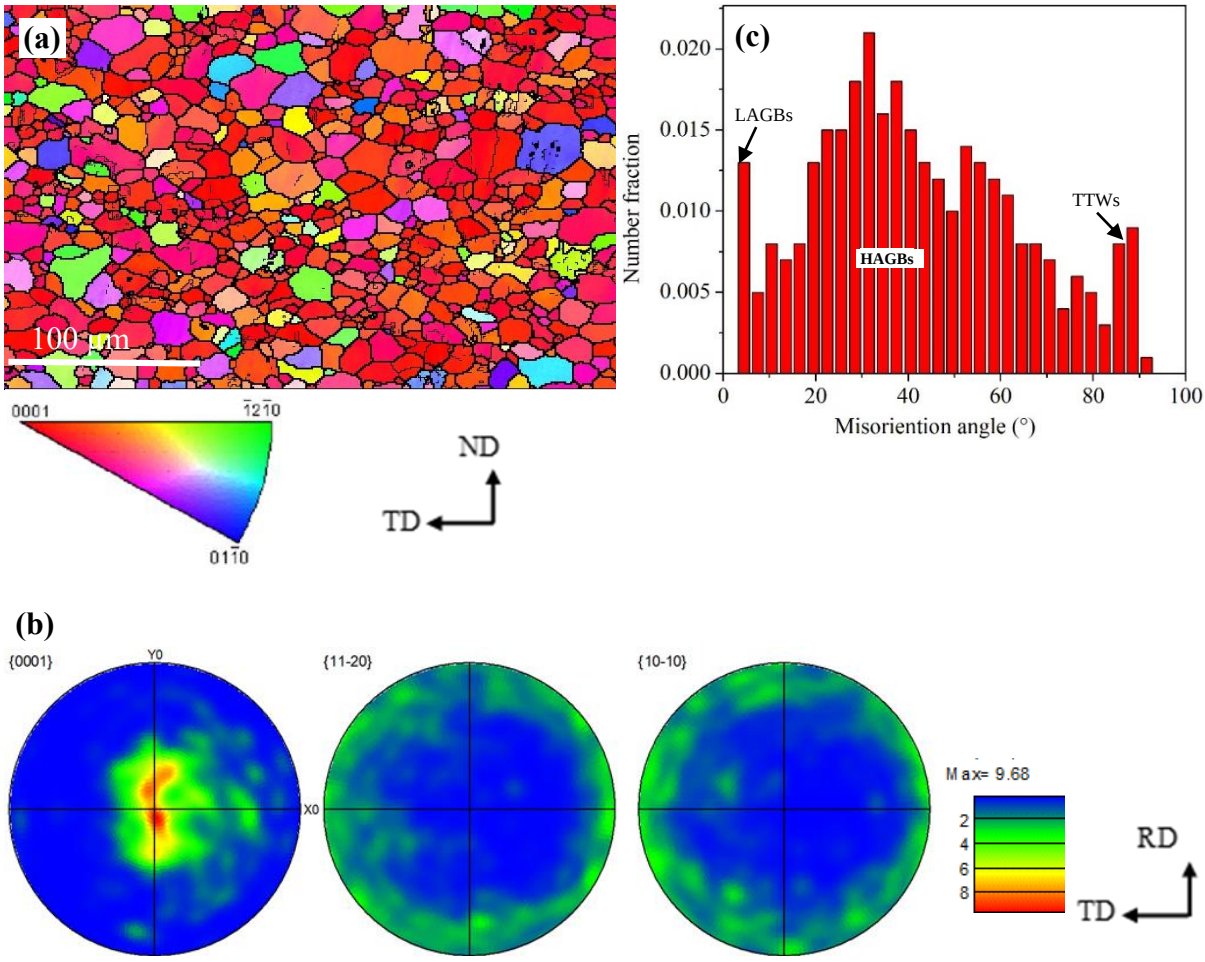

Figure 3.8 Shows the middle of the AZ31 layer for annealed sheet II. (a) IPF figure of the AZ31 layer; (b) (0001) pole figure; (c) distributions of misorientation angle.

The sheet II was subjected to high strain (50% reduction) during the hot rolling process. Figure 3.6a shows the IF map of the as-rolled AZ31 layer which also reveals columnar grain structure (deformed and fine substructure grains) with average grain size was 4.4μm. The average grain size of the as-rolled AZ31layer decreases with the increase of the reduction strain. Figure 3.6b shows a strong (0001) with a maximum index of 22.71 which is tilted by 30° away from the normal direction ND toward RD. The texture intensity of sheet II is lower than the intensity of sheet I which is related to the amount of strain. Hot-rolled AZ31usually exhibit (0001) pole figure orientation distribution around ND wider in RD than in TD [119]. In addition, the pyramidal slip system $\langle c+a\rangle$ ($\{11\bar{2}2\}\langle 11\bar{2}3\rangle$) is responsible for splitting of the basal pole towards the RD for the hot

rolled AZ31 [104, 119, 120]. Figure 3.6c shows distributions of misorientation angle which consist of two main peaks with rang ~5°-8° and ~85°-90°. The first beak represents LAGBs while the second peak represents HAGBs (TTWs; $\{10\bar{1}2\}\langle 10\bar{1}1\rangle$). In addition, there is small fraction of double twins (DTWs; $\{10\bar{1}1\}-\{10\bar{1}2\}\langle 10\bar{2}0\rangle$) around 35° [40, 41]. The number of CTWs $\{10\bar{1}1\}\langle 10\bar{2}0\rangle$ are limited because of it transform to DTWs, $\{10\bar{1}1\}-\{10\bar{1}2\}\langle 10\bar{2}0\rangle$[118, 121]. It has been reported that the DTWs reduce ductility of Mg alloys and led to shear failure at low strain[122]. Hot rolling is associated with a large strain deformation led to reduce the critical resolved shear stress (CRSS) of pyramidal $\langle c+a\rangle$ slip system and non-basal slip system may become activate [104, 123, 124]. DRX has been taken place during hot rolling for both sheet I and sheet II, which involve to convert the LAGBs to HAGBs [117].

During the annealing heat treatment, recovery, recrystallization, and grain growth have been taken place with different rates on different regions of the AZ31 layer which was depending on their local stored energies. The microstructure evaluation after annealing treatment at 400 °C for 12h shows that there is no the presence of any elongated grains which indicate that the microstructure has been recrystallized and grown to some extent. Figure 3.6 shows IPF map, (0001) PF, and distributions of misorientation angle in areas far from the interface AZ31/Ti of the sheet I. Equiaxed coarse grains are formed after the heat treatment. The average grain size was 9.28 μm, as shown in figure 3.7a. The deformed grains and non-indexed areas with higher internal stored energy were recrystallized. The (0001) PF shows double-peak basal pole intensity which is tilted about ±25° from the ND towards the TD, as shown in figure 3.7b. The basal texture intensity was significantly reduced from 26.22 to 7.51 [31, 104].

The annealing process has the most significant enhancement of AZ31layer texture, which was weakening the severely deformed grains of texture component [82, 104, 125]. Qiao et al.[102] and Nie et al.[31] have reported the mechanism of LAGBs transformation into HAGBs by migration of the grain boundaries of the sub-grains. Figure 3.7c shows distributions of a misorientation angle which is exhibited by a random distribution of grain boundaries with the domination of HAGBs. This indicates that the static recrystallization process (SRX) had taken place during annealing heat treatment [81, 125].

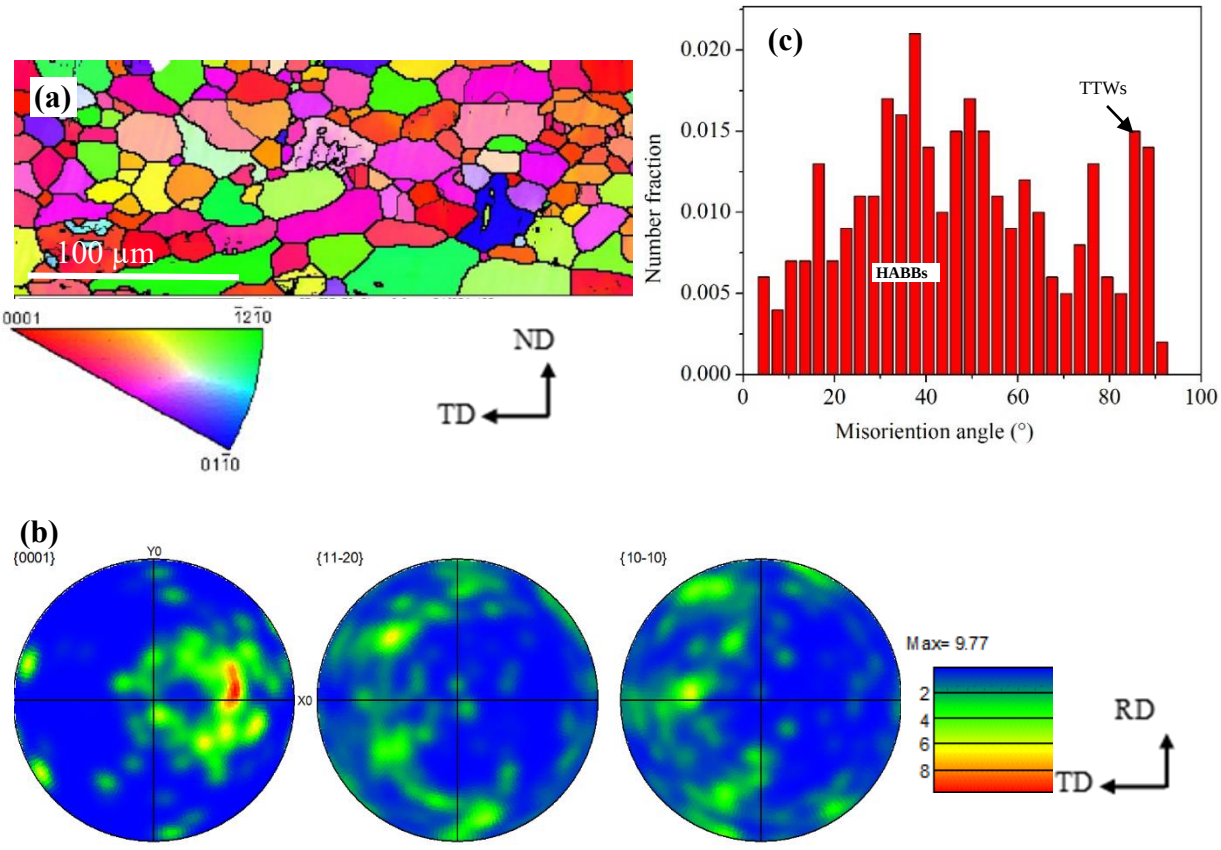

Figure 3.9 Shows annealed sheet II for AZ31 layer close to interface; (a) IPF figure of the AZ31 layer; (b) (0001) pole figure; (c) large deformed grains, substructure grains, and recrystallization grains in the IPF figure; (d) distributions of misorientation angle.

During the annealing process, the stored energy from plastic deformation could be the driving force for SRX [81, 126].

Figure 3.8 shows IPF map, (0001) PF, and distributions of misorientation angle in areas far from the AZ31/Ti interface after annealing of the sheet II. Figure 3.8a shows IPF map which reveals recrystallized texture with an average grain size of 8.97 µm. Figure 3.8b shows (0001) PF a significant change in pole intensity distribution comparing with as-rolled sheet II. After the annealing treatment, the basal pole intensity decreased from 22.71 to 9.68. The result shows that single pole intensity maxima splitting along the RD, and a wide pole intensity distribution inclined -5° from the ND to word RD. Hong-Fei et al.[103] have reported that the most recrystallized grains tilt away from the ND depend on the degree of deformation. A sample with deformation higher than 30% shows double pole

tilts toward TD while a sample with high plastic deformation shows tilting toward RD. The basal plan pole tilting will affect the mechanical anisotropy along (RD) and (TD) during tension test at room temperature. The annealing heat treatment is effective in the weakening of the basal texture intensity of as-rolled clad sheet due to SRX. Figure 3.8c shows a wide misorientation distribution histogram in the range of the angle between 20° and 60° (HAGBs) which confirms the SRX.

Figure 3.9 shows IPF map, (0001) PF, and distributions of misorientation angles in areas close to AZ31/Ti interface after annealing of the sheet II. Coarse grains are formed at the AZ31 layer close to the interface after annealing heat treatment. The average grain size was 13.03 μm, as shown in figure 3.9a. Figure 3.9b shows double-peak (0001) PF with intensity of 9.77 which is tilted about 50° from the ND toward TD. Figure 3.9c shows a misorientation distribution of grain boundaries which exhibits two strong beaks at ~35° and ~85°. The first beak represents the recrystallized grains which support the above discussion the increase in grain boundary misorientation and the conversion of LAGBs into HAGBs. Another peak represents the probability of the TTWs $\{10\bar{1}2\}\langle 10\bar{1}1\rangle$ existing [93]. The grain sizes of AZ31layer close to the interface are larger than those in the areas far from the interface. With high friction at the interface, high deformation energy is stored, which provides a larger driving force for recrystallization. It can be observed that the microstructure, after annealing heat treatment, becomes and HAGBs and with small amounts of twins at the interface (see the supplementary Fig.3.S1). The twins and twin-grain boundary (GB) lead the activation of nucleation which leads to form a new grains DTWs ($\{10\bar{1}1\}-\{10\bar{1}2\}\langle 10\bar{2}0\rangle$) and CTWs ($\{10\bar{1}1\}\langle 10\bar{2}0\rangle$). Chao et al.[126]. suggested that high dislocation densities were preferential nucleation sites during SRX of the AZ31 Mg alloy. Their observation depends on the modeling of fine grains and twins texture before and after annealing heat treatments. As a result of annealing heat treatment, SRX causes the weakening of AZ31layer the basal texture which it is not eliminated [82, 127]. Kawamoto et al.[32] studied Mg/Ti interface crystal orientation using EBSD (see the supplementary Fig. S2). They confirm that twins formed
at the interface after applying the strain. Guan et al. had reported that DTWs could weaken the deformed texture and for the first time provided direct evidence that recrystallized grains originating from double twins can form the rare earth texture during annealing

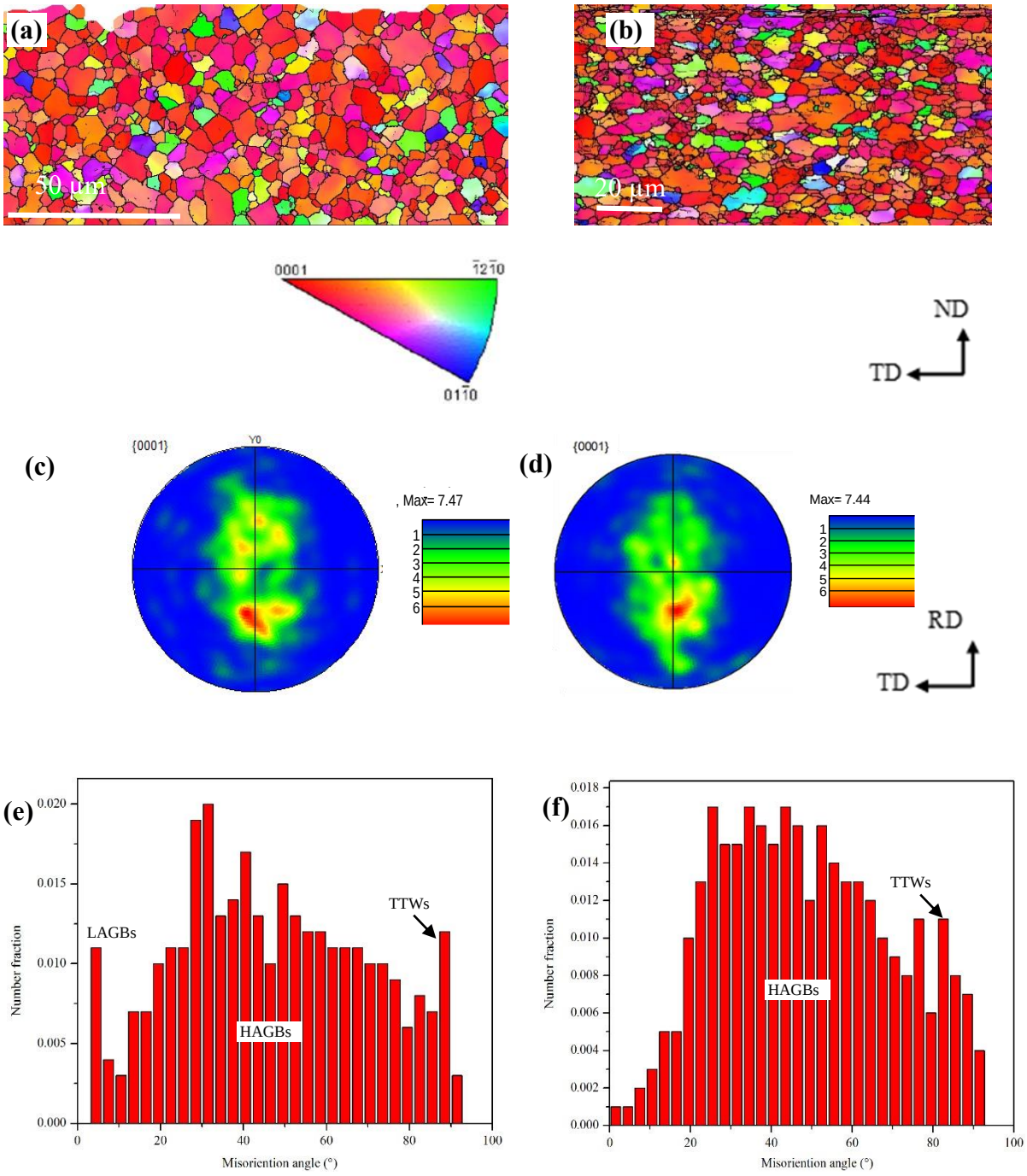

Figure 3.10 Shows sheet I Ti layer in as-rolled and annealed state. (a-b) IPF map; (c-d) (0001) pole figure; (e-f) distributions of misorientation angle.

recrystallized grain nucleation, grain growth and texture evolution of Mg alloy after heat treatment[118].

3.4.2.2. The Ti Layer

Figure 3.10 shows EBSD inverse pole figure map, (0001) PF, and distributions of misorientation angle of the sheet I Ti layer in as-rolled and annealed state. A few studies have reported the hot-rolling texture of the pure Ti, and all investigation has been done using X-ray diffraction (XRD) pole figures[128]. The results reveal that uniform grains with an average grain size of 2.83μm and 3.35μm for as-rolled and annealed, respectively, as shown in figure 3.10 a and figure 3.10 b. The Ti layers were subjected to a low deformation strain due to the different flow stress of the Ti and AZ31. In this work, a thin Ti layer (0.2±0.02mm) were used to clad the AZ31 which was subjected to shear deformation generated by friction from both AZ31 layer and rolls. The hot-rolling and annealing heat treatment were carried out at a temperature lower than the recrystallization temperature of Ti (≥ 500 ºC) [95, 96]. Therefore, it is considered to be in a deformed or recovered state, i.e.,unrecrystallized. The (0001) PF of as rolled and annealed Ti layers represented in figure 3.9 c and figure 3.9d. There was a slight decrease in the texture intensity after annealing. Both as-rolled and annealed texture show single pole basal texture split to the RD, and the maximum intensity of (0001) poles shifted by 35-45° towards RD from ND. The distribution of the grain boundaries misorientation angle illustrated in figure 3.9e and figure 3.9 f confirm a wider distribution of HAGBs in the range of the angle between 20°and 80° with a small fraction of LAGBs and TTWs in the as-rolled layer which disappeared after heat treatment. Dragomir et al. [129] studied hot rolled commercially pure titanium at 268 °C to a different reduction 40%-80%; they found that the (0001)PF was split to the RD in the initial state, and then the orientation become TD at a higher strain of 80%. Bouhattate et al.[130] simulated experimental data of cold and hot-rolled commercial pure Ti texture with a different strain. They show that the (0001) PF split along of RD for the hot-rolled sample with a strain of 20% for both experimental and simulated. Figure 3.11 depicts EBSD inverse pole figure map, (0001) PF, and distribution of grain boundaries misorientation angles for as-rolled and annealed state sheet II. The Ti layers in the sheet II exhibited a similar texture as in the sheet I, which has confirmed the Ti layer subjected to low deformation stain in both sheets I and II. The average grain size was of 2.86 μm and 4.41μm for as-rolled and annealed sheets, respectively, as shown in figure

3.10 a and b. The (0001) PF shows single pole basal texture split to the RD by 35-45° towards RD from ND, as shown in figure 3.11c and figure 3.11d.

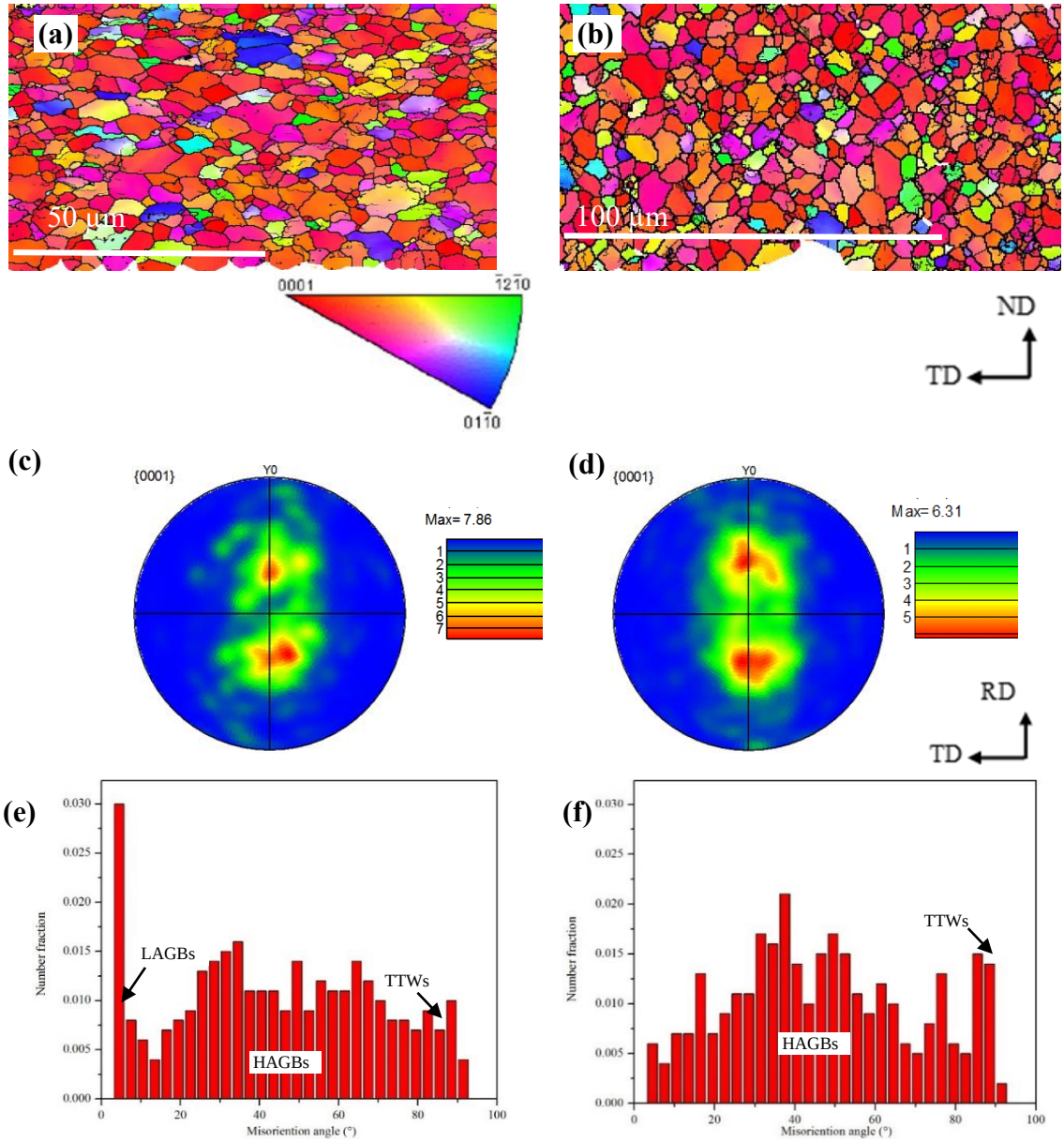

Figure 3.11 Shows sheet II Ti layer in as-rolled and annealed state: (a-b) IPF map; (c-d) (0001) pole figure; (e-f) distributions of misorientation angle.

The distribution of the grain boundaries misorientation angle is shown in figure 3.11e and figure 3.11f which exhibits HAGBs in the range of the angle between 20°and 80° with a small fraction of LAGBs and TTWs in the as-rolled sheet which was disappeared after heat treatment.

3.4.2. Mechanical Properties

The mechanical properties were investigated by conducting nanoindentation and tensile tests at room temperature. The annealing heat treatment process could affect mechanical properties of the clad sheets. The effect of the clad sheets texture on the mechanical properties studied as well.

3.4.2.1. Nanoindentation Test Results

The nanoindentation is useful characterization technique which reflects the strength of the clad sheet layers. Nanoindentation test was conducted to study the mechanical properties of the clad sheets layers. Indentation test was performed on Ti/AZ31/Ti cross section for assembly sample, sheet I, and sheet II in as-rolled and annealed conditions, as shown in figure 3.12a. The hardness of the Ti layers is much higher than that of the AZ31 layer in all conditions. After the hot-rolling, the hardness of the AZ31 layer enhanced while Ti layer showed slightly increasing. The hardness of as-rolled AZ31 layer is slightly higher than the AZ31 layer in the assembly sample, which is likely associated with twins, shear bands microstructures, and high texture intensity generated during the hot rolling process. Also, hardness measurements showed that increase in hardness values with increasing rolling reduction. This could be attributed to fine grain size and the increase in shear bands density[126, 131].

The shear bands hardness has been discussed by Fatemi-Varzaneh et al.[83] in the AZ31 Mg alloy. Also, the shear bands may consider as a grain refining mechanism. Thus, the tensile strength of the clad sheets enhanced while reduced the ductility.

Further annealing heat treatment, the hardness of the AZ31 layer was decreased. The hardness value decreased attributed to the recovery and recrystallization during heat treatment[126, 132]. Average hardness values of assembly sample, the clad sheet I and sheet II are shown in the figure 3.12b. The hardness of the annealed Ti layer is higher than that in assembly and as-rolled samples, which may associate with the diffusion of A1 to Ti side during heat treatment [72, 133, 134]. The nanoindentation load-displacement curves of the as-rolled and annealed clad sheet II are presented in figure 3.12c. A maximum load of 30 mN was applied, and the indentation depth in the range of 2000-3500 nm. The AZ31 layer showed quite a difference in indentation depth before and father heat treatment. The

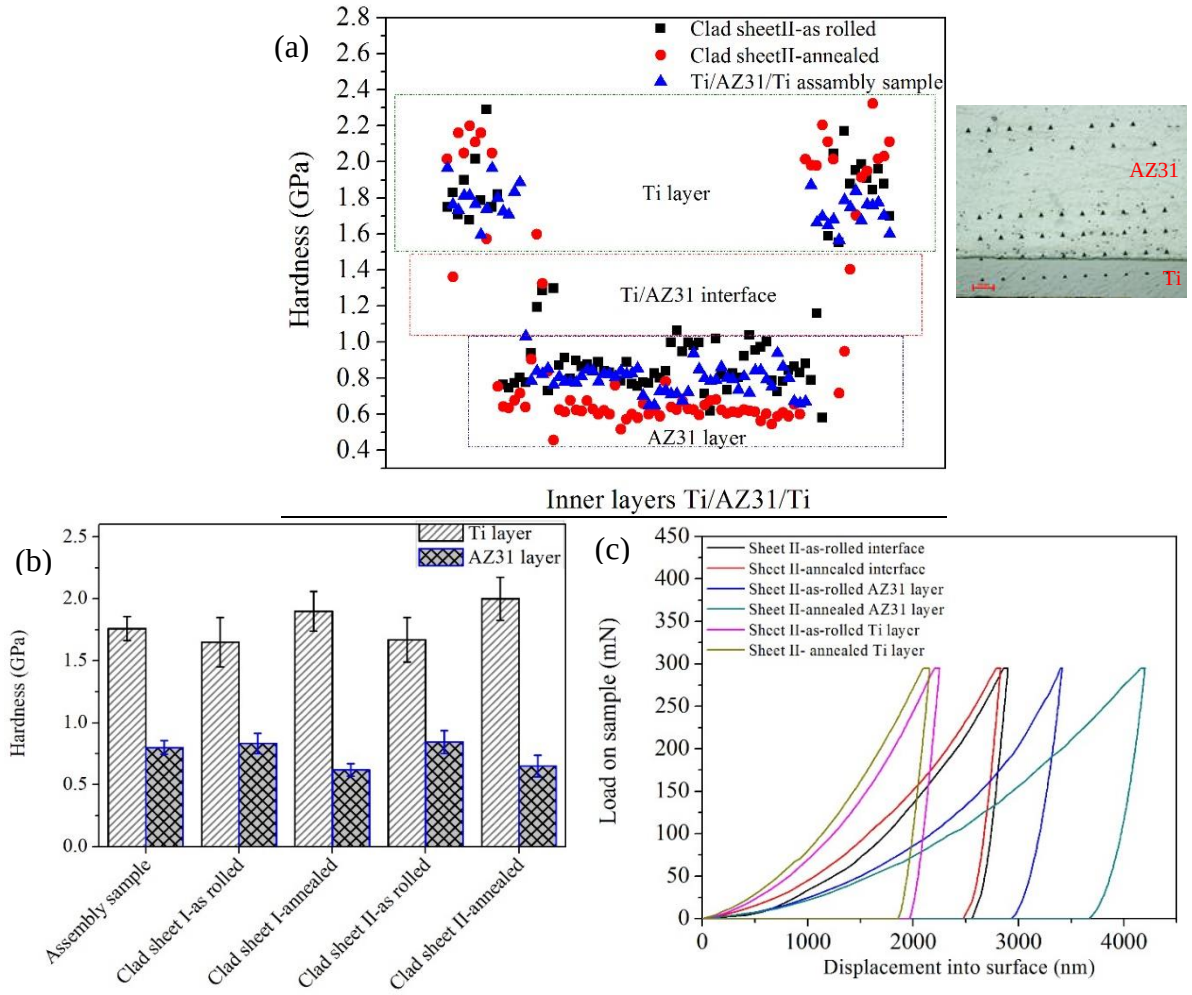

Figure 3.12 (a) local nanoindentation evolution through the cross-section of the sheet II; (b) average hardness values of assembly sample, the clad sheet I and II; (c) nanoindentation load-displacement curves of the sheet II.

hardness values are increasing, and indentation depth decreasing are agree with the fact that hardness has increased with the higher resistance of the as-AZ31 layer to the indenter.

3.4.2.2. The Tensile Properties of Clad Sheets

Figure 3.13 a shows the stress-strain curves of the AZ31 and clad sheet II (as-rolled and annealed conditions). The tensile properties are summarized in figure 3.13b; for the ultimate tensile strength (UTS), 0.2% yield stress (YS), and the elongation in the RD and TD directions. The tensile tests were conducted at room temperature. The as-rolled sheets show that increased the flow stress and significantly decreased the elongation. The UTS and YS of as-rolled sheet II reached to 365 MPa and 280 MPa, respectively, which was

~26% and 25% higher than that of AZ31 alloy (290 MPa and 224 MPa). The elongation was 13% which was ~ 23% lower than that of AZ31 alloy (17%). This is generally attributed to dislocation strengthening mechanisms during the hot-rolling process in which the higher density of dislocations and finer microstructures (twins and shear bands) are pinned the dislocations and caused strengthening in the AZ31 layer. In general, materials processed through severe plastic deformation showing very limited ductility due to the fine-grained microstructure. It is reported that shear bands and acts as stress concentration point which leads to failure the materials at low elongation [109, 110].

It can be seen that the annealed sheets exhibit lower UTS and YS than the as- rolled sheets which are a good agreement with the texture evolved after the heat treatment. The clad sheets mechanical properties are controlled by the components texture, and layered structural design. The elongation of the sheet II is significantly improved following the annealing treatment at 400°C for 12 h. The elongation reached 35% and 26% in RD and TD respectively which is ~51% and 35% higher than of as-received AZ31. The AZ31 is the largest constituent layer in the clad sheets which control the mechanical performance due to its sensitivity to cracks[135]. Therefore, the annealing heat treatment is highly significant. The texture evolution of the AZ31layer obtained by annealing heat treatment is the essential step to improve the sheets mechanical properties. On the other hand, the Ti cladding layer has better formability than the AZ31 alloy which may impose the maximum tensile stress. However, the Ti layers were subjected to work hardening due to mechanical cleaning and rolling process[95]. Therefore, Ti may fail at lower elongation since the annealing heat treatment carried out at a temperature lower than Ti recrystallization temperature. The mechanical performance of the clad sheet can be calculated using the rule of mixtures (eq.1) [135, 136]

$$\sigma_{clad} = \sigma_{Ti} * v_{Ti} + \sigma_{AZ31} * v_{AZ31} \quad \ldots\ldots\ldots\ldots\ldots\ldots\ldots\ldots (1)$$

where σ_{clad} is strength of the clad sheet, (σ_{Ti} ; σ_{AZ31}) and (v_{Ti} ; v_{AZ31}) are the strength and volume fraction of Ti and AZ31, respectively. The results show that the experimental result agrees with the theoretical calculation. The bonding strength between the AZ31/Ti plays a critical role on the mechanical properties of the clad sheets. It has been reported that the interface bonding effect the load transfer and the stress redistribution during the deformation [135, 136]. Kawamoto et al.[49] studied stain transfer through

Mg/Ti interface. They found that the Mg twinning is associated with Ti dislocation motion. In this study, the AZ31/Ti interface crystallographic orientation is controlled by AZ31 twining, which agrees with Kawamoto et al. conclusion; AZ31/Ti crystallographic orientation is provided in the supplementary materials. Brittle/ductile composite materials can sustain large plastic deformation without failure through the structure design such as layered, networks, and bi-layer. Huang et al.[136] studied the strain delocalization and constrained crack distribution of layerd Ti/Al composite material. They found that constrain interface may restrect the extensvie crack and relieved the localized strain at the interface. The elongation of the sheet II in the RD and TD directions show 35% and 26%, respectively which is related to anisotropic properties of AZ31 layer texture. It can be seen that the YS of sheet depend in the sample direction; where the TD tensile samples show an increase of the YS and decrease of elongation comparing to the RD samples[95]. In addition, the mechanical properties of the sheet II is same as or higher than that magnesium alloy that processed by plastic deformation and annealed [81, 123, 131]. Therefore, the sheet II exhibits a combination of strength and ductility. Suggested that the shape of (0001) basal plane effect the planer anisotropy, which means the probability of activation slip systems according to Schmid factor in RD higher than TD[95, 119, 120].

The sheet II presented ductility behavior higher than the AZ31, which is related to unique layered structural design. As shown in figure 3.13b, the annealed sheets II showed better mechanical properties than those of sheet I. The reasons for this variations can be related to the bonding strength between the Ti/AZ31, which enhanced as a function of large rolling reduction and post heat treatment. This is a further support to the effect of the interdiffusion layer on the interface strength.

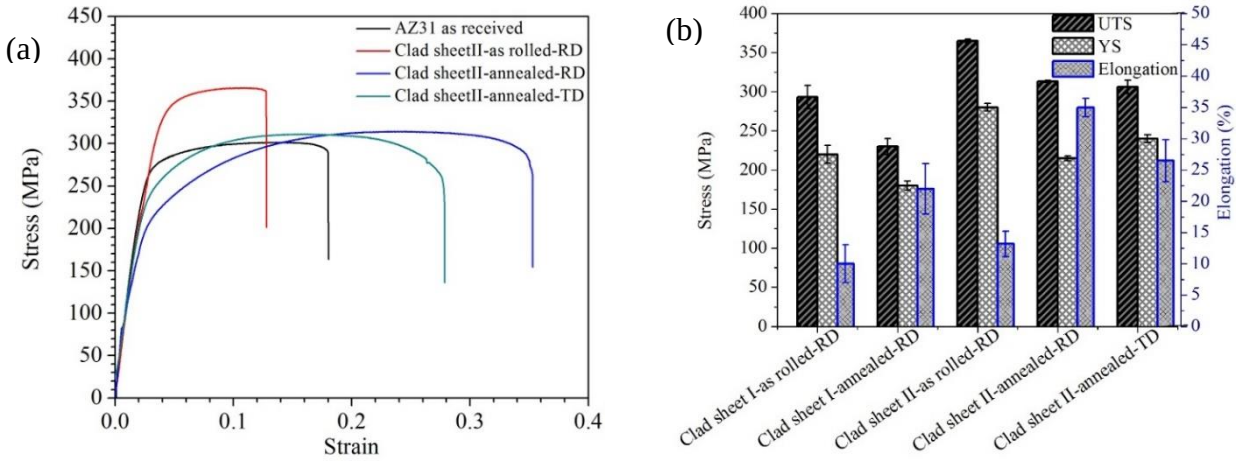

Figure 3.13 (a) stress-strain curves of the AZ31 and clad sheet II in as-rolled and annealed conditions; (b) summarized average of the UTS, YS, and the elongation.

3.4.2.3. Fracture morphology of clad sheets

The fracture surface of the sheet II in as-rolled and annealed conditions are shown in figure 3.14 The fracture was governed by the failure of the AZ31 layer, nucleation, and growth of cracks. Compared the failure surface of the sheet II before and after annealing treatment, the Ti layers in both conditions show equiaxed dimples on the failure surface, which leads to ductile fracture of the Ti layer, as shown in figure 3.13a and figure 3.13b. Figure 3.9c shows surface of as-rolled AZ31 layer with large voids (indicated by red circle), shear bands (indicated by blue arrow), and tear ridges (indicated by yellow arrow). The fracture surface features are typical intergranular fracture which occurs due to high dislocation densities (shear bands). As a result, shear bands areas are potential stress concentration sites which susceptible to void and crack formation starts early. This causes reduction of the clad sheet ductility [109]. After annealing, the AZ31 layer exhibits ductile fractures with fine equiaxed dimples that leads to significant increase in tensile ductility, as shown in figure 3.14d. Thus, modifying shear banding structure can lead relatively high elongation. Subsequent annealing heat treatment is believed to recovery and recrystallization of the deformed materials, which lead to homogenous microstructure and delay the cracking formation in AZ31layer.

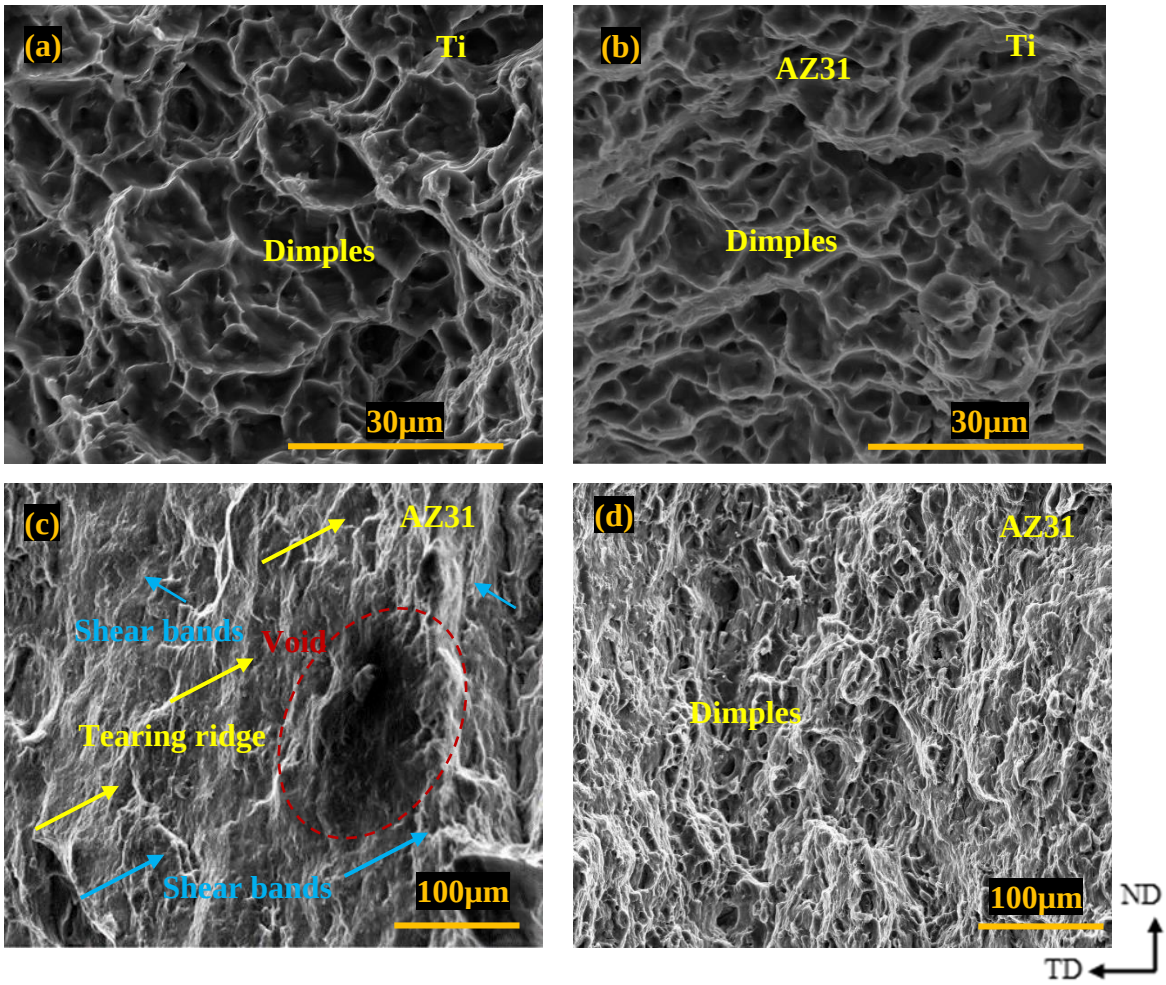

Figure 3.14 The SEM of tensile fracture profile of the Sheet II (a) as-rolled and (b) annealed-Ti layer; (e) as-rolled and (f) annealed-AZ31-layer.

3.5. Conclusions

1. The single-pass hot-rolling followed by heat treatment is a successful way to fabricate lightweight Ti/AZ31/Ti clad sheets with excellent corrosion resistance and mechanical properties.
2. The tensile test was performed at RT for as-rolled and annealed clad sheets which reflect the heat treatment on the changes of the microstructure and texture.
3. The AZ31 layer controlled the tensile properties of the clad sheets since it is the major component of the clad sheet. The clad sheets showed strong basal texture in the AZ31 layer due to twins and shear bands.

4. The shear bands were caused by the strain localization which leads to failure of the sheets at lower elongation. The texture of the AZ31 layer was significantly improved after the annealing heat treatment (i.e., SRX) for 400 ◦C for 12h.
5. The clad sheets elongation was improved flowing annealing heat treatment which can be explained by the texture evolution in the AZ31 layer and interfacial bonding strength between the Ti-AZ31. The sheet II showed the best mechanical properties with the YS, UTS, and elongation reaching 215MPa, 313MPa, and 35% respectively in the RD and 240 MPa, 306MPa and 26 % respectively in the 26.46 TD.

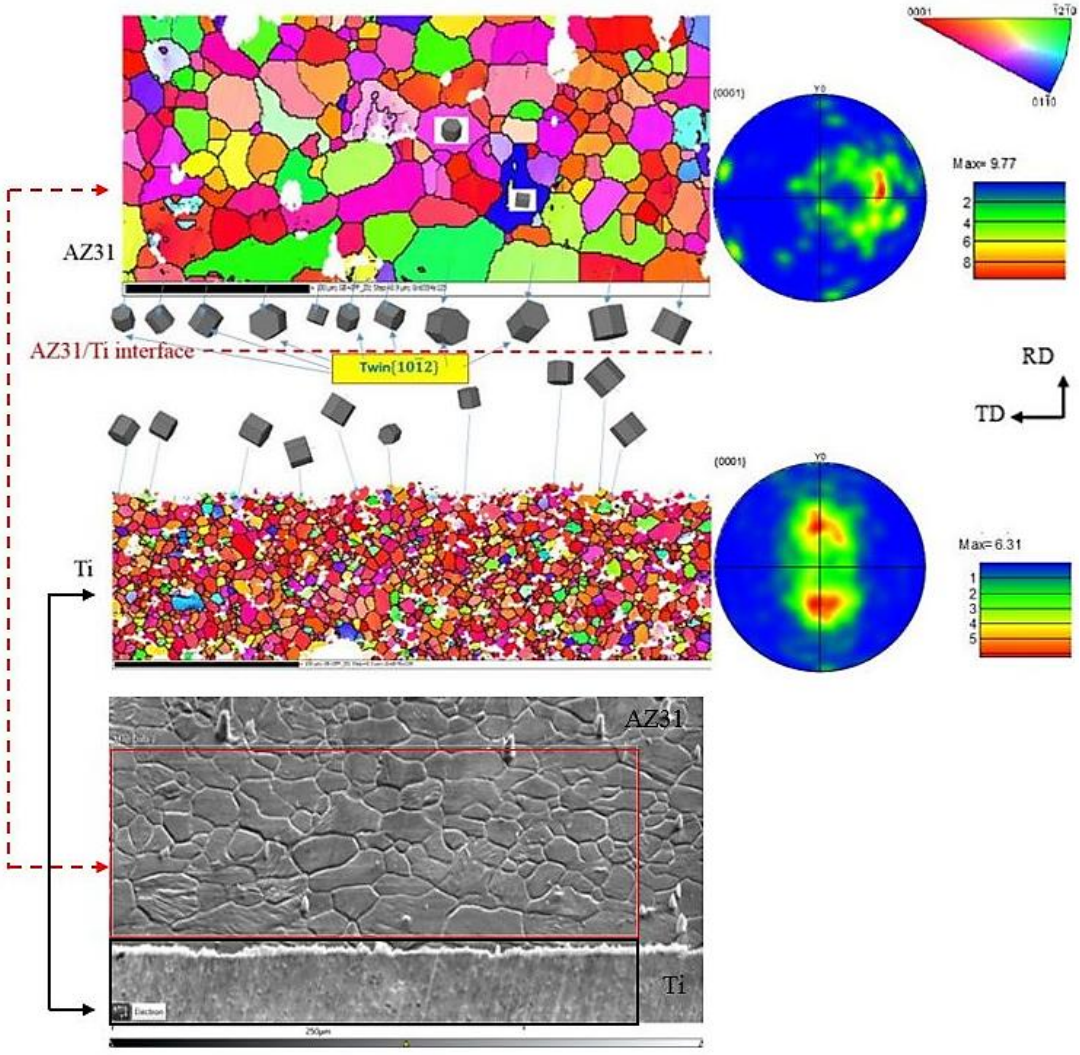

Figure 3.S1 Illustrates the interface of annealed clad sheet II.

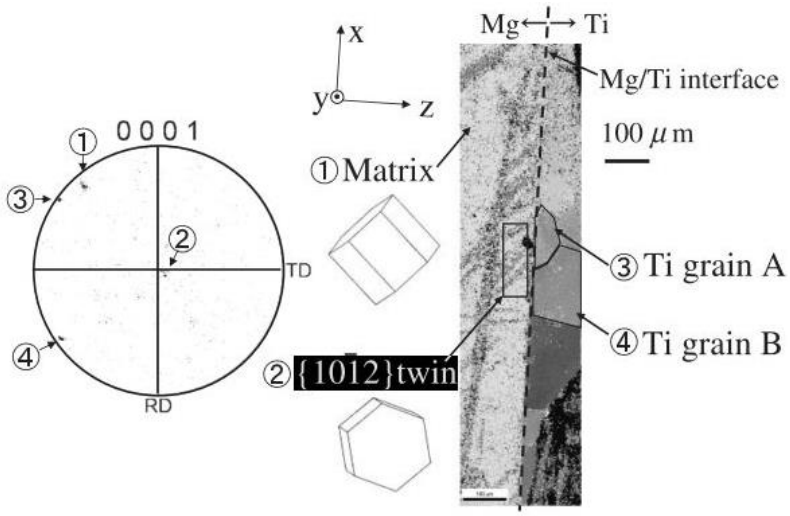

Figure 3.S2 Shows Mg/Ti interface crystal orientation using EBSD[32].

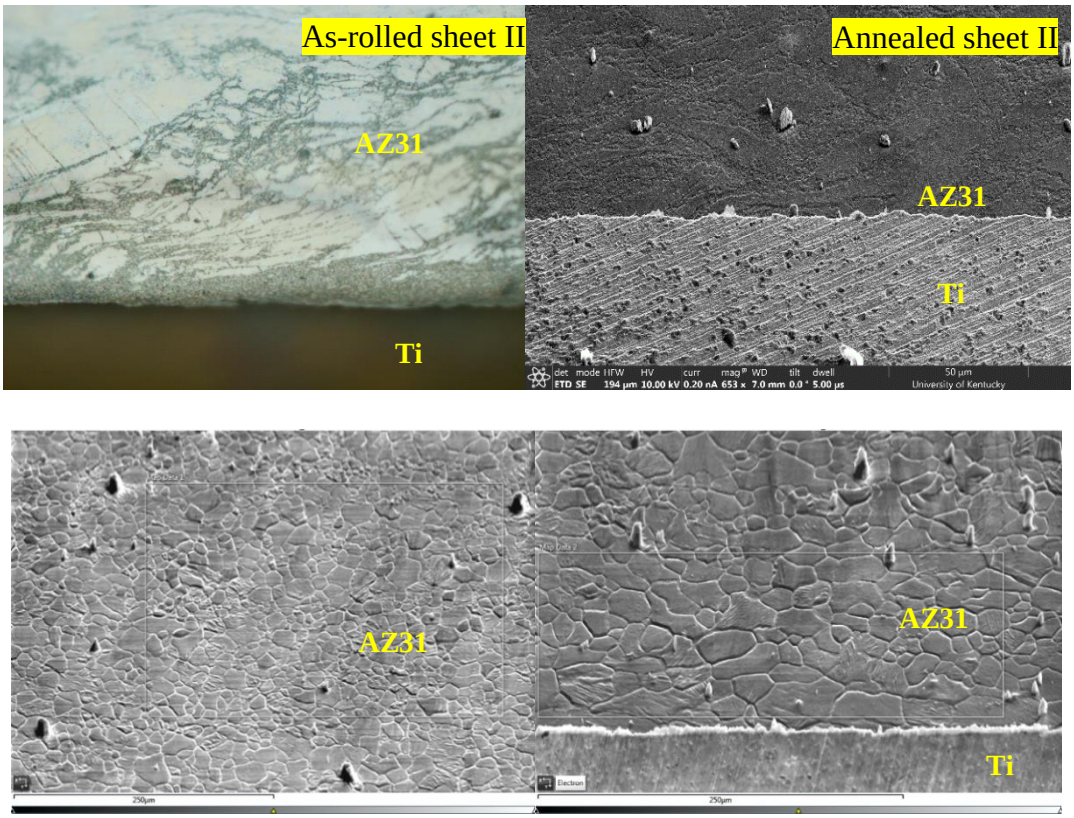

Figure 3.S3 Shows the interface of as-rolled and annealed clad sheet I &II.

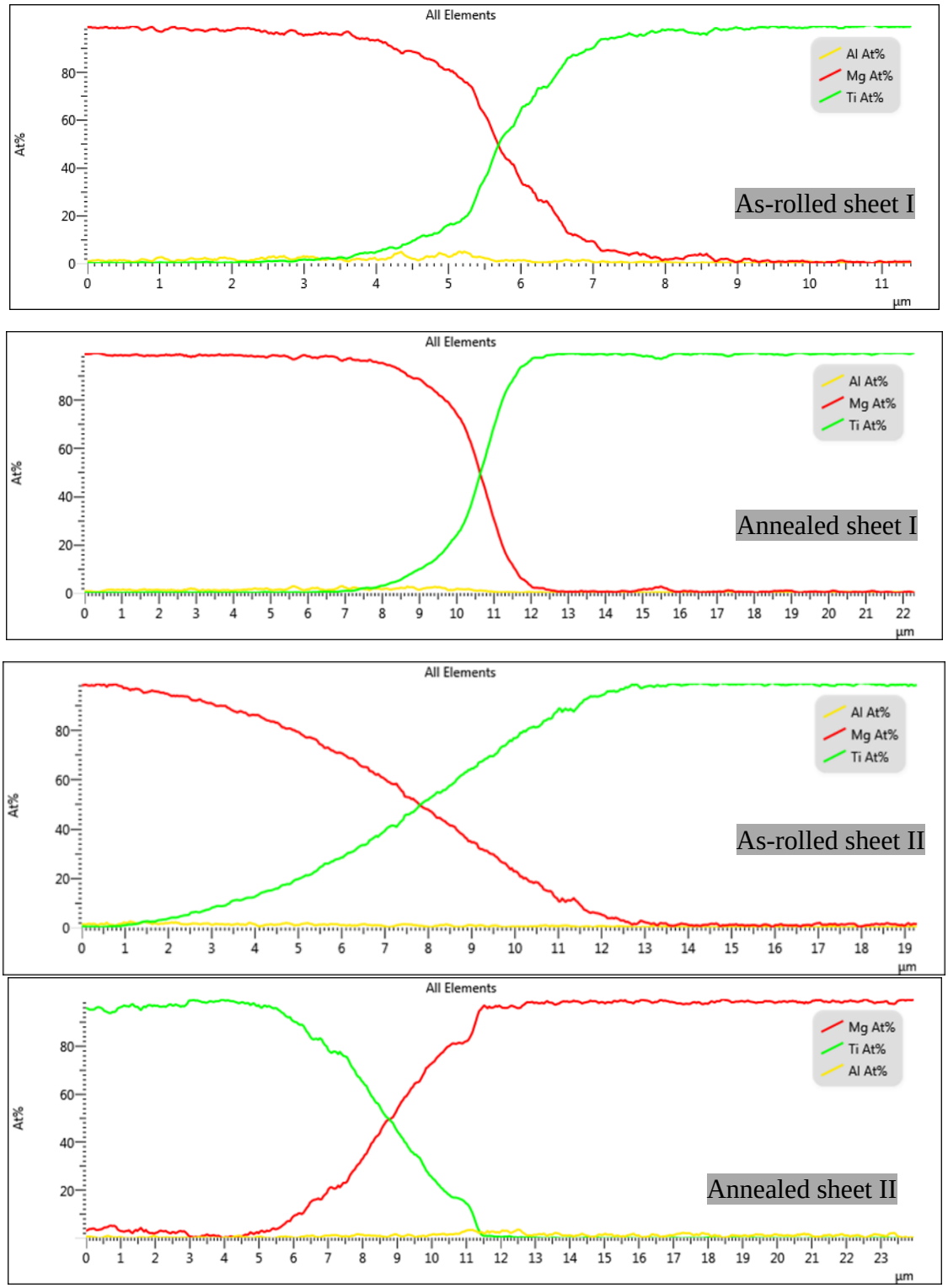

Figure 3.S4 Shows the interface line scan of as-rolled and annealed clad sheet I &II.

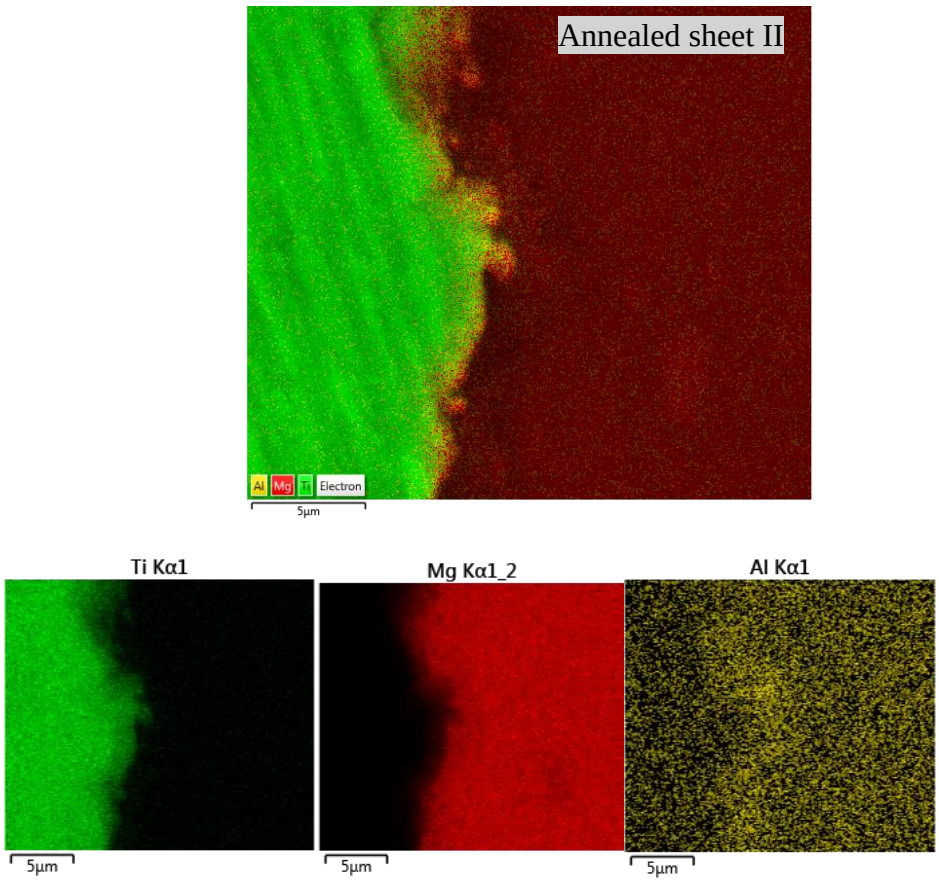

Figure 3.S5 Shows the interface map scan of clad sheet I &II.

CHAPTER 4. Microstructure and mechanical properties of Ti particles reinforced AZ31 –Mg alloy matrix composites through ARB and subsequent annealing

4.1. Summary

This work aims to study the effects of dispersed pure titanium particles (150 mesh) with 0, 2.3, 3.5, 4.9, and 8.6 wt. % on the microstructure and mechanical properties of AZ31-Mg alloy matrix. Mg-Ti composites were processed through a three accumulative roll bonding (ARB) process using thickness reductions of 50% each pass followed by heat treatment at 400 °C for 12 h in an argon atmosphere. Mechanical properties of Mg-0 and Mg-2.3Ti composite were enhanced by ~ 8% and 13 % in YS and ~ 30% and 32 % in UTS, respectively. Meanwhile, the elongation of the composite was decreased by 63% and 70%. After heat treatment, the results showed a decrease in yield strength and increased in the elongation to fracture. The mechanical properties of the Mg-0 and Mg-2.3Ti composite were enhanced; ultimate tensile strength by 9% and 7%, and elongation by 40% and 67%, while the yield strength was decreased by 28% and 36% compared with the initial AZ31. Enhancement of strength and ductility were developed based on the operation of two mechanisms: developing a random matrix texture by ARB, and dispersion of ductile titanium particles. ARB is an efficient process to fabricate an Mg-Ti composite material.

4.2. Introduction

Magnesium is lighter than aluminum and steel by 35% and 78%, respectively. Magnesium-based composite materials have become more attractive in the transportation industry and aerospace applications due to their combined desirable properties such as lightweight, high strength, and high recyclability. Magnesium alloy AZ31 (Mg-3%Al-1%Zn) has been used in industrial applications because of its good mechanical properties, damping characteristics, machinability, and low casting costs[53, 137]. However, it is difficult to form Mg alloys at an ambient temperature because Mg alloys have a hexagonal close-packed (HCP) structure [138], and the axial ratio(c/a) is 1.624 smaller than the ideal value[32]. Only the basal slip system is active at room temperature, while the other slip systems (prismatic and pyramidal) are inactive. Therefore, insufficient plastic deformation occurs at room temperature [36-39]. During severe plastic deformation processing high temperature (i.e., hot rolling and extrusion), other non-basal slip systems or twinning systems are activated. In general, HCP materials have slip systems: basal $\{0001\}\langle 11\bar{2}0\rangle$, prismatic $\{10\bar{1}0\}\langle 11\bar{2}0\rangle$ and pyramidal $\{10\bar{1}1\}\langle 11\bar{2}0\rangle$ [33, 34]. Therefore, the texture control is an effective way to enhance the ductility of Mg and its alloys at room temperature[139]. Severe plastic deformation (SPD) is a process in which a large strain is applied at a temperature below recrystallization temperature without thermal treatment to produce ultrafine-grained (UFG) structures. There are several processes which have been developed to produce high strain in metals accompanied with changes in sample dimensions such as equal-channel angular pressing (ECAP), high-pressure torsion (HPT), multi-axial forging (MAF), and accumulative roll-bonding (ARB)[37, 140-143].

Composite materials are alternating which have significant advantages due to the combination of their desirable properties, such as strength and ductility. Ceramic and intermetallic compounds were employed as reinforcements to Mg- alloys such as SiC, TiC and TiB_2, Al_20_3, and graphene nano-platelets [144-148]. However, all of these hard and brittle reinforcements lead to a decrease in the ductility of the composites[52]. Alam et al. [54] claimed that there is an improvement in the microstructure and mechanical properties of AZ41 and AZ50 Mg alloys by adding nano-sized Al_2O_3 particles and Ca. Mg-based composites can improve formability and toughness by the dispersion of ductile particles,

which are deformed plastically with stress lower than the maximum strength of the Mg matrix. The dispersion particles prevent stress concentration and cracking at Mg grain boundaries. Ti has been reported as a suitable dispersoid because it has a very low solid solubility, and there is no affinity and no intermediate reaction layer in the Mg-Ti binary phase diagram [22, 32, 50-52]. Kitazono et al. [53] synthesized Mg/Ti composites by accumulative diffusion-bonding (ADB). The mechanical properties of the AZ91Mg alloy were improved by the dispersion of Ti particles in the AZ91matrix. They suggested that the development of a random texture improved ductility due to severe plastic deformation and stress relaxation in Ti particles. Esen et al. [19] prepared Ti–Mg composite rods by hot rotary swaging from elemental powders of titanium and magnesium. The composite was in-vivo tested in Ringer's solution which can be used in the human body. In this study, Ti particles (0, 2.3, 3.5, 4.9, and 8.6 wt. %) were used to improve AZ31 ductility. We proposed the accumulative roll bonding (ARB) process which is known as a useful severe plastic deformation technique to fabricate metal-metal composites material. The materials synthesized were studied for microstructural and mechanical properties. The reinforced the composites with Ti particles were compared to that of unreinforced samples.

4.3. Materials and Experimental procedures

AZ31 magnesium alloy (Mg–3wt. % Al–1 wt. % Zn, provided by Magnesium Elektron) was used as a matrix, and high purity (99.9%) titanium particles (spherical -150 mesh, provided by Alfa Aesar) were added as ductile reinforcements. The AZ31 sheet was 0.80±0.1mm in thickness. The samples were 25mm in width 50mm in length, and 0.80±0.1 mm in thickness (5ply plates) of the AZ31 with five weight percentage of Ti 0, 2.3, 3.5, 4.9, and 8.6 as starting materials. The samples were named as (Mg-0 Ti, …, Mg-8.6 Ti) in correspondence to the Ti weight percentage in the composite. Before stacking the AZ31 layers, the Ti particles were distributed on the bonding interface. First, the samples were assembled by the uniaxial hot press with a load of 5 tons at 300 °C for 20 min to bond the AZ31 layers and avoid Ti particles oxidation [53]. Opposite corners of the assembled samples were fastened tightly by steel wires to prevent sliding of the AZ31 layers during ARB. Second, the assembly samples were heated in an argon atmosphere furnace at 450°C for 15 min, and then three ARB cycles were done using thickness reductions of 50% each pass [140]. The detailed schematic diagram of the ARB process is illustrated in figure 4.1.

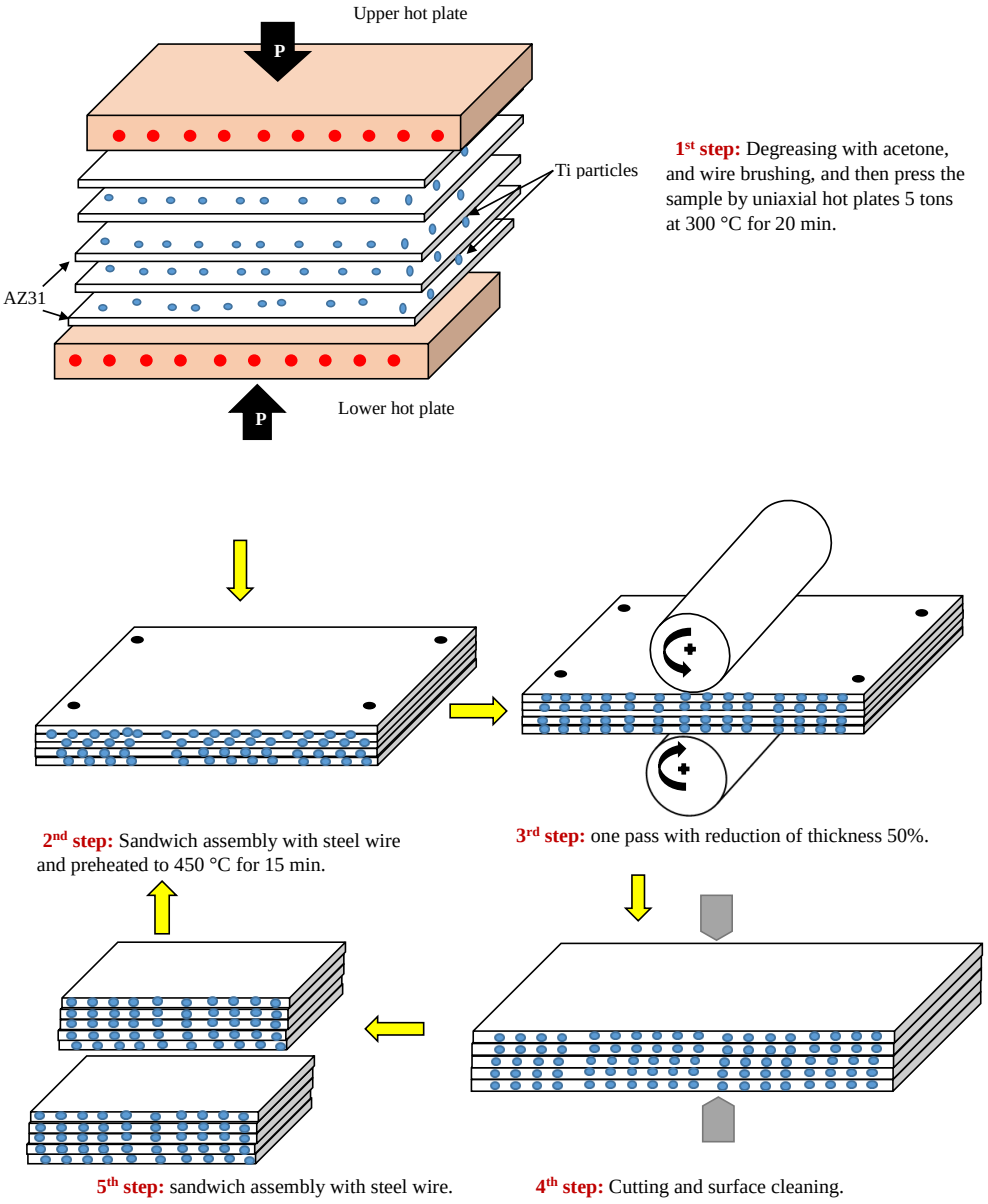

Figure 4.1 Schematic diagram of the ARB process.

The ARB process was carried out without lubricant using rolling mills with 101.15 mm diameter. After each ARB cycle, the sample was cut into two halves using a shear cutting machine, surface treatment, assembly, and rolled [66, 149]. To achieve good bonding between layers, the AZ31 plates were decreased by an ultrasound bath using acetone for 15 min and roughened using a rotating “stainless steel” wire brush [8, 11, 150]. Surface treatment was done for the assembly samples and between the ARB cycles. Heat

treatment was carried out at 400 °C for 12 h in an argon atmosphere. Optical microscopy (OM), X-ray diffraction (XRD), scanning electron microscopy (SEM), energy dispersive spectroscopy (EDS), electron backscatter diffraction (EBSD), nanoindentation, and tensile tests were used to characterize the samples before and after heat treatment. The samples were mounted using a non-conductive epoxy. The surface was prepared using silicon carbide abrasive papers for grinding and MasterPolish (0.05 µm) polishing liquid with a ChemoMet cloth for mechanical polishing. Electrochemical polisher was used to polish AZ31 matrix; an electrolyte (methanol: ethanol: nitric acid = 10:10:3) at room temperature and voltage of 27-30V to obtain high-quality EBSD patterns[49, 100]. EBSD was performed on the as-rolled and annealed samples Mg– 0 Ti and Mg– 4.9 Ti using FEI (Helios NanoLab 660) equipped with an electron backscatter diffraction (EBSD) system. The EBSD data were analyzed using HKL channel 5 software. Hardness was evaluated by nanoindentation (Agilent G200). The tensile tests conducted at room temperature with a strain rate of 0.5mm/min. Tensile specimens with 10mm gauge length were machined by an electric discharge machine (EDM) in rolling direction (RD) [76].

4.4. Results and discussion

4.4.1. Effect of accumulative roll bonding (ARB) on the microstructure

Optical micrographs of the ARBed Mg– 4.9 composites materials are shown in figure 4.2. It can be seen the bonding line and agglomeration of the Ti particles in the first ARB cycle (figure 4.2a). The Ti particle distribution in the AZ31 matrix became more uniform after the second and third ARB cycles, as shown in figure 4.2 b-d. The bonding lines disappeared after the three ARB cycles which indicate that ARB is an effective process to fabricate Mg-Ti composite material [39, 142, 151, 152]. In this study, several weights percentages of Ti particles (0, 2.3, 3.5, 4.9, and 8.6) were added to the AZ31 matrix. The microstructures of the AZ31-Ti composite with four different weight contents of Ti after three ARB cycles are shown in figure 4.3. The composite material showed no visual defects such as interface debonding, cracks, or pores after three ARB cycles for both AZ31/AZ31 and Ti/AZ31 interfaces.

The Ti particles were quite uniformly distributed without agglomeration in the matrix; neither clusters of Ti particles nor new phases were created during the ARB process

AZ31

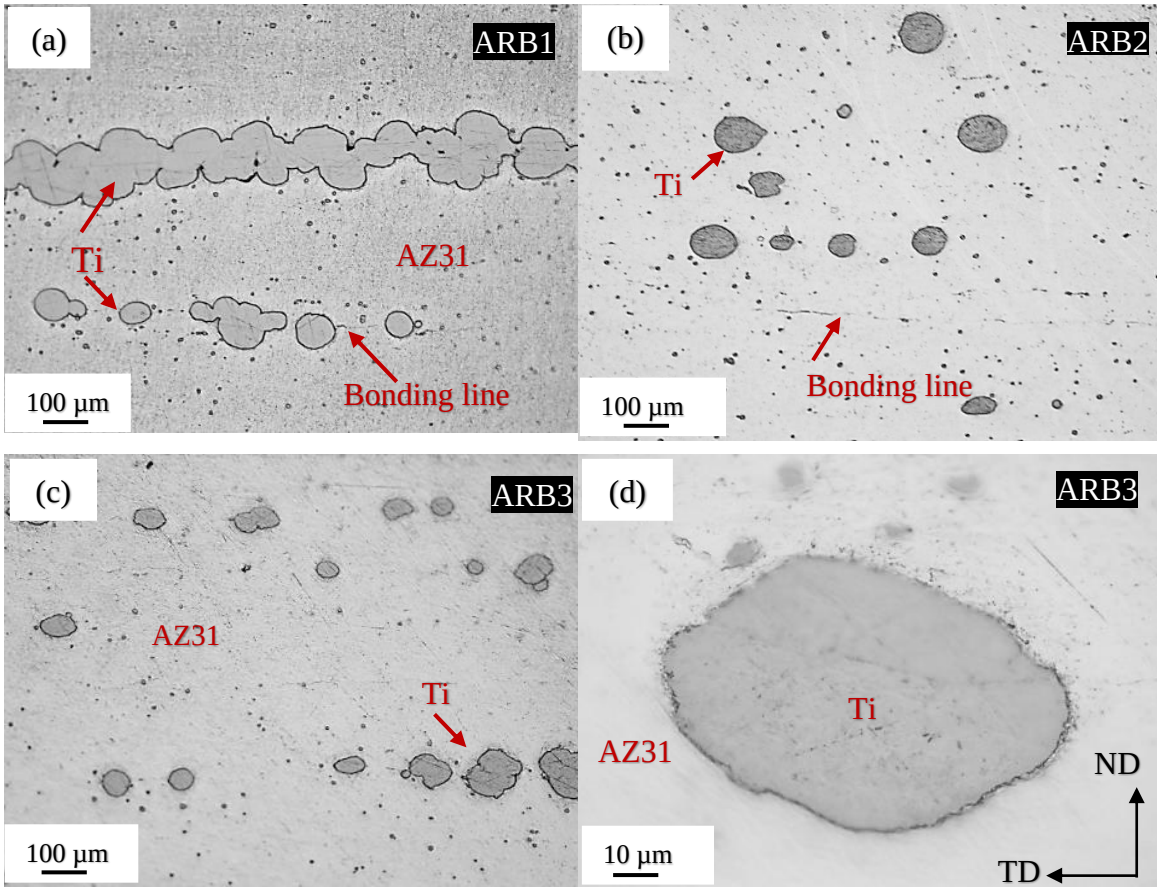

Figure 4.2 Microstructure of the Mg–4.9Ti composite processed by accumulative roll bonding. (a) ARB1, (b) ARB2, (c) ARB3, (d) high magnification of (c).

[22, 52]. Figure 4.4 shows X-ray diffraction patterns of AZ31, Ti- particles, Mg–4.9 Ti, and Mg–4.9 Ti in annealed condition after three ARB cycles.

Furthermore, no changes of the Ti particle shape or particle size were detected during ARB cycles. This is related to the high strength of Ti, and the flow deformation of the matrix is not enough to deform the Ti particles. It has been reported that the particles shape and size may affect the mechanical properties of the composite materials [22, 53]. In this work, the Ti reinforcement particles found with round edges, therefore no stress concentration would occur due to sharp edges[153, 154]. The total reduction and equivalent plastic strain can be calculated from equations 1and 2[17, 155].

$$\text{Total reduction (\%)} = \left(1 - \frac{1}{2^n}\right) \times 100 \qquad (1)$$

$$\text{Equivalent plastic strain } \varepsilon = n\left(\frac{2}{\sqrt{3}}\right)\ln\left(\frac{1}{2}\right) = 0.8n \qquad (2)$$

where n is the number of ARB cycles

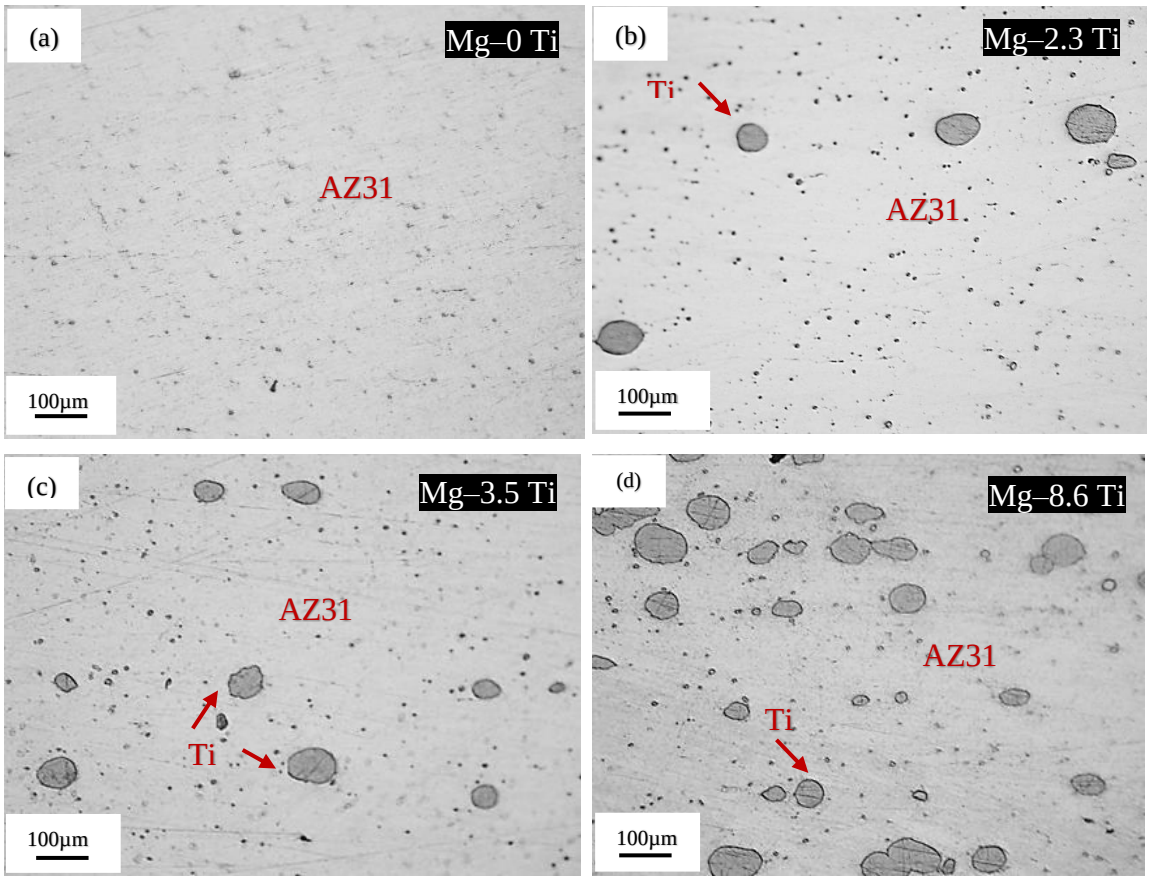

Figure 4.3 The microstructure of the composite processed by three ARB passes. (a) Mg–0 Ti, (b) Mg–2.3 Ti, (c) Mg–3.5 Ti and (d) Mg–8.6 Ti.

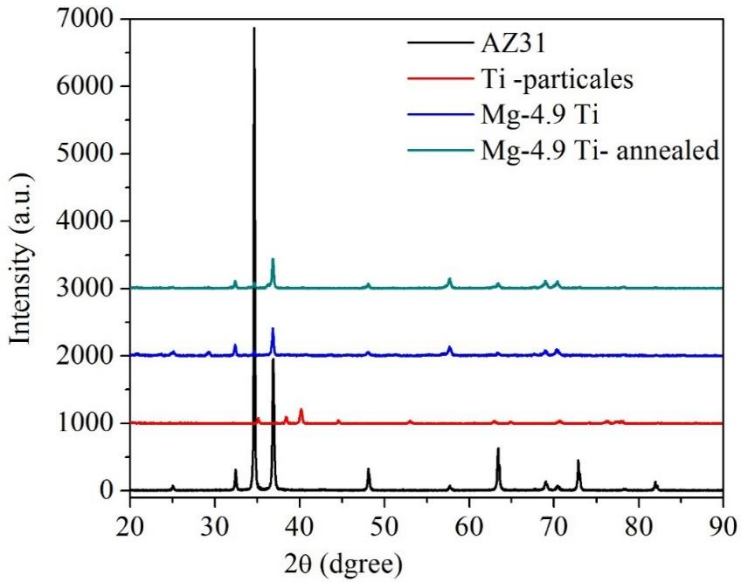

Figure 4.4 Shows X-ray diffraction patterns of AZ31, Ti- particles, Mg–4.9 Ti , and Mg–4.9 Ti annealed.

4.4.2 Texture analysis

To study the effect of Ti addition on the AZ31 matrix texture, EBSD was conducted for the as-ARBed and annealed condition for the Mg–0 Ti and Mg–4.9 Ti samples after three ARB cycles. The results of texture analysis based on the EDSD scan was performed on the TD plane. SEM images and pole figures corresponding to the AZ31 matrix of a composite structure Mg–0 Ti and Mg–4.9 Ti are shown in figure 4.4. Dynamic recrystallization (DRX) has taken place in the AZ31 matrix where recrystallized grains grew by the migration of grain boundaries during the ARB process. As shown in figure 4.5a, the microstructure of Mg–0 Ti was populated by recrystallized grains. In addition, heating between ARB passes may cause partial recrystallization and remove the accumulated strain [39, 142]. The (0001) PF showed strong basal texture with maximum pole intensity of 16.04, which tilted at 15° away from normal direction ND toward TD, as shown in figure 4.5(a-1). Zhan et al.[39, 142] have reported improved mechanical properties of the AZ31 after three ARB cycles at 300 °C and 400°C with 50% reduction. According to them, the basal texture was weakened as a result of repeating the ARB process and the DRX, which agrees with my research results.

To further understand the effect of Ti particles (Mg–4.9 Ti) on the AZ31 matrix texture, the EBSD scan was conducted at two sites. Site1 was in areas without Ti particles and site2 around Ti particles, as shown in figure 4.4b and 4.4c, respectively. Recrystallized grains were found in the site1 which is similar to Mg–0 Ti matrix, as shown in figure 4.5 b. Also, the (0001) PF showed a strong basal texture with maximum pole intensity of 12.63 and tilted at 15° away from ND toward TD, as shown in figure 4.5 (b-1). Pérez et al. [50]. has studied Mg-Ti composites (5 to 15 vol. % of Ti) processed by powder metallurgy followed by hot extrusion at 400°C. According to them, the basal texture intensity decreased with increasing Ti volume fraction. Elongated matrix grains formed in the vicinity of the Ti particles in site2 (figure 4.5c), which means a strong interaction between AZ31 and Ti particles during the ARB process. The Ti particles resist the AZ31 deformation flow that leads to forming the AZ31 fiber texture around Ti particles [22, 52]. The site2 showed a strong basal texture with maximum pole intensity of 15.12 and -5° away from normal direction ND toward TD, as shown in figure 4.5(c-1). The Ti particle

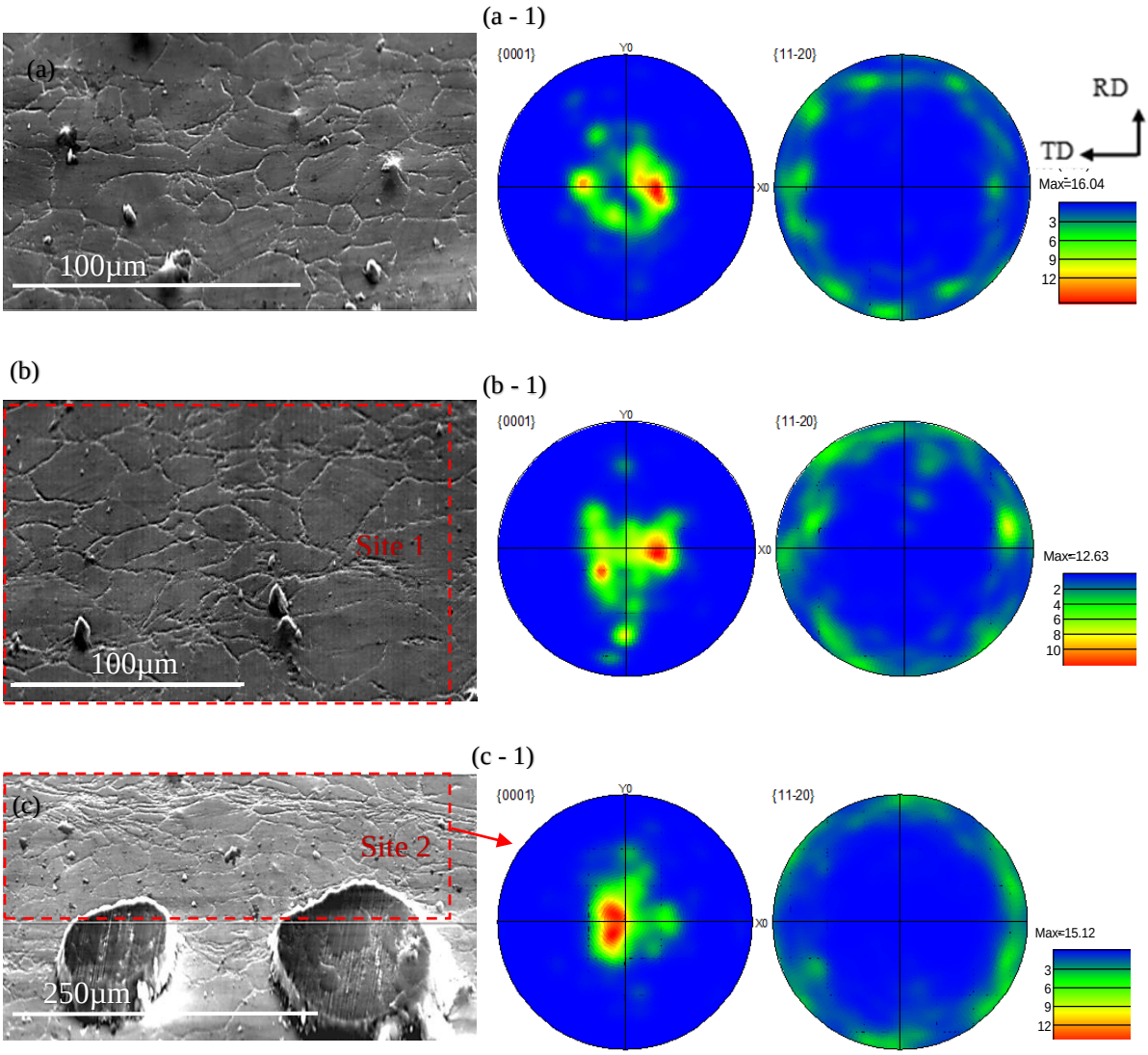

Figure 4.5 SEM and pole figures corresponding to AZ31 matrix after three ARBed cycles: (a) Mg–0 Ti, (b) Mg–4.9 Ti site 1, (c) Mg–4.9 Ti site 2.

zones were disturbed by the texture to re-arrange. In addition, Ti particles are located between the stacking AZ31 sheets during the ARB process, so that the texture changes from rolling texture to the large shear texture (site2) between bonded surfaces [156]. Thus, the AZ31 texture intensity is high in the vicinity of the Ti particles.

Heat treatment was carried out at 400 ºC for12h to relive the internal stress in the matrix during the ARB process. EBSD was used to analysis the texture changes after post heat treatment. Figure 4.6 shows SEM images and the pole figures of the Mg-Ti composites

with Mg–0Ti and Mg–4.9 Ti after three ARB passes. Static recrystallization (SRX) and grain growth occurred upon heat treatment. As shown in figure 4.6a- c, the grains become larger and more equiaxed, and the matrix fiber texture around the Ti particles disappeared. Furthermore, the basal texture intensity was weakened due to static recrystallization during heat treatment. The comparison of the pole figures of the ARBed and annealed samples reveals that the heat treatment has significantly influenced the texture intensity. The basal texture intensity of the Mg–0Ti sample was reduced from 16.04 to 7.16. The (0001) PF shows multi basal poles along the TD, as shown in figure 4.6(a-1). Also, the EBSD was conducted in two sites for the sample with Mg–4.9 Ti. Site1 shows lower basal texture intensity than the as-rolled condition where the (0001) PF reduced from 12.63 to 9.65 (figure 4.6(b-1)), while the site2 (0001) PF was reduced from 15.12 to 6.20, as shown in figure 4.5(c-1).

4.4.3. Hardness measurements

Nanoindentation measurements were conducted on polished samples before and after heat treatment. Berkovich indenter was used with a test load of 30 gf and a dwell time of 15 s. The hardness tests were conducted randomly on the Mg-Ti composite material, and the averages of the values were reported. Figure 4.7 shows the room temperature results of the nanoindentation measurements of as received AZ31 and Mg-Ti composite materials reinforced with different Ti content. The result reveals that the hardness values were significantly increased after three ARB cycles compared to initial hardness of the AZ31. In addition, the hardness values increased with an increase in the weight percentage of Ti content in the matrix. The hardness value was 0.85, 0.95, and 1.025 GPa for the as-ARBed condition of the Mg-0 Ti, Mg-4.9 Ti, and Mg-8.6 Ti, respectively. The hardness of the unreinforced Mg-0 Ti and Mg-4.9 Ti has increased by about 43% and 60%, respectively, compared to the AZ31. This is attributed to: (a) grain refining during ARB, (b) the formation of localized plastic deformation (fiber texture) around the Ti particles, which was caused by plastic deformation incompatibility between the reinforcement and matrix, and (c) the presence of relatively harder phase Ti particles in the matrix [22, 52, 55, 153]. Furthermore, the internal stresses developed in the metal matrix composite materials,

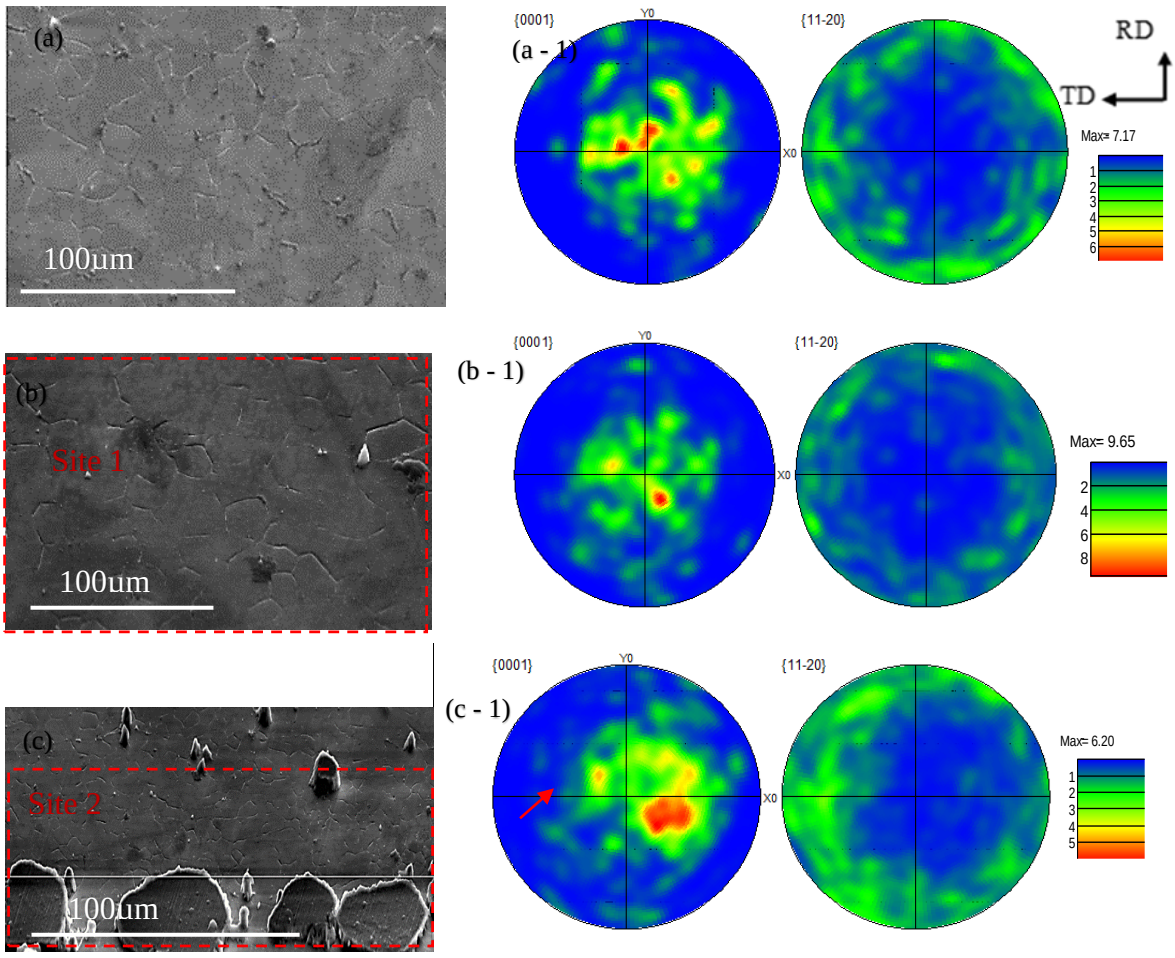

Figure 4.6 SEM and pole figures corresponding to AZ31 matrix after three ARBed cycles and annealing heat treatment: (a) Mg–0 Ti, (b) Mg–4.9 Ti site 1, (c) Mg–4.9 Ti site 2.

which caused by various factors. It has been reported that the increase of the Ti particle fraction leads to increase in internal stress between Ti reinforcement and matrix due to the differences in their thermal expansion coefficients and the modulus of elasticity [157, 158].

Softening behavior and stress relieve upon heat treatment of the metal matrix composite materials were investigated [159, 160]. Figure 4.7 shows the hardness as a function of Ti content in the matrix. The hardness decreased after heat treatment at 400 °C for 12h. This may be attributed to the relaxation of the internal stress and grain coarsening during heat treatment. It can be seen that the recrystallization has changed the texture of the ARBed materials completely (figure 4.5). The hardness values were 0.61, 0.78, and 0.79 GPa for the Mg-0, Mg-4.9, and Mg-8.6 wt. % Ti, respectively. The hardness of the

as-received AZ31 increased by ~ 3.5% and 32.5% compared to Mg-0 Ti and Mg-4.9 Ti, respectively.

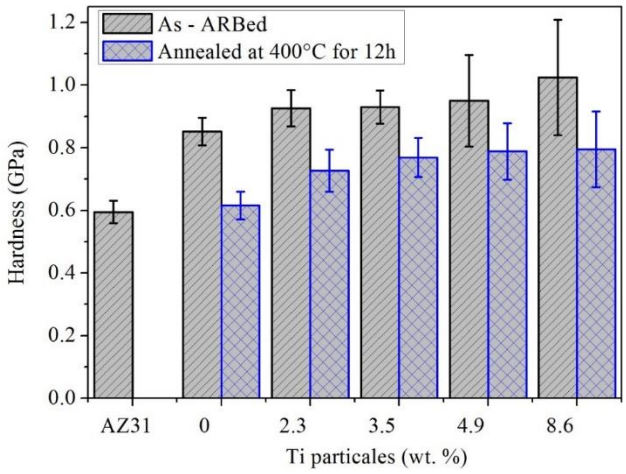

Figure 4.7 Nanoindentation measurements of as received AZ31 and Mg-Ti composite material reinforced with different Ti content.

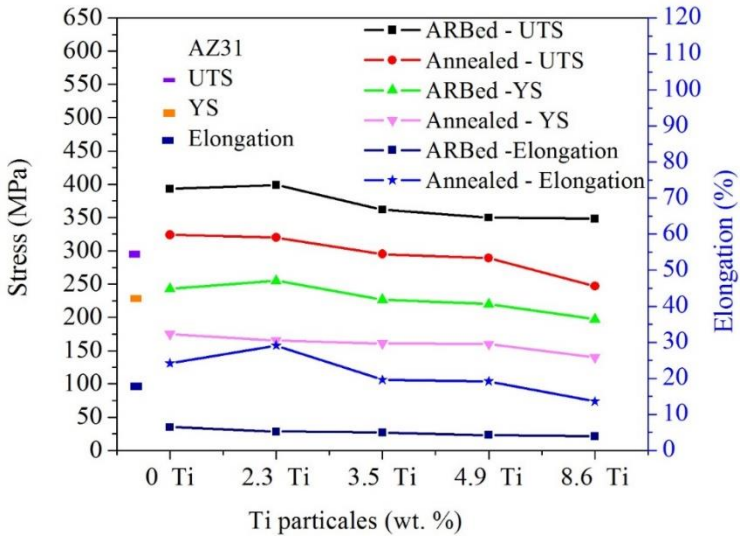

Figure 4.8 Room temperature tensile properties of AZ31-Ti composite materials.

4.4.4. Tensile test measurements

Figure 4.8 shows the ultimate tensile strength (UTS), 0.2% yield strength (YS), and elongation of the composites as a function of the weight percentage of Ti particles before and after heat treatment. The results show that the UTS and YS of the as-ARBed composite were enhanced after three ARB cycles when compared to the initial AZ31. The Mg–0 Ti

and Mg-2.3 Ti have the highest strength values. The Mg-0 and Mg-2.3Ti composites showed ~ 8% and 13 % higher YS and ~ 30% and 32 % higher UTS, respectively. Meanwhile, the elongation of the composite decreased by 63% and 70% for the Mg-0 and Mg-2.3Ti composite, respectively. The remarkable increases in the UTS and YS were attributed to grain refinement and fiber texture developed around Ti particles during ARB [157, 158]. Dislocations formed around the Ti particles due to plastic incompatibility between the Ti and AZ31- matrix. The high-density of dislocations in the matrix further increased the mechanical properties of the composite. The presence of the second phase in the composite matrix could restrict the dislocation motion in the matrix, leading to an increase in the YS [51]. However, a decrease in tensile properties with increasing Ti content could be related to the bonding strength between matrix and Ti particles (poor interfacial bonding). Furthermore, stress concentration developed around the reinforcement under tensile load, which may cause local damage when the local stress is higher than the bonding strength of the matrix and reinforcement particles. Therefore, the unreinforced (Mg-0Ti) shows higher mechanical properties in comparison to the other reinforced matrix which is related to absent of local damage in the matrix (interface debonding)[51]. As discussed in the texture section, the texture intensity is significant in understanding the influence of Ti particulates on matrix tensile properties. In general, Mg alloys deformed by different dislocations slips systems and twinning which associated with critical resolved shear stress (CRSS) which depend on the orientation of the crystal.

Heat treatment, at 400 C for 12 h in atmospheric argon, was conducted on ARBed samples to reveal the texture and SRX effect on the tensile properties. Subsequent annealing produces a 5% decrease in the UTS and YS, and simultaneously the elongation increased up to 24.2 and 29.1 for the Mg-0 and Mg-2.3Ti composite in comparison to the ARBed samples, respectively. Figure 4.6 shows that annealing led to decrease in the texture intensity of the basal when compared with as-ARBed the basal texture intensity. As discussed in the previous section, the SRX has the major role in softening the metal composite matrix. Improvement in the elongation following the heat treatment is consistent with the texture evolution and matrix internal stresses relief. Comparing to the initial AZ31, the results showed a decrease in yield strength and an increase in the elongation to fracture. The UTS is higher than the initial AZ31 while the YS shows a sharp decrease. The

mechanical of properties were enhanced by adding 2.3wt. % of Ti; ultimate tensile strength by 7%, and elongation by 62%, while the yield strength was dropped by 36%. Also, the YS of the reinforced composite is lower than the unreinforced (AZ31-0 Ti), which agrees with the results reported by Pe´rez-Prado et al.[50]. Hence, the change in mechanical properties upon heat treatment, especially the increase in ductility with a small decrease of strengths, can be attributed to (a) relief of residual stresses in the matrix around the Ti particles, (b) an increase in the average grain size, and (c) a reduction of the basal texture intensity due to SRX. Based on the above results, the ARB followed by heat treatment strongly contributed to the enhancement in the strength and ductility of the composites compared with AZ31.

Table 4.1 summarized the available tensile properties and their fabrication methods for AZ31 and pure Mg- base composites with reinforcements by hard and ductile particles such as SiC, Al_2O_3, and Ti. From the table 1, it can be seen that ARB is a more significant process in making Mg-Ti composites than the other processes available in the literature.

Table 4.1. Comparison between this study and literature of Mg-Ti composite materials.

Material	Method of Preparation	0.2% YS (MPa)	UTS (MPa)	Elongation (%)
AZ31B		225	302	17.4
Mg-0 Ti	ARB	243	393	6.47
	ARB and annealed	175	324	24.2
Mg -2.3 Ti	ARB	255	399	5.3
	ARB and annealed	165	320	29.1
Mg-3.5 Ti	ARB	227	362	5
	ARB and annealed	161	295	19.6
Mg-4.9 Ti	ARB	220	350	4.3
	ARB and annealed	160	289	19.2
Mg-8.6 Ti [Present study]	ARB	197	348	4
	ARB and annealed	140	247	13.6
ZK51 [161]	Hot extrusion	229	315	8.5
ZK51-SiC		302	355	3.2
ZK51-Ti		295	386	16.9
Mg [50]	Hot extrusion	233±3	256±3	4±0.5
Mg-5Ti		201±5	223±10	5.5±1
Mg-10Ti		200±4	225	6±1
Mg-15Ti		196±5	215±8	5±1
Mg-0Ti[52]	Spark plasma sintering and hot extrusion	182	223	14.3
Mg-1Ti		180	221	16.1
Mg-3Ti		184	224	14.9
Mg-5Ti		179	218	15.5
AZ31B/ Al_2O_3[162]	Hot extrusion	204±8	317±5	22±2.4
AZ31 matrix [145] AZ31-SiC	Hot rolling	208 258	269 308	16.9 5.4

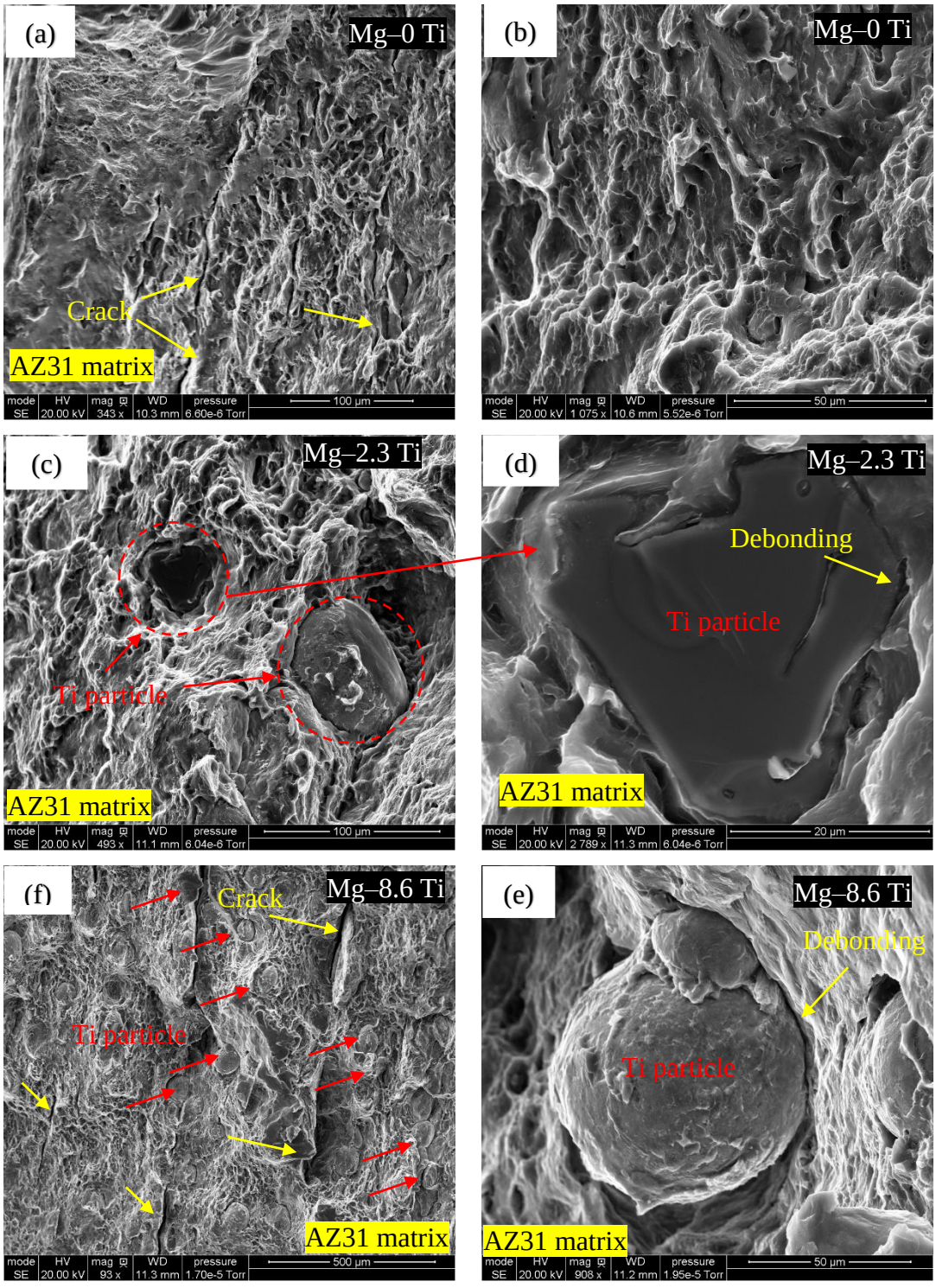

Figure 4.9 SEM of factured surface of tensile test samples for heat treated sample: (a-b) Mg–0 Ti, (c-d) Mg–2.3 Ti, and (e-f) Mg–8.6 Ti.

In addition, the tensile properties of the composites after heat treatment are superior to those of the Mg alloys such as pure Mg, and ZK51, and AZ31 alloys made by extrusion and rolled condition.

Further analysis needs to be done to test these materials for corrosion, damping, fatigue, and high temperature tensile. Studying the electrochemical property can provide a better understanding of using the Mg-Ti composite materials for biomedical applications.

4.4.5. Fracture behavior

Fracture surface investigation was conducted on the fractured tensile samples which provide a deep understanding of fracture mechanisms of the composite materials. Figure 4.9 shows the fractured surface for heat treated Mg-0 Ti, Mg-2.3 Ti, and Mg-8.6 Ti. The fractured surfaces show dimples formed in the AZ31matrix and debonding of Ti particles, suggesting ductile fracture. The dimples on the fracture surface represent the plasticity of the AZ31 matrix after heat treatment which is consistent with the ductility results obtained from tensile testing (figure 4.8).

The Ti particles in Mg-2.3 Ti and Mg-8.6 Ti samples are observed at the fractured surface. This means that there is poor bonding between the Ti particles and AZ31 matrix. This led to the fracture of the composite at low tensile strength values due to limited load transfer between the matrix and Ti particles. However, the Mg-2.3 Ti sample (figure 4.9 d) shows that cracks extended from the Mg-matrix into the Ti particle. This indicates load

transfer from the AZ31 matrix to the Ti particle which increases the ductility of the composite due to large stresses carried by the Ti particles. This behavior shows the benefit of introducing ductile reinforcements to the AZ31 matrix in comparison to that of those hard particles reinforcements [163, 164]. In this research, the fracture pattern is consistent with previous research [22, 52, 153, 159, 165].

4.5. Conclusions

The Ti particle dispersion AZ31 was successfully processed through ARB process. The microstructure and mechanical properties were evaluated. The results can be summarized as follows:

1. Mg-Ti composite materials with different Ti content (Mg–0 to Mg–8.6 Ti) can successfully be made by ARB. Addition of Ti particles improves the UTS, 0.2%YS, and degrades the ductility of the composite for as-ARBed condition, whereas post heat treatment leads to significant decrees of the UTS, 0.2% YS and a significant increase of the ductility to fracture.
2. Detailed texture studies using EBSD analysis revealed recrystallization and residual stress relieve due to heat treatment when compared to the as-ARBed (non-heat treated composites).
3. Mechanical properties of the heat treated composites showed a significant increase in ductility with a reduction in yield strength which is caused by texture weakening due to matrix recrystallization.
4. Ti particle reinforced magnesium and its alloys can be superior to that of using hard reinforcing particles such as SiC and Al_2O_3.
5. The fracture of Ti particles was the main failure mechanism in the Mg/Ti composites.
6. Ti particles could be used as ductile reinforcement for the ductility of magnesium matrix composite materials.

CHAPTER 5. Conclusion and Future Work

5.1. Overall Conclusions

The present research contributes to the understanding of the Mg-Ti composite materials and develops new lightweight materials. The composite materials were prepared through cladding, multi-layered, and Ti particles addition to AZ31-Mg alloy matrix. The Mg-Ti sheets were processed successfully with the single-pass hot roll-bonding (RB) and accumulative roll-bonding (ARB). The microstructure and texture evaluation were investigated, and the mechanical properties were evaluated using microhardness and tensile tests at room temperature. The conclusions drawn from this research are:

5.1.1. Ti/AZ31 multilayer structures

1. Plastic deformation (rolling deformation) and heat treatment cannot cause the formation of intermetallic compounds near the AZ31/Ti interface.
2. There exists inter-diffusion of Ti, Mg, and Al across the AZ31/Ti interface, which is driven by the concentration gradient. The plastic deformation associated with the thickness reduction enhances the inter-diffusion.
3. The thickness of the inter-diffusion layer increases with the increase of the annealing time and the thickness reduction.
4. The indentation hardness of the AZ31 plates in the sandwiched structures decreases with increasing annealing time due to the grain growth and the decrease in the dislocation density.
5. For the same heat-treated sandwiched structures, the bonding strength increases with thickness reduction; for the same sandwiched structures, the bonding strength increases with increasing annealing time and temperature.
6. Under tensile loading, the AZ31 plate fails first in the sandwiched structures.

5.1.2. Titanium Clad-AZ31 Magnesium

1. The single-pass hot-rolling and annealing heat treatment is a successful way of fabricating lightweight Ti/AZ31/Ti clad sheets with excellent corrosion resistance and mechanical properties.

2. The tensile test was performed at RT for as-rolled and annealed clad sheets; the tensile test results can be correlated with the changes in the microstructure and texture caused by heat treatment.
3. The AZ31 layer controlled the tensile properties of the clad sheets since it was the major component of the clad sheet. The clad sheets showed strong basal texture in the AZ31 layer due to twins and shear bands.
4. The shear bands were caused by the strain localization which leads to failure of the sheets at lower elongation. The texture of the AZ31 layer was significantly improved after the heat treatment (i.e., SRX) at 400 ◦C for 12h.
5. The clad sheets elongation was improved by heat treatment. This can be explained by the texture evolution in the AZ31 layer and interfacial bonding strength between Ti and AZ31. The sheet II showed the best mechanical properties with the YS, UTS, and elongation reaching 215MPa, 313MPa, and 35% respectively in the RD and 240 MPa, 306 MPa and 26 % respectively in the 26.46 TD.

5.1.3. Ti particles reinforced AZ31-Mg alloy matrix composites

1. Mg-Ti composite materials with different Ti content (Mg–0 to Mg–8.6 Ti) can successfully be produced via (ARB). Addition of Ti particles improves the UTS, 0.2%YS, but degrades the ductility of the composite for ARBed condition, whereas post heat treatment leads to significant improvement in the UTS, 0.2% YS and a significant increase in the ductility to fracture.
2. Detailed texture studies using EBSD analysis revealed recrystallization and residual stress relieve due to heat treatment when compared to the as-ARBed (non-heat treated composite).
3. Mechanical properties for heat treated composite showed a significant increase in ductility values with a reduction in yield strength which is related to texture weakening due to matrix recrystallization.
4. Ti particle reinforced magnesium and its alloys can be superior to that of hard reinforcing particles such as SiC and Al_2O_3.
5. Fracture surface characterization the Mg/Ti composites revealed that Ti particle fracture was the main failure mechanism.

6. Ti particles could be used as ductile reinforcement for the ductility of magnesium matrix composites materials.

5.2. Recommendations for future work

In the current study, Mg-Ti materials are produced using severe plastic deformation techniques followed by heat treatment. The results showed that mechanical properties were improved due to the changes in the texture of AZ31 matrix and Ti as ductile dispersions.

Further investigation are recommended to develop this composite material. Future work can be divided into the following research areas:

1. The bonding strength of the Mg/Ti can be significantly influenced by reduction percentage and post heat treatment. Future studies should focus on the development of heat treatment temperature and time, in which the bonding strength of the Mg/Ti interface can be optimized.
2. Formability of the Mg-Ti at an elevated temperature should be investigated.
3. The effect of adding an intermediate layer (aluminum or zirconium) between AZ31 and Ti on the bonding strength should be studied.
4. The microstructure and texture of Mg/Ti interface should be investigated for deep understanding the structural failure during the uniaxial tensile test; strain and energy transfer through the AZ31/Ti interface.
5. The structural design effect of Mg-Ti should be optimized to find the ideal combination of multilayers Mg-Ti for engineering applications.
6. Corrosion behavior of Mg-Ti should be investigated.

Bibliography

1. Danaie, M., et al., *Hydrogen storage in bulk Mg–Ti and Mg–stainless steel multilayer composites synthesized via accumulative roll-bonding (ARB).* International Journal of Hydrogen Energy, 2011. **36**(4): p. 3022-3036.
2. Choi, Y.J., et al., *Hydrogen storage properties of the Mg–Ti–H system prepared by high-energy–high-pressure reactive milling.* Journal of Power Sources, 2008. **180**(1): p. 491-497.
3. Choi, Y.J., et al., *Chemical vapor synthesis of Mg–Ti nanopowder mixture as a hydrogen storage material.* International Journal of Hydrogen Energy, 2009. **34**(18): p. 7700-7706.
4. Hoffmann, I., et al., *Mg-Ti: A Possible Biodegradable, Biocompatible, Mechanically Matched Material for Temporary Implants.* MRS Proceedings, 2011. **1301**.
5. Song, G.-L., et al., *The corrosion and passivity of sputtered Mg–Ti alloys.* Corrosion Science, 2016. **104**: p. 36-46.
6. Hansen, N., *Dispersion strengthening of aluminium-aluminium-oxide products.* Acta Metallurgica, 1970. **18**(1): p. 137-145.
7. Eizadjou, M., H. Danesh Manesh, and K. Janghorban, *Mechanism of warm and cold roll bonding of aluminum alloy strips.* Materials & Design, 2009. **30**(10): p. 4156-4161.
8. Jamaati, R. and M.R. Toroghinejad, *Investigation of the parameters of the cold roll bonding (CRB) process.* Materials Science and Engineering: A, 2010. **527**(9): p. 2320-2326.
9. Aklh YAHIRO , T.M., Takeshl YOSHIDA ,Takeshl YOSHIDA, *Developmentof Nonferrous Clad Plate and Sheet by warmRolling with Different Temperatureof Materials.* ISIJ Intemational 1991. **31**(6): p. 647-654.
10. Eizadjou, M., H. Danesh Manesh, and K. Janghorban, *Investigation of roll bonding between aluminum alloy strips.* Materials & Design, 2008. **29**(4): p. 909-913.
11. Li, L., K. Nagai, and F. Yin, *Progress in cold roll bonding of metals.* Sci Technol Adv Mater, 2008. **9**(2): p. 023001.

12. Tsuji, N., et al., *ARB (Accumulative Roll-Bonding) and other new Techniques to Produce Bulk Ultrafine Grained Materials.* Advanced Engineering Materials, 2003. **5**(5): p. 338-344.
13. Azushima, A., Kopp, R., Korhonen, A., Yang, D. Y., Micari, F., Lahoti, G. D., ... & Yanagida, A., *Severe plastic deformation (SPD) processes for metals* CIRP Annals-Manufacturing Technology, 2008. **57**(2): p. 716-735.
14. Saito, Y., et al. "." 47.2 (1999): , *Novel ultra-high straining process for bulk materials—development of the accumulative roll-bonding (ARB) process.* Acta materialia, 1999. **47**(2): p. 579-583.
15. Su, L., Lu, C., Deng, G., Tieu, K., & Sun, X. , *Microstructure and mechanical properties of 1050/6061 laminated composite processed by accumulative roll bonding.* Adv. Mater. Sci, 2013. **33**: p. 33-37.
16. Wu, K., et al., *Microstructure and mechanical properties of the Mg/Al laminated composite fabricated by accumulative roll bonding (ARB).* Materials Science and Engineering: A, 2010. **527**(13-14): p. 3073-3078.
17. Tsuji, N., Saito, Y., Lee, S. H., & Minamino, Y., *ARB (Accumulative Roll-Bonding) and other new techniques to produce bulk ultrafine grained materials.* Advanced Engineering Materials 2003. **5**(5): p. 338-344.
18. Hoffmann, I., *MAGNESIUM-TITANIUM ALLOYS FOR BIOMEDICAL APPLICATIONS.* 2014.
19. Esen, Z., et al., *Titanium–magnesium based composites: Mechanical properties and in-vitro corrosion response in Ringer's solution.* Materials Science and Engineering: A, 2013. **573**: p. 119-126.
20. J. G. ZHENG, P.G.P., J. W.STEEDS, *Microstructure of vapour quenched Ti–29wt% Mg alloy solid solution.* JOURNAL OF MATERIALS SCIENCE, (1997) **32**: p. 3089 — 3099.
21. Takumi Haruna, D.M., Yuichi Nakagawa, Naoji Yamashita and Toshio Oishi, *Corrosion Resistance of TitaniumMagnesium Alloy in Weak Acid Solution Containing Fluoride Ions.* Materials Transactions, 2013. **54**(2): p. 143 - 148.
22. Pérez, P., G. Garcés, and P. Adeva, *Mechanical properties of a Mg–10 (vol.%)Ti composite.* Composites Science and Technology, 2004. **64**(1): p. 145-151.

23. Phasha, M., K. Maweja, and C. Babst, *Mechanical alloying by ball milling of Ti and Mg elemental powders: Operation condition considerations.* Journal of Alloys and Compounds, 2010. **492**(1-2): p. 201-207.
24. Aonuma, M. and K. Nakata, *Effect of alloying elements on interface microstructure of Mg–Al–Zn magnesium alloys and titanium joint by friction stir welding.* Materials Science and Engineering: B, 2009. **161**(1-3): p. 46-49.
25. Commin, L., et al., *Friction stir welding of AZ31 magnesium alloy rolled sheets: Influence of processing parameters.* Acta Materialia, 2009. **57**(2): p. 326-334.
26. Liu, L., D. Ren, and F. Liu, *A Review of Dissimilar Welding Techniques for Magnesium Alloys to Aluminum Alloys.* Materials, 2014. **7**(5): p. 3735-3757.
27. Tan, C., et al., *Microstructure and mechanical properties of laser welded-brazed Mg/Ti joints with AZ91 Mg based filler.* Materials & Design, 2016. **99**: p. 127-134.
28. Topic, I., H.W. Höppel, and M. Göken, *Friction stir welding of accumulative roll-bonded commercial-purity aluminium AA1050 and aluminium alloy AA6016.* Materials Science and Engineering: A, 2009. **503**(1-2): p. 163-166.
29. Xu, C., et al., *Tungsten Inert Gas Welding–Brazing of AZ31B Magnesium Alloy to TC4 Titanium Alloy.* Journal of Materials Science & Technology, 2016. **32**(2): p. 167-171.
30. Chang, H., et al., *Microstructure and mechanical properties of the Mg/Al multilayer fabricated by accumulative roll bonding (ARB) at ambient temperature.* Materials Science and Engineering: A, 2012. **543**: p. 249-256.
31. Nie, H., et al., *Texture Evolution of Single-Pass Hot-Rolled 5052/AZ31/5052 Clad Sheets.* Jom, 2016.
32. Kawamoto, H., et al., *Analysis of Strain Transfer through the Mg/Ti Interface Using Crystallographic Orientation Analysis Based on Electron Back-Scattered Diffraction Patterns.* Materials Transactions, 2008. **49**(5): p. 1107-1111.
33. Florina D. Dumitru1, G.D., Oscar F. Higuera-Cobos2 and José M. Cabrera-Marrero3,4, *Effect of severe plastic deformation on an extruded ZK60 magnesium alloy.* 2016.

34. Asano, K., H. Enoki, and E. Akiba, *Synthesis process of Mg–Ti BCC alloys by means of ball milling.* Journal of Alloys and Compounds, 2009. **486**(1-2): p. 115-123.

35. Luque, A., M. Ghazisaeidi, and W.A. Curtin, *Deformation modes in magnesium (0001) and (0 1 ¯11) single crystals: simulations versus experiments.* Modelling and Simulation in Materials Science and Engineering, 2013. **21**(4): p. 045010.

36. Kim, H.K. and W.J. Kim, *Microstructural instability and strength of an AZ31 Mg alloy after severe plastic deformation.* Materials Science and Engineering: A, 2004. **385**(1-2): p. 300-308.

37. Miyahara, Y., Z. Horita, and T.G. Langdon, *Exceptional superplasticity in an AZ61 magnesium alloy processed by extrusion and ECAP*. Materials Science and Engineering: A, 2006. **420**(1-2): p. 240-244.

38. del Valle, J.A., F. Carreño, and O.A. Ruano, *Influence of texture and grain size on work hardening and ductility in magnesium-based alloys processed by ECAP and rolling.* Acta Materialia, 2006. **54**(16): p. 4247-4259.

39. Zhan, M.Y., et al., *Microstructure and mechanical properties of Mg–Al–Zn alloy sheets severely deformed by accumulative roll-bonding.* Journal of Materials Science, 2007. **42**(22): p. 9256-9261.

40. Yang, H.J., et al., *EBSD Study on Deformation Twinning in AZ31 Magnesium Alloy During Quasi-in-Situ Compression.* Advanced Engineering Materials, 2008. **10**(10): p. 955-960.

41. Alaneme, K.K. and E.A. Okotete, *Enhancing plastic deformability of Mg and its alloys—A review of traditional and nascent developments.* Journal of Magnesium and Alloys, 2017. **5**(4): p. 460-475.

42. Ion, S.E., F. J. Humphreys, and S. H. White. , *Dynamic recrystallisation and the development of microstructure during the high temperature deformation of magnesium.* Acta Metallurgica 1982. **30**(10): p. 1909-1919.

43. del Valle, J.A., M.T. Pérez-Prado, and O.A. Ruano, *Texture evolution during large-strain hot rolling of the Mg AZ61 alloy.* Materials Science and Engineering: A, 2003. **355**(1-2): p. 68-78.

44. Hoseini, M., et al., *Comparative effect of grain size and texture on the corrosion behaviour of commercially pure titanium processed by equal channel angular pressing.* Corrosion Science, 2009. **51**(12): p. 3064-3067.
45. Aung, N.N. and W. Zhou, *Effect of grain size and twins on corrosion behaviour of AZ31B magnesium alloy.* Corrosion Science, 2010. **52**(2): p. 589-594.
46. Hamu, G.B., D. Eliezer, and L. Wagner, *The relation between severe plastic deformation microstructure and corrosion behavior of AZ31 magnesium alloy.* Journal of Alloys and Compounds, 2009. **468**(1-2): p. 222-229.
47. Guo, Q., et al., *Grain refinement in as-cast AZ80 Mg alloy under large strain deformation.* Materials Characterization, 2007. **58**(2): p. 162-167.
48. Jin, L., et al., *Mechanical properties and microstructure of AZ31 Mg alloy processed by two-step equal channel angular extrusion.* Materials Letters, 2005. **59**(18): p. 2267-2270.
49. Hiroaki Kawamoto, S.M., Kaori Yano, Kenji Ohkubo and Tetsuo Mohri, *Analysis of Strain Transfer through the Mg/Ti Interface Using Crystallographic Orientation Analysis Based on Electron Back-Scattered Diffraction Patterns.* Materials Transactions, 2008. **49**(5): p. 1107 -1111.
50. Pérez, P., *Influence of titanium volume fraction on the mechanical properties of Mg–Ti composites.* International journal of materials research, 2009. **100**(3): p. 366-369.
51. S.F. Hassan, M.G., *D evelopment of ductile magnesium composite materials using titanium as reinforcement.* Journal of Alloys and Compounds 2002. **345** p. 246–251.
52. Junko Umeda, M.K., Katsuyoshi Kondoh *, EL-Sayed Ayman, Hisashi Imai, *Microstructural and mechanical properties of titanium particulate reinforced magnesium composite materials.* Materials Chemistry and Physics, 2010. **123**: p. 649-657.
53. Kitazono, K., Susumu Komatsu, and Yuki Kataoka. , *Mechanical properties of titanium particles dispersed magnesium matrix composite produced through accumulative diffusion bonding process.* Materials transactions, 2011. **52**(2): p. 155-158.

54. Alam, M.E., et al., *Improving microstructural and mechanical response of new AZ41 and AZ51 magnesium alloys through simultaneous addition of nano-sized Al2O3 particulates and Ca.* Journal of Alloys and Compounds, 2013. **574**: p. 565-572.
55. Meenashisundaram, G.K. and M. Gupta, *Low volume fraction nano-titanium particulates for improving the mechanical response of pure magnesium.* Journal of Alloys and Compounds, 2014. **593**: p. 176-183.
56. Teng, X., et al., *Micro-machinability of nanoparticle-reinforced Mg-based MMCs: an experimental investigation.* The International Journal of Advanced Manufacturing Technology, 2016.
57. Kumar, A., et al., *Improved Compressive, Damping and Coefficient of Thermal Expansion Response of Mg–3Al–2.5La Alloy Using Y2O3 Nano Reinforcement.* Metals, 2017. **7**(3): p. 104.
58. Dai, J.H., et al., *First principles study on stability and hydrogen adsorption properties of Mg/Ti interface.* Phys Chem Chem Phys, 2015. **17**(25): p. 16594-600.
59. Ozgur Duygulu, A.A.K., Gizem Oktay,and Filiz Cinar Sahin, *Diffusion Bonding of Magnesium, Zirconium and Titanium as Implant Material* Materials Science Forum 2007. **546**(549): p. 417-420.
60. Motevalli, P.D. and B. Eghbali, *Microstructure and mechanical properties of Tri-metal Al/Ti/Mg laminated composite processed by accumulative roll bonding.* Materials Science and Engineering: A, 2015. **628**: p. 135-142.
61. Gao, M., et al., *Dissimilar Ti/Mg alloy butt welding by fibre laser with Mg filler wire – preliminary study.* Science and Technology of Welding and Joining, 2013. **16**(6): p. 488-496.
62. Dehsorkhi, R.N., F. Qods, and M. Tajally, *Investigation on microstructure and mechanical properties of Al–Zn composite during accumulative roll bonding (ARB) process.* Materials Science and Engineering: A, 2011. **530**: p. 63-72.
63. Jamaati, R. and M.R. Toroghinejad, *Manufacturing of high-strength aluminum/alumina composite by accumulative roll bonding.* Materials Science and Engineering: A, 2010. **527**(16-17): p. 4146-4151.

64. Mahdavian, M.M., L. Ghalandari, and M. Reihanian, *Accumulative roll bonding of multilayered Cu/Zn/Al: An evaluation of microstructure and mechanical properties.* Materials Science and Engineering: A, 2013. **579**: p. 99-107.
65. Mozaffari, A., H. Danesh Manesh, and K. Janghorban, *Evaluation of mechanical properties and structure of multilayered Al/Ni composites produced by accumulative roll bonding (ARB) process.* Journal of Alloys and Compounds, 2010. **489**(1): p. 103-109.
66. Y Saito, H.U., N Tsuji, T Sakai, *Novel ultra-high straining process for bulk materials—development of the accumulative roll-bonding (ARB) process. .* Acta materialia, 1999. **47.2**: p. 47.2.
67. Kim, J.-S., et al., *Improvement of interfacial bonding strength in roll-bonded Mg/Al clad sheets through annealing and secondary rolling process.* Materials Science and Engineering: A, 2015. **628**: p. 1-10.
68. Lee, J.E., et al., *Effects of annealing on the mechanical and interface properties of stainless steel/aluminum/copper clad-metal sheets.* Journal of Materials Processing Technology, 2007. **187-188**: p. 546-549.
69. Matsumoto, H., S. Watanabe, and S. Hanada, *Fabrication of pure Al/Mg–Li alloy clad plate and its mechanical properties.* Journal of Materials Processing Technology, 2005. **169**(1): p. 9-15.
70. Nagai, T., et al., *Development of dissimilar metal transition joint by hot roll bonding technique.* Nippon Genshiryoku Gakkai-Shi, 1994. **36**(12): p. 1137-1146.
71. Ma, M., X. Meng, and W. Liu, *Microstructure and Mechanical Properties of Ti/Al/Ti Laminated Composites Prepared by Hot Rolling.* Journal of Materials Engineering and Performance, 2017. **26**(7): p. 3569-3578.
72. Luo, J.-G. and V.L. Acoff, *Using cold roll bonding and annealing to process Ti/Al multi-layered composites from elemental foils.* Materials Science and Engineering: A, 2004. **379**(1-2): p. 164-172.
73. Ma, M., et al., *Microstructure and mechanical properties of Al/Ti/Al laminated composites prepared by roll bonding.* Materials Science and Engineering: A, 2015. **636**: p. 301-310.

74. Nie, H., et al., *Texture Evolution of Single-Pass Hot-Rolled 5052/AZ31/5052 Clad Sheets.* JOM, 2016. **68**(8): p. 2274-2287.
75. Pang, J.C., et al., *Mechanical properties of Ti–(SiCp/Al) laminated composite with nano-sized TiAl3 interfacial layer synthesized by roll bonding.* Materials Science and Engineering: A, 2013. **582**: p. 294-298.
76. Kashaev, N., et al., *Comparative study of mechanical properties using standard and micro-specimens of base materials Inconel 625, Inconel 718 and Ti-6Al-4V.* Journal of Materials Research and Technology, 2013. **2**(1): p. 43-47.
77. Pan, D., K. Gao, and J. Yu., *Cold roll bonding of bimetallic sheets and strips.* . Materials science and technology, 1989. **5**(9): p. 934-939.
78. Ohsaki, S., et al., *Bulk mechanical alloying of Cu–Ag and Cu/Zr two-phase microstructures by accumulative roll-bonding process.* Acta Materialia, 2007. **55**(8): p. 2885-2895.
79. Guo, L. and F. Fujita, *Influence of rolling parameters on dynamically recrystallized microstructures in AZ31 magnesium alloy sheets.* Journal of Magnesium and Alloys, 2015. **3**(2): p. 95-105.
80. Huang, Y., et al., *Dynamic recrystallization and mechanical properties of friction stir processed Mg-Zn-Y-Zr alloys.* Journal of Materials Processing Technology, 2017. **249**: p. 331-338.
81. Jäger, A., et al., *Influence of annealing on the microstructure of commercial Mg alloy AZ31 after mechanical forming.* Materials Science and Engineering: A, 2006. **432**(1-2): p. 20-25.
82. Guan, D.R., W. MarkMa, Le Wynne, Brad Gao, Jun heng, *Twin recrystallization mechanisms and exceptional contribution to texture evolution during annealing in a magnesium alloy.* Acta Materialia, 2017. **126**: p. 132-144.
83. Fatemi-Varzaneh, S.M., A. Zarei-Hanzaki, and J.M. Cabrera, *Shear banding phenomenon during severe plastic deformation of an AZ31 magnesium alloy.* Journal of Alloys and Compounds, 2011. **509**(9): p. 3806-3810.
84. Sauvage, X., G. P. Dinda, and Gerhard Wilde., *Non-equilibrium intermixing and phase transformation in severely deformed Al/Ni multilayers.* Scripta Materialia, 2007. **56**(3): p. 181-184.

85. Habibnejad-Korayem, M., R. Mahmudi, and W.J. Poole, *Enhanced properties of Mg-based nano-composites reinforced with Al2O3 nano-particles.* Materials Science and Engineering: A, 2009. **519**(1-2): p. 198-203.
86. Asadi, P., G. Faraji, and M.K. Besharati, *Producing of AZ91/SiC composite by friction stir processing (FSP).* The International Journal of Advanced Manufacturing Technology, 2010. **51**(1-4): p. 247-260.
87. Chang, H., et al., *Texture evolution of the Mg/Al laminated composite fabricated by the accumulative roll bonding.* Scripta Materialia, 2009. **61**(7): p. 717-720.
88. Peláez, D., et al., *Mechanical and microstructural evolution of Mg AZ31 alloy using ECASD process.* Journal of Materials Research and Technology, 2015. **4**(4): p. 392-397.
89. Pripanapong, P., Umeda, J., Imai, H., Takahashi, M., & Kondoh, K. , *Tensile Strength of Ti/Mg Alloys Dissimilar Bonding Material Fabricated by Spark Plasma Sintering.* . International Journal of Engineering Innovations and Research, 2016. **5**(4): p. 253.
90. Tan, C., et al., *Enhanced interfacial reaction and mechanical properties of laser welded-brazed Mg/Ti joints with Al element from filler.* Materials Letters, 2016. **167**: p. 38-42.
91. Pripanapong, P., et al., *Corrosion Behavior and Strength of Dissimilar Bonding Material between Ti and Mg Alloys Fabricated by Spark Plasma Sintering.* Materials (Basel), 2016. **9**(8).
92. Sheng, L.Y., Fang Yang, T. F. Xi, Chen Lai, and H. Q. Ye, *Influence of heat treatment on interface of Cu/Al bimetal composite fabricated by cold rolling.* Composites Part B: Engineering, 2011. **42**(6): p. 1468-1473.
93. Nie, H., et al., *The Microstructure, Texture and Mechanical Properties of the Rolled Al/Mg/Al Clad Sheets.* Journal of Materials Engineering and Performance, 2016. **25**(11): p. 4695-4705.
94. Çetin, A., et al., *Laminated Metal Composites by Infiltration.* Metallurgical and Materials Transactions A, 2011. **42**(11): p. 3509-3520.

95. Inoue, H., M. Ishio, and T. Takasugi, *Texture, Tensile Properties and Press Formability of Mg-3Al-1Zn/Ti Clad Sheets Produced by Roll-Bonding.* Materials Science Forum, 2005. **495-497**: p. 645-650.

96. Inoue, H., *Mechanical Properties and Formability of Titanium-Clad Magnesium Alloy Sheets.* Proceedings of the 8th Pacific Rim International Congress on Advanced Materials and Processing., 2013. **Springer, Cham**: p. 1109-1114.

97. Liu, H.S., Zhang, B., & Zhang, G. P . , *Microstructures and mechanical properties of Al/Mg alloy multilayered composites produced by accumulative roll bonding.* Journal of Materials Science & Technology, 2011. **27**(1): p. 15-21.

98. Wei, Y., et al., *Formation process of the bonding joint in Ti/Al diffusion bonding.* Materials Science and Engineering: A, 2008. **480**(1-2): p. 456-463.

99. Liu, C., et al., *Polishing-assisted galvanic corrosion in the dissimilar friction stir welded joint of AZ31 magnesium alloy to 2024 aluminum alloy.* Materials Characterization, 2009. **60**(5): p. 370-376.

100. Vander Voort, G.F., Steven R. Lampman, Bonnie R. Sanders, Gayle J. Anton, Carol Polakowski, Jill Kinson, Kathryn Muldoon, Scott D. Henry, and William W. Scott Jr. , *ASM handbook." Metallography and microstructures 9.* ASM handbook, 2004. **9**: p. 44073-0002.

101. Kim, J.S., et al., *Novel strip-cast Mg/Al clad sheets with excellent tensile and interfacial bonding properties.* Sci Rep, 2016. **6**: p. 26333.

102. Qiao, Y., et al., *Microstructures, Textures and Mechanical Properties Evolution during Cold Drawing of Pure Mg.* Microscopy Research, 2013. **01**(02): p. 8-15.

103. Sun, H.-F., Shu-Jin Liang, and Er-De Wang, *Mechanical properties and texture evolution during hot rolling of AZ31 magnesium alloy.* Transactions of Nonferrous Metals Society of China, 2009. **19**: p. 349-354.

104. Sun, H.F., Liang, S. J., & Wang, E. D., *Mechanical properties and texture evolution during hot rolling of AZ31 magnesium alloy. .* Transactions of Nonferrous Metals Society of China, 2009. **19**: p. 349-354.

105. Hamad, K. and Y.G. Ko, *A cross-shear deformation for optimizing the strength and ductility of AZ31 magnesium alloys.* Sci Rep, 2016. **6**: p. 29954.

106. Tan, J.C., and M. J. Tan. , *Dynamic continuous recrystallization characteristics in two stage deformation of Mg–3Al–1Zn alloy sheet.* Materials Science and Engineering: A, 2003. **339**(124-132).
107. Jia, W.P., et al., *Texture evolution of AZ31 magnesium alloy sheets during warm rolling.* Journal of Alloys and Compounds, 2015. **645**: p. 70-77.
108. Wang, Y., et al., *Formation and microstructure of shear bands during hot rolling of a Mg–6Zn–0.5Zr alloy plate with a basal texture.* Journal of Alloys and Compounds, 2015. **644**: p. 147-154.
109. Sandlöbes, S., et al., *The relation between ductility and stacking fault energies in Mg and Mg–Y alloys.* Acta Materialia, 2012. **60**(6-7): p. 3011-3021.
110. Shi, Z.-Z. and X.-F. Liu, *Characteristics of cross grain boundary contraction twin pairs and bands in a deformed Mg alloy.* Journal of Alloys and Compounds, 2017. **692**: p. 274-279.
111. Chun, Y.B. and C.H.J. Davies, *Texture effects on development of shear bands in rolled AZ31 alloy.* Materials Science and Engineering: A, 2012. **556**: p. 253-259.
112. Yan, H., et al., *Twins, shear bands and recrystallization of a Mg–2.0%Zn–0.8%Gd alloy during rolling.* Scripta Materialia, 2011. **64**(2): p. 141-144.
113. Baldi, A., et al., *Mg/Ti multilayers: Structural and hydrogen absorption properties.* Physical Review B, 2010. **81**(22).
114. Rousselot, S., D. Guay, and L. Roué, *Synthesis of fcc Mg–Ti–H alloys by high energy ball milling: Structure and electrochemical hydrogen storage properties.* Journal of Power Sources, 2010. **195**(13): p. 4370-4374.
115. Lei, X., et al., *Microstructure and Mechanical Properties of Magnesium Alloy AZ31 Processed by Compound Channel Extrusion.* Materials Transactions, 2011. **52**(6): p. 1082-1087.
116. Choi, S., E. Shin, and B. Seong, *Simulation of deformation twins and deformation texture in an AZ31 Mg alloy under uniaxial compression.* Acta Materialia, 2007. **55**(12): p. 4181-4192.
117. Tan, J.C., and M. J. Tan. , *"Dynamic continuous recrystallization characteristics in two stage deformation of Mg–3Al–1Zn alloy sheet.".* Materials Science and Engineering A319–321 (2001), 2003. **339**(1): p. 124-132.

118. Guan, D.R., W. Mark Gao, Junheng Sharp, Joanne Wynne, Brad Ma, Le, *Individual effect of recrystallisation nucleation sites on texture weakening in a magnesium alloy: Part 1- double twins.* Acta Materialia, 2017. **135**: p. 14-24.

119. Yan, H., R.S. Chen, and E.H. Han, *Room-temperature ductility and anisotropy of two rolled Mg–Zn–Gd alloys.* Materials Science and Engineering: A, 2010. **527**(15): p. 3317-3322.

120. Kaiser, F., Bohlen, J., Letzig, D., Kainer, K. U., Styczynski, A., & Hartig, C. , *Influence of rolling conditions on the microstructure and mechanical properties of magnesium sheet AZ31*. . Advanced Engineering Materials, 2003. **5**(12): p. 891-896.

121. Niknejad, S., S. Esmaeili, and N.Y. Zhou, *The role of double twinning on transgranular fracture in magnesium AZ61 in a localized stress field.* Acta Materialia, 2016. **102**: p. 1-16.

122. Barnett, M.R., *Twinning and the ductility of magnesium alloys.* Materials Science and Engineering: A, 2007. **464**(1-2): p. 8-16.

123. Luo, D., et al., *Effect of Rolling Route on Microstructure and Tensile Properties of Twin-Roll Casting AZ31 Mg Alloy Sheets.* Materials (Basel), 2016. **9**(6).

124. Qin, Y., et al., *Microstructure and texture evolution in multi-pass warm rolled AZ31 magnesium alloy.* MATEC Web of Conferences, 2015. **21**: p. 03003.

125. Miao, Q., et al., *Fabrication of excellent mechanical properties AZ31 magnesium alloy sheets by conventional rolling and subsequent annealing.* Materials Science and Engineering: A, 2011. **528**(22-23): p. 6694-6701.

126. Chao, H.Y., et al., *Static recrystallization kinetics of a heavily cold drawn AZ31 magnesium alloy under annealing treatment.* Materials Characterization, 2011. **62**(3): p. 312-320.

127. Li, J.Y., et al., *Effects of Annealing Treatment on Texture and Stamping Properties of AZ31 Magnesium Alloy.* Materials Science Forum, 2011. **686**: p. 101-106.

128. Singh, A.K., and R. A. Schwarzer., *Texture and anisotropy of mechanical properties in titanium and its alloys.* Z. Metallkd, 2000. **91**(9): p. 702.

129. Dragomir, I.C., et al., *Evolution of dislocation density and character in hot rolled titanium determined by X-ray diffraction.* Materials Characterization, 2005. **55**(1): p. 66-74.
130. Bouhattate, J., et al., *Texture Prediction of Cold- and Hot-Rolled Titanium Using Processing Path Model.* Journal of Materials Engineering and Performance, 2010. **20**(2): p. 177-184.
131. Ko, Y.G. and K. Hamad, *Structural features and mechanical properties of AZ31 Mg alloy warm-deformed by differential speed rolling.* Journal of Alloys and Compounds, 2018. **744**: p. 96-103.
132. Lu, L., et al., *Effect of annealing on microstructure evolution and mechanical property of cold forged magnesium pipes.* Materials & Design, 2012. **39**: p. 131-139.
133. Yang, D., et al., *Ultrafine equiaxed-grain Ti/Al composite produced by accumulative roll bonding.* Scripta Materialia, 2010. **62**(5): p. 321-324.
134. Maier, V., H.W. Höppel, and M. Göken, *Nanomechanical behaviour of Al-Ti layered composites produced by accumulative roll bonding.* Journal of Physics: Conference Series, 2010. **240**: p. 012108.
135. Feng, B., et al., *On the rule of mixtures for bimetal composites.* Materials Science and Engineering: A, 2017. **704**: p. 173-180.
136. Huang, M., et al., *Revealing extraordinary tensile plasticity in layered Ti-Al metal composite.* Sci Rep, 2016. **6**: p. 38461.
137. Hidetoshi Somekawa, H.H., Hiroyuki Watanabe , Kenji Higashi *Diffusion bonding in superplastic magnesium alloys.* Materials Science and Engineering, 2003. **A339**: p. 328-333.
138. Britton, T.B., F.P.E. Dunne, and A.J. Wilkinson, *On the mechanistic basis of deformation at the microscale in hexagonal close-packed metals.* Proceedings of the Royal Society A: Mathematical, Physical and Engineering Science, 2015. **471**(2178): p. 20140881.
139. Yang, Q., et al., *Effect of Multi-Pass Bending Deformation on Microstructure Evolution and Mechanical Properties of AZ31 Alloy Sheet.* Materials Research, 2016. **19**(2): p. 322-327.

140. Meiyan, Z.H.A.N., L. I. Chunming, and Datong ZHANG Weiwen ZHANG. , *Processing of AZ31 magnesium alloy by accumulative roll-bonding at gradient temperature.* Acta Metallurgica Sinica (English letters), 2012. **25**(1): p. 65-75.
141. Wang, Q.D., Chen, Y. J., Lin, J. B., Zhang, L. J., & Zhai, C. Q. , *Microstructure and properties of magnesium alloy processed by a new severe plastic deformation method.* Materials Letters, 2007. **61**(23): p. 4599-4602.
142. ZHAN, M.-y., Yuan-yuan LI, and Wei-ping CHEN., *Improving mechanical properties of Mg-Al-Zn alloy sheets through accumulative roll-bonding.* Transactions of Nonferrous Metals Society of China, 2008. **18**(2): p. 309-314.
143. Pérez-Prado, M.T., J.A. del Valle, and O.A. Ruano, *Effect of sheet thickness on the microstructural evolution of an Mg AZ61 alloy during large strain hot rolling.* Scripta Materialia, 2004. **50**(5): p. 667-671.
144. Reddy, M.P., et al., *Enhanced performance of nano-sized SiC reinforced Al metal matrix nanocomposites synthesized through microwave sintering and hot extrusion techniques.* Progress in Natural Science: Materials International, 2017.
145. Wang, X., et al., *Microstructural modification and strength enhancement by SiC nanoparticles in AZ31 magnesium alloy during hot rolling.* Materials Science and Engineering: A, 2018. **715**: p. 49-61.
146. Kumar, P., et al., *Strength of Mg–3%Al alloy in presence of graphene nano-platelets as reinforcement.* Materials Science and Technology, 2018: p. 1-10.
147. Xiuqing, Z., et al., *The mechanical properties of magnesium matrix composites reinforced with (TiB2+TiC) ceramic particulates.* Materials Letters, 2005. **59**(17): p. 2105-2109.
148. Paramsothy, M., et al., *Enhancing tensile/compressive response of magnesium alloy AZ31 by integrating with Al2O3 nanoparticles.* Materials Science and Engineering: A, 2009. **527**(1-2): p. 162-168.
149. Liu, H.S., B. Zhang, and G.P. Zhang, *Microstructures and Mechanical Properties of Al/Mg Alloy Multilayered Composites Produced by Accumulative Roll Bonding.* Journal of Materials Science & Technology, 2011. **27**(1): p. 15-21.
150. Yan, H. and J.G. Lenard, *A study of warm and cold roll-bonding of an aluminium alloy.* Materials Science and Engineering: A, 2004. **385**(1-2): p. 419-428.

151. Pérez-Prado, M.T., d. Valle, and O.A. Ruano, *Grain refinement of Mg–Al–Zn alloys via accumulative roll bonding.* Scripta Materialia, 2004. **51**(11): p. 1093-1097.
152. Roostaei, A.A., et al., *An investigation into the mechanical behavior and microstructural evolution of the accumulative roll bonded AZ31 Mg alloy upon annealing.* Materials & Design, 2011. **32**(5): p. 2963-2968.
153. Sankaranarayanan, S., S. Jayalakshmi, and M. Gupta, *Effect of addition of mutually soluble and insoluble metallic elements on the microstructure, tensile and compressive properties of pure magnesium.* Materials Science and Engineering: A, 2011. **530**: p. 149-160.
154. Hassan, S.F. and M. Gupta, *Effect of particulate size of Al2O3 reinforcement on microstructure and mechanical behavior of solidification processed elemental Mg.* Journal of Alloys and Compounds, 2006. **419**(1-2): p. 84-90.
155. Kuśnierz, J., & Bogucka, J. , *Accumulative roll-bonding (ARB) of Al 99.8%*. Archives of Metallurgy and Materials, 2005. **50**(1): p. 219-230.
156. Utsunomiya, H., et al., *Grain refinement of magnesium alloy sheets by ARB using high-speed rolling mill.* Journal of Physics: Conference Series, 2009. **165**: p. 012011.
157. SEETHARAMAN, S., *Synthesis and characterization of new titanium containing magnesium materials* Doctoral dissertation, 2014.
158. Wang, X.M., et al., *Processing, Microstructure and Mechanical Properties of Ti6Al4V Particles-Reinforced Mg Matrix Composites.* Acta Metallurgica Sinica (English Letters), 2016. **29**(10): p. 940-950.
159. Seetharaman, S., Jayalakshmi Subramanian, and Manof Gupta. , *Improving the Mechanical Properties of Mg-5.6Ti-3Al Composite through Nano-Al2O3 Addition with Recrystallisation Heat Treatment* Journal of Engineering Science, 2013. **9**(1).
160. Chawla, N., and Y-L. Shen. , *Mechanical behavior of particle reinforced metal matrix composites.* Advanced engineering materials, 2001. **3**(6): p. 357-370.
161. Xi, Y.L., et al., *Titanium alloy reinforced magnesium matrix composite with improved mechanical properties.* Scripta Materialia, 2006. **54**(1): p. 19-23.

162. Paramsothy, M., et al., *Al(2)O(3) Nanoparticle Addition to Commercial Magnesium Alloys: Multiple Beneficial Effects.* Nanomaterials (Basel), 2012. **2**(2): p. 147-162.
163. Shen, M.J., M.F. Zhang, and W.F. Ying, *Processing, microstructure and mechanical properties of bimodal size SiCp reinforced AZ31B magnesium matrix composites.* Journal of Magnesium and Alloys, 2015. **3**(2): p. 162-167.
164. Hassan, S.F. and M. Gupta, *Development of high performance magnesium nano-composites using nano-Al2O3 as reinforcement.* Materials Science and Engineering: A, 2005. **392**(1-2): p. 163-168.
165. Sankaranarayanan, S., S. Jayalakshmi, and M. Gupta, *Effect of individual and combined addition of micro/nano-sized metallic elements on the microstructure and mechanical properties of pure Mg.* Materials & Design, 2012. **37**: p. 274-284.

VITA

NAME: Baleegh Alobaid

EDUCATION:

Technical College of Baghdad/ Baghdad -Iraq

Department of Welding Engineering

1996-2000, B.Sc.

University of Technology Baghdad/ Baghdad -Iraq

Department of Metallurgical Engineering

2001-2004, M.Sc.

WORK EXPERIENCE:

Oil refinery,

2005-2009

University of Al-Muthanna/ Samawah -Almutanna-Iraq/ College of engineering

2009-2012

Previous Publication

Chapter	Publication	Publication status
Chapter 2	Microstructure and mechanical behavior of hot-rolled AZ31/Ti multilayers Baleegh Alobaid [a,b], Fuqian Yang [a], and Yang-Tse Cheng [a]	Submitted
Chapter 3	Three layered Titanium Clad-AZ31 Magnesium alloy Sheet by Single-Pass Hot-Rolling Baleegh Alobaid [a,b], Fuqian Yang [a], and Yang-Tse Cheng [a]	Prepared
Chapter 4	Microstructure and mechanical properties of Ti particles reinforced AZ31 –Mg alloy matrix composites through ARB and subsequent annealing Baleegh Alobaid [a,b], Fuqian Yang [a], and Yang-Tse Cheng	Prepared

a . Materials Program, Department of Chemical and Materials Engineering, University of Kentucky, Lexington, Kentucky, USA 40506

b. College of Engineering, Muthanna University, Samawah, Muthanna, Iraq 66001